

# **Quantum Transport of Alkane Derivatives in Nanoscale Structures**

**Abdullah Alshehab**

PhD Thesis in Physics



Submitted in partial fulfilment of the requirements for the degree of Doctor of  
Philosophy

April 2022

# **Declaration**

Except where stated otherwise, this thesis is a result of the author's original work and has not been submitted in whole or in part for the award of a higher degree elsewhere. This thesis documents work carried out between October 2018 and March 2022 at Lancaster University, UK, under the supervision of Professor. Colin J. Lambert and funded by King Faisal University, Saudi Arabia.

**Abdullah Alshehab**

April 2022

## **Acknowledgment**

I would like to express deepest gratitude to Prof. Colin John Lambert for the excellent supervision and guidance I received. This thesis would never completed without his enormous support and excellent guidance. I would also like to express my grateful admiration to Dr. Ali Ismael, none of this work would have been accomplished without his insightful comments and suggestions, dedicated time, and guidance. Also, many thanks to Theory of molecular-Scale groups especially Dr. Majed Alshammari and Dr. Turki Alotaibi.

I would like also to thank my sponsor, King Faisal University -KSA, for given me this great opportunity to study a Ph.D. in the United Kingdom.

I would like to thank the collaborating experimental groups. I would like to thank all my friends and colleagues in Colin's group.

Last but not the least, I would like to thank my family: my father, mother, my brothers and sisters and not forget to thank my wife and my daughter Misk.

Above all, my great thanks to ALLAH for his mercy and blessing.

Abdullah

## Abstract

As a result of recent developments, alkane derivatives have been used in many applications, including sensors for safety and security. This thesis provides a theoretical contribution to these developments by exploring molecular junctions formed from nearly 40 alkane derivatives including linear chains and rings. This study also employs 4 different anchor groups such as amine, thiol, direct carbon and thiomethyl.

Within this thesis, I will provide a simple introduction to the theoretical tools used to explore electron transport through single-molecule junctions. In Chapter 2, Density Functional Theory (DFT) and its applications within the SIESTA code will be discussed. This allows computation of ground state wave functions for molecules and provides the underlying Hamiltonians for molecular junctions which are used as a starting point for transport calculations. Chapter 3, provides the theoretical framework that is used to calculate electron transport properties such as electrical conductance  $G$  and thermopower  $S$ . This is based on Green's and Dyson's equation and is embodied in the GOLLUM code, which is the second major tool used during in this thesis. In chapter 3, I present some solutions of Green's functions for infinite and semi-infinite chains and the transmission coefficient equations that implemented in the GOLLUM code.

Chapter 4 is the first results chapter in this thesis, which provides thorough and vigorous theoretical investigations about series of alkane chains using different anchor groups including amine ( $\text{NH}_2$ ), thiol (S), direct carbon contact (C), and thiomethyl (SMe). Thus, I demonstrate the impact of using different terminal groups on the electrical conductance of alkane molecules. As expected, the conductance of alkane chains decreases exponentially with length, regardless of the type of anchor groups. However, the precise value of the conductance differs from one anchor to another.

The theoretical predictions of the four anchors are checked against the STM measurements and are found to be well supported by the experimental measurements.

Chapter 5 is the second results chapter in my thesis, and investigates a series of alkane chains and their corresponding symmetric and asymmetric alkane rings were explored. The electrical conductance and Seebeck coefficient of three linear chains and six rings were investigated using DFT. Remarkably, I found that the conductances of the double-branched alkane rings were smaller than those of the corresponding individual chains and much smaller than the value predicted by Kirchhoff's law. This result is well supported by previous published work. The Seebeck coefficients of the rings were also higher than those of the corresponding chains, which is consistent with the presence of phase coherent tunnelling in the alkane rings. Further characterizations of asymmetric rings found that their conductances and Seebeck coefficients were between those of their corresponding shorter and longer chains. With the elongation of the longer chain, the conductance of the asymmetric ring became close to that of the shorter chain. This suppression of conductance in symmetric rings agrees with experimental results using the scanning tunneling microscope break junction (STM-BJ) method.

### List of publication during PhD studies

1. Wang, X., Ismael, A., Almutlg, A., Alshammari, M., Al-Jobory, A., Alshehab, A., Bennett, T.L.R., Wilkinson, L.A., Cohen, L.F., Long, N.J., Robinson, B.J. and Lambert, C. (2021). Optimised power harvesting by controlling the pressure applied to molecular junctions. *Chemical Science*, 12(14), pp.5230–5235.
2. Ismael, A., Al-Jobory, A., Wang, X., Alshehab, A., Almutlg, A., Alshammari, M., Grace, I., Bennett, T., Wilkinson, L., Robinson, B., Long, N. and Lambert, C., **2020**. Molecular-scale thermoelectricity: as simple as ‘ABC’. *Nanoscale Advances*, 2(11), pp.5329-5334.

## Table of Contents

Acknowledgment .....	3
Abstract .....	4
List of publication during PhD studies .....	6
Chapter 1 .....	18
1.1 Molecular electronics and thermopower.....	18
1.2 Thesis outline .....	20
Bibliography .....	22
Chapter 2 .....	33
2.1 Introduction.....	33
2.2 The Schrödinger Equation and Variational Principle .....	34
2.3 Born-Oppenheimer approximation .....	36
2.4 The Hohenberg-Kohn Theorems .....	39
2.5 The Kohn-Sham Theorems .....	41
2.6 The Exchange Correlation Functionals.....	42
2.6.1 Local Density Approximation (LDA).....	43
2.6.2 Generalized Gradient Approximation (GGA) .....	43
2.7 Pseudopotentials .....	44
2.8 SIESTA .....	45
2.9 Conclusion .....	45
Bibliography .....	46
Chapter 3 .....	51
Theory of Quantum Transpor .....	51
3.1 Introduction.....	51
3.2 Landauer formula and thermoelectric coefficient.....	52
3.3 Green's function for the double-infinite chain in one- dimension.....	56
3.4 Green's functions for the semi-infinite chain in one- dimension .....	58
3.5 Dyson's equation and Green's function for a scattering system.....	59
3.6 Green's functions and Dyson's equation applications.....	63
3.6.1 A dangling system.....	63
3.6.2 A scattering system with only one atom .....	66

3.6.3 Breit-Wigner resonance .....	70
3.7 Conclusion .....	71
Bibliography .....	72
Further investigations of anchoring groups on linear alkane chains.....	73
4.1 Introduction.....	73
4.2 Motivation.....	73
4.3 Optimised DFT Structures of Isolated Molecules .....	74
4.3.1 Geometries of the isolated alkane chains terminated with an amine anchor .....	74
4.4 Frontier orbitals for the studied molecules .....	75
4.5 Binding energy of linear chains on gold.....	79
4.6 DFT Calculations .....	80
4.7 Optimised DFT Structures of Compounds in their Junctions.....	80
4.8 Transport calculations.....	81
4.8.1 Transmission coefficient of alkane chains with Amine as terminal group.....	81
4.8.2 Comparison between theory and experiment of amine anchor.....	83
4.9 Studied alkane chains with thiol as terminal group .....	85
4.9.1 Geometries of the isolated alkane chains terminated with a thiol anchor.....	85
4.10 Frontier orbitals for studied molecules .....	86
4.11 Binding energy of linear chain on gold.....	90
4.12 Optimised DFT Structures of Compounds in their Junctions.....	90
4.13 Transmission coefficient of alkane chains with Thiol as terminal group .....	91
4.13.1 Comparison between theory and experiment of thiol anchor .....	93
4.14 Alkane chains with carbon as a terminal group.....	95
4.14.1 Geometries of the isolated alkane chains terminated directly with a carbon anchor.....	95
4.15 Frontier orbitals for the studied molecules .....	96
4.16 Binding energy of linear chain on gold.....	100
4.17 Optimised DFT Structures of Compounds in their Junctions.....	101
4.18 Transmission coefficient of alkane chains with carbon as terminal group.....	102
4.18.1 Comparison between theory and experiment of carbon anchor.....	104
4.19 Transmission coefficient of alkane chains with Thiomethyl as terminal group .....	105
4.20 STM versus DFT Conductance of four different terminal groups.....	106
4.21 Exponential decay $\beta$ calculations .....	108
4.21.1 Comparison between theory and experiment of $\beta$ factor .....	110



4.21 Conclusion .....	111
Bibliography .....	112
Chapter 5 .....	116
Non-classical electron transport in the sigma systems of alkane rings.....	116
5.1 Motivation.....	117
5.3 Optimized DFT Structures of Isolated Molecules .....	118
5.3.1 Geometries of the isolated alkane chains.....	118
5.3.2 Geometries of the isolated symmetric alkane rings .....	118
5.3.3 Geometries of the isolated asymmetric alkane rings .....	119
5.4 Frontier orbitals of the studied molecules.....	120
5.5 Binding energy of two terminal groups on gold .....	124
5.6 DFT Calculations .....	125
5.7 Optimised DFT Structures of Compounds in their Junctions.....	125
5.8 Transport calculations.....	126
5.8.1 Transmission coefficient of alkane chains using (Au-SMe) as terminal group.....	126
5.8.2 Transmission coefficient of alkane rings using (Au-S) as terminal group .....	127
5.9 Applying the Kirchhoff's law in the Nano-scale structures.....	130
5.9.1 Conductance of linear chain versus symmetric rings .....	132
5.9.2 Conductance of linear chains versus asymmetric rings .....	133
5.10 Classical and non-classical trends (families) .....	135
5.10.1 Comparison between theoretical simulations and experimental measurements.....	140
5.10.2 Units of the Y-axis .....	147
5.11 Seebeck coefficient .....	149
5.11.1 Seebeck coefficients of linear chains .....	150
5.11.2 Seebeck coefficient of symmetric alkane rings .....	151
5.11.3 Seebeck coefficient of asymmetric alkane rings.....	152
5.11.3 Comparison between theoretical simulations and experimental measurements.....	153
5.12 Conclusion .....	155
Bibliography .....	157
Chapter 6.....	161
Conclusion and Future Work.....	161
6.1 Conclusion .....	161
6.2 Future work.....	163

Bibliography .....	164
--------------------	-----

## List of Figures

Figure 3. 1. Double-infinite chain in one- dimension on-site energies $\epsilon_0$ and couplings $-\gamma$ .	56
Figure 3. 2. The structure of retarded Green's function of an infinite one-dimensional chain. The excitation at $l = j$ causes wave to propagate left and right with amplitudes $B$ and $A$ respectively.	57
Figure 3. 3. Semi-infinite chain in one- dimension with on-site energies $\epsilon_0$ and couplings $-\gamma$ .	58
Figure 3. 4. A one-dimensional scatterer connected to one-dimensional leads before perturbation $\alpha = \beta = 0$ .	60
Figure 3. 5. A one-dimensional scatterer connected to one-dimensional leads after perturbation $\alpha$ and $\beta \neq 0$ .	60
Figure 3. 6. A dangling system.	64
Figure 3. 7. Transmission coefficients of dangling system against electron energy $E$ . In this system $\alpha = 0.6$ , $\gamma = 1$ and $\epsilon_1 = 0$ .	66
Figure 3. 8. Open system with only one atom in the SR before the perturbations $\alpha, \beta$ .	67
Figure 3. 9. Open system with only one atom in the SR after the perturbation.	68
Figure 3. 10. Transmission coefficient versus energy $E$ for only one atom in the SR.	69
Figure 4. 1. Alkane chains: Fully relaxed isolated molecules, of different length 3-10 carbon atoms. (Left panel) shows the odd chains <b>C<sub>3</sub></b> , <b>C<sub>5</sub></b> , <b>C<sub>7</sub></b> and <b>C<sub>9</sub></b> while (right panel) represents the even ones <b>C<sub>4</sub></b> , <b>C<sub>6</sub></b> , <b>C<sub>8</sub></b> and <b>C<sub>10</sub></b> , both chains are terminated with amine anchors.	74
Figure 4. 2. An example of alkane molecule terminated with an amine anchor on a gold tip : (Left) Binding energy of <b>C<sub>6</sub></b> alkane molecule to gold as a function of molecule-contact distance. The equilibrium distance (i.e. the minimum of the binding energy curve) is found to be approximately 3 Å, for Au-Amine. (Right) its idealised ad-atom configuration at the Au lead interface Au-Amine. Key: C = grey, H = white, N = blue, Au = dark yellow.	80
Figure 4. 3. Examples of fully relaxed alkane derivatives in Au molecule Au junctions. (Left panel) shows odd number of linear chains <b>C<sub>3</sub></b> , <b>C<sub>5</sub></b> , <b>C<sub>7</sub></b> and <b>C<sub>9</sub></b> (top to bottom) connected to gold electrodes via amine anchor groups. (Right panel) shows even number of linear chains <b>C<sub>4</sub></b> , <b>C<sub>6</sub></b> , <b>C<sub>8</sub></b> and <b>C<sub>10</sub></b> (top to bottom) with the same anchor groups.	81
Figure 4. 4. Transmission coefficient curves of alkane chains . (Left panel) and (right panel) represent transmission coefficients $T(E)$ of alkane chains with odd (left) and even (right) number of carbon atoms against electron energy $E$ .	82
Figure 4. 5. Transmission coefficient curves of alkane chains with (Au-Amine) for both odd and even number of carbon atoms of linear chains against electron energy $E$ .	82
Figure 4. 6. Length dependence of the conductance of a single-molecule Au  linear chains  Au junction with Au-Amine covalent bonds connecting the ends of the alkane to gold electrodes. The purple line and the green dashed line show the DFT conductances for odd and even number of $-CH_2$ units respectively.	83

Figure 4. 7. STM measurements versus DFT simulation of alkane chains terminated with  $\text{NH}_2$  anchor. Two set of measurements from different experimental group (blue- and red-line), and DFT calculations (black-line). 85

Figure 4. 8. Alkane chains: Fully relaxed isolated molecules, of different length 3-10 carbon atoms. (Left panel) shows the odd chains  $\text{C}_3$ ,  $\text{C}_5$ ,  $\text{C}_7$  and  $\text{C}_9$  while (right panel) represents the even ones  $\text{C}_4$ ,  $\text{C}_6$ ,  $\text{C}_8$  and  $\text{C}_{10}$ , both chains are terminated with thiol anchors. 86

Figure 4. 9. An example of alkane molecule terminated with a thiol anchor on a gold tip :( Left) Binding energy of  $\text{C}_4$  alkane molecule to gold as a function of molecule-contact distance. The equilibrium distance (i.e. the minimum of the binding energy curve) is found to be approximately 2.4 Å, for Au-S. (Right) its idealised ad-atom configuration at the Au lead interface Au-thiol. Key: C = grey, H = white, S = light yellow, Au = dark yellow. 90

Figure 4. 10. Examples of fully relaxed alkane derivatives in Au|molecule|Au junctions. (Left panel) shows odd number of linear chains  $\text{C}_3$ ,  $\text{C}_5$ ,  $\text{C}_7$  and  $\text{C}_9$  (top to bottom) connected to gold electrodes via thiol anchor groups. (Right panel) shows even number of linear chains  $\text{C}_4$ ,  $\text{C}_6$ ,  $\text{C}_8$  and  $\text{C}_{10}$  (top to bottom) with the same anchor groups. 91

Figure 4. 11. Transmission coefficients curves of alkanes chains with (Au-S) . (Left panel) and (right panel) represent transmission coefficients  $T(E)$  of alkane chains with odd (left) and even (right) number of carbon atoms against electron energy  $E$ . 92

Figure 4. 12. Transmission coefficients of alkanes chains with (Au-S) for both odd and even number of carbon atoms of linear chains against electron energy  $E$ . 92

Figure 4. 13. Length dependence of the conductance of a single-molecule Au| linear chains |Au junction with Au-S covalent bonds connecting the ends of the alkane to gold electrodes. The purple line and the green dashed line show the DFT conductances of odd and even number of  $-\text{CH}_2$  units respectively. 93

Figure 4. 14. STM measurements versus DFT simulation of alkane chains terminated with thiol anchor. The black dashed line shows the DFT calculations whereas the red line represents experimental measurements of  $\text{C}_6$ ,  $\text{C}_8$  and  $\text{C}_{10}$  94

Figure 4. 15. Chain-length dependence of the single-junction Au |alkane linear chain | Au conductance for two different terminal groups. (Left panel) and (right panel) represent logarithmic conductances of DFT and STM (left to right), as a function of length for two different terminal groups Au- Amine (theoretical blue-dashed line of left panel and experimental blue and blue-dot lines of right panel) and Au-S (theoretical red-dashed line of left panel and experimental red line of right panel). 95

Figure 4. 16. Alkane chains: Fully relaxed isolated molecules, of different length 3-10 carbon atoms. (Left panel) shows the odd chains  $\text{C}_3$ ,  $\text{C}_5$ ,  $\text{C}_7$  and  $\text{C}_9$  while (right panel) represents the even ones  $\text{C}_4$ ,  $\text{C}_6$ ,  $\text{C}_8$  and  $\text{C}_{10}$ , both chains are terminated with carbon anchors ( $\text{CH}_3$ ). 96

Figure 4. 17. An example of alkane molecule terminated with a carbon on a gold tip :( Left) Binding energy of  $\text{C}$  alkane molecule to gold as a function of molecule-contact distance. The equilibrium distance (i.e. the minimum of the binding energy curve) is found to be approximately 2.3 Å, for Au-C. (Right) its idealised ad-atom configuration at the Au lead interface Au-thiol. Key: C = grey, H = white, Au = dark yellow. 100

Figure 4. 18. Examples of fully relaxed alkane derivatives in Au|molecule|Au junctions. (Left panel) shows odd number of linear chains  $\text{C}_3$ ,  $\text{C}_5$ ,  $\text{C}_7$  and  $\text{C}_9$  (top to bottom) connected to gold

electrodes via direct carbon anchor groups. (Right panel) shows even number of linear chains **C<sub>4</sub>**, **C<sub>6</sub>**, **C<sub>8</sub>** and **C<sub>10</sub>** (top to bottom) with the same anchor groups. 101

Figure 4. 19. Transmission coefficients curves of alkanes chains with (C-Au) . (Left panel) and (right panel) represent transmission coefficients  $T(E)$  of alkane chains with odd (left) and even (right) number of carbon atoms against electron energy  $E$ . 102

Figure 4. 20. Transmission coefficients of alkanes chains with (C-Au) for both odd and even carbon atoms of linear chains against electron energy  $E$ . 103

Figure 4. 21. Length dependence of the conductance of a single-molecule Au| linear chains |Au junction with C-Au covalent bonds connecting the ends of the alkane to gold electrodes. The purple line and the green dashed line show the DFT conductances of odd and even number of  $-CH_2$  units respectively. 103

Figure 4. 22. STM measreaments versus DFT simulation of alkane chains terimenated with carbon anchor. The black dashed line shows the DFT calculations where the red line represents experimental measurements. 104

Figure 4. 23. Alkane chains: Fully relaxed isolated molecules, of different length of carbon atoms, mainly even chains **C<sub>4</sub>**, **C<sub>6</sub>**, **C<sub>8</sub>** and **C<sub>10</sub>**, and all are terminated with SMe anchors. 105

Figure 4. 24. Transmission coefficient curves of alkanes chains . Transmission coefficient  $T(E)$  curves of even alkane chains against electron energy  $E$ . 106

Figure 4. 25. Chain-length conductance dependence of Au |alkane linear chain | Au junctions for four different terminal groups. Logarithmic conductance of DFT and STM (left to right), as a function of the chain length of four different terminal groups Au- C (purple line), Au-S (green line), Au-SMe (blue line) and Au-Amine (red line). 107

Figure 5. 1. Alkane chains: Fully relaxed isolated molecules, with 6, 8 and 10 carbon atoms (excluding the 2 carbon atoms within the SMe anchors). (a), (b) and (c): represent **C<sub>6</sub>**, **C<sub>8</sub>** and **C<sub>10</sub>** chains with (SMe) top to bottom respectively..... 118

Figure 5. 2. Alkane symmetric rings: Fully relaxed isolated symmetric rings, with 6-6, 8-8 and 10-10 carbon atom branches: (a), (b) and (c): represent **C<sub>6</sub>C<sub>6</sub>**, **C<sub>8</sub>C<sub>8</sub>** and **C<sub>10</sub>C<sub>10</sub>** rings with (SMe) top to bottom respectively. .... 119

Figure 5. 3. Alkane asymmetric rings: Fully relexed isolated asymmetric rings, with 6-8, 6-10 and 8-10 carbon atom branches. (a), (b) and (c): represents **C<sub>6</sub>C<sub>8</sub>**, **C<sub>6</sub>C<sub>10</sub>** and **C<sub>8</sub>C<sub>10</sub>** rings with (SMe) top to bottom respectively. .... 120

Figure 5. 4. An example of alkane molecule terminated with a thiol anchor and thiomethyl on a gold tip :( Left) Binding energy of **C<sub>4</sub>** alkane chain and **C<sub>6</sub>C<sub>6</sub>** symmetric ring to gold as a function of molecule-contact distance. The equilibrium distances (i.e. the minimum of the binding energy curve) are found to be approximately 2.4 and 2.8 Å, for Au-S and Au-SMe (red and green curves). (Right) its idealised ad-atom configuration at the Au lead interface Au-thiol and Au-SMe. Key: C = grey, H = white, S = light yellow, Au = dark yellow..... 124

Figure 5. 5. Examples of fully relaxed alkane derivatives in Au|molecule|Au junctions: (a), (b) and (c). 6, 8 and 10 linear chains connect to gold electrodes via thiomethyl anchor groups (Au-SMe). .... 125

Figure 5. 6. Transmission coefficients of alkanes with 6, 8 and 10 carbon atoms. Transmission coefficients $T(E)$ of alkane chains against electron energy $E$ , alkane chain $C_6$ (black-line), alkane chain $C_8$ (blue-line), and alkane chain $C_{10}$ (red-line). .....	126
Figure 5. 7. Examples of alkane ring derivatives in Au molecule Au junctions: (a), (b) and (c): A double-branch $n = 6, 8$ and $10$ alkane symmetric rings with (Au-S). .....	127
Figure 5. 8. Transmission coefficient curves of alkane symmetric rings. Transmission coefficients $T(E)$ of alkane symmetric rings against electron energy $E$ , alkane ring size $C_6C_6$ (black-line), alkane ring size $C_8C_8$ (blue-line), and alkane ring size $C_{10}C_{10}$ (red-line). .....	128
Figure 5. 9. Examples of alkane ring derivatives in Au molecule Au junctions: (a), (b) and (c): The length of top-branches are $n = 6, 6$ and $8$ while bottom- branches $n=8, 10$ and $10$ asymmetric alkane rings with (Au-S).....	129
Figure 5. 10. Transmission coefficient curves of alkane asymmetric rings. Transmission coefficients $T(E)$ of alkane asymmetric rings against electron energy $E$ , alkane ring size $C_6C_8$ (black-line), alkane ring size $C_6C_{10}$ (blue-line), and alkane ring size $C_8C_{10}$ (red-line). .....	129
Figure 5. 11. Electrical circuit with resistors ( $R_1$ and $R_2$ ), where they connected in parallel. ....	130
Figure 5. 12. Different scenarios for quantum circuits. (a): The conductance of a molecule is $G$ (due to there is only one pathway). (b): Classically, the conductance of a ring formed from two conductors connect in parallel, is equal to the sum of the individual conductances ( $G_1 + G_2$ ). .....	131
Figure 5. 13. Transmission coefficient curves of the three alkane rings of family-6. Transmission coefficients $T(E)$ of family-6 against electron energy $E$ .....	136
Figure 5. 14. Transmission coefficient curves of the three alkane rings of family-8. Transmission coefficients $T(E)$ of family-8 against electron energy $E$ .....	136
Figure 5. 15. Transmission coefficient curves of the three alkane rings of family-10. Transmission coefficients $T(E)$ of family-10 against electron energy $E$ .....	137
Figure 5. 16. Conventional and non-conventional tunnelling transport of three families. The theoretical conductances of three alkane ring families: small cavity family $C_6$ including $C_6C_6$ , $C_6C_8$ and $C_6C_{10}$ , medium cavity family $C_8$ including $C_8C_8$ , $C_6C_8$ and $C_8C_{10}$ , and large cavity family $C_{10}$ including $C_{10}C_{10}$ , $C_6C_{10}$ and $C_8C_{10}$ . .....	138
Figure 5. 17. Testing the validity of DFT predictions (the Kirchhoff's law validity). Conductance comparison of linear chains (blue lines) and alkane rings (red lines). (Left panel) represents DFT predictions while (right panel) STM experimental measurements. Note: $n = C_6, C_8$ and $C_{10}$ for chains and $C_6C_6, C_8C_8$ and $C_{10}C_{10}$ for rings. ....	141
Figure 5. 18. Length dependence conductance of Au chains/rings Au junction, with Au-SMe for chains and Au-S for rings covalent bonds connecting the ends of the alkane to the gold electrodes. The blue and dashed blue lines represent the DFT simulations while the red and dashed red lines represent the STM measurements. ....	142
Figure 5. 19. Comparison between DFT simulations against STM measurements of the small group, $C_6$ versus $C_6C_8$ or $C_6C_{10}$ . The red dashed- line represents the theory while the blue dashed- line represents the experiment. ....	143
Figure 5. 20. Comparison between DFT simulations against STM measurements of the medium group, $C_8$ versus $C_6C_8$ or $C_8C_{10}$ . The red dashed- line represents the theory while the blue dashed- line represents the experiment. ....	144

Figure 5. 21. Comparison between DFT simulations against STM measurements of the medium group, $C_{10}$ versus $C_6C_{10}$ or $C_8C_{10}$ . The red dashed- line represents the theory while the blue dashed- line represents the experiment. ....	145
Figure 5. 22. Conventional and non-conventional tunnelling transport. Comparison between the theory and experimental conductances of three alkane ring families: small, medium and large cavities $C_6$ , $C_8$ and $C_{10}$ respectively.....	146
Figure 5. 23. Same plotting scale of Y-axes (amending Figure). Family 6, family 8 and family 10, (top to bottom). ....	148
Figure 5. 24. Seebeck coefficient $S$ as a function of Fermi energy $E_F$ for 3 alkane chains. Seebeck coefficient $S$ of alkane chains of size $C_6$ , alkane chain $C_8$ , and alkane chain $C_{10}$ . .	151
Figure 5. 25. Seebeck coefficients $S$ as a function of Fermi energy $E_F$ for 3 alkane symmetric rings. Small symmetric rings of size $C_6C_6$ , medium size $C_8C_8$ , and large size $C_{10}C_{10}$ .....	151
Figure 5. 26. Seebeck coefficients $S$ as a function of Fermi energy $E_F$ for 3 alkane rings. Seebeck coefficients $S$ of asymmetric alkane rings of small cavity $C_6C_8$ , medium cavity $C_6C_{10}$ , and large cavity $C_8C_{10}$ respectively. ....	152
Figure 5. 27. Schematic illustration of chapter 5 summarized the trend of $G$ for chains and rings.....	156
 Figure 6. 1. The structure of 1,4,7,10,13,16-Hexaoxacyclooctadecane molecule.....	163

## List of Tables

Table 4. 1. Comparison between the Frontier molecular orbitals of alkane chain, including C <sub>3</sub> , C <sub>4</sub> and C <sub>5</sub> in the gas phase.....	76
Table 4. 2. Comparison between the frontier molecular orbitals of alkane chain, including C <sub>6</sub> , C <sub>7</sub> and C <sub>8</sub> in the gas phase. ....	76
Table 4. 3. Comparison between the frontier molecular orbitals of alkane chain, including C <sub>9</sub> and C <sub>10</sub> in the gas phase.....	77
Table 4. 4. Conductances of two STM measurements and DFT simulations of linear alkane chains terminated with NH <sub>2</sub> anchors. Simulations are taken at the DFT-predicted Fermi ( $E - EF = 0$ eV).....	84
Table 4. 5. Comparison between the frontier molecular orbitals of alkane chain, including C <sub>3</sub> , C <sub>4</sub> and C <sub>5</sub> in the gas phase.....	87
Table 4. 6. Comparison between the frontier molecular orbitals of alkane chain, including C <sub>6</sub> , C <sub>7</sub> and C <sub>8</sub> in the gas phase. ....	88
Table 4. 7. Comparison between the frontier molecular orbitals of alkane chain, including C <sub>9</sub> and C <sub>10</sub> in the gas phase.....	89
Table 4. 8. Comparison between the frontier molecular orbitals of alkane chain, including C <sub>3</sub> , C <sub>4</sub> and C <sub>5</sub> in the gas phase.....	97
Table 4. 9. Comparison between the frontier molecular orbitals of alkane chain, including C <sub>6</sub> , C <sub>7</sub> and C <sub>8</sub> in the gas phase.....	97
Table 4. 10. Comparison between the frontier molecular orbitals of alkane chain, including C <sub>9</sub> and C <sub>10</sub> in the gas phase.....	98
Table 5. 1. Comparison between the Frontier molecular orbitals of alkane chain, including C <sub>6</sub> , C <sub>8</sub> and C <sub>10</sub> in the gas phase. ....	121
Table 5. 2. Frontier molecular orbitals of symmetric rings, including C <sub>6</sub> C <sub>6</sub> , C <sub>8</sub> C <sub>8</sub> and C <sub>10</sub> C <sub>10</sub> in the gas phase. ....	122
Table 5. 3. Frontier molecular orbitals of asymmetric rings, including C <sub>6</sub> C <sub>8</sub> , C <sub>6</sub> C <sub>10</sub> and C <sub>8</sub> C <sub>10</sub> in the gas phase. ....	123
Table 5. 4. Conductances of linear chains, C <sub>6</sub> , C <sub>8</sub> and C <sub>10</sub> , and alkane symmetric rings, C <sub>6</sub> C <sub>6</sub> , C <sub>8</sub> C <sub>8</sub> and C <sub>10</sub> C <sub>10</sub> . These results are determined at the DFT-predicted Fermi ( $E - EF = 0$ ). ....	132
Table 5. 5. Conductances of linear chains, C <sub>6</sub> , C <sub>8</sub> and C <sub>10</sub> , and asymmetric alkane rings including C <sub>6</sub> C <sub>8</sub> , C <sub>6</sub> C <sub>10</sub> and C <sub>8</sub> C <sub>10</sub> . These results are determined at the DFT-predicted Fermi ( $E - EF = 0$ ). ....	134
Table 5. 6. shows three families: family-6, family-8 and family-10. Each family includes three rings, the three rings have a common branch. The common branches of the three rings are C <sub>6</sub> , C <sub>8</sub> and C <sub>10</sub> (family-6, family-8 and family-10 respectively). ....	135
Table 5. 7. Conductances of three families: small, medium and large (family-6, family-8 and family-10), each family includes three different cavities. These values are determined at the DFT-predicted Fermi energy ( $E - EF = 0$ eV). ....	139



Table 5. 8. DFT predicted versus STM measured Seebeck coefficients of 9 alkane derivatives in $\mu\text{V/K}$ unit. ....	154
---	-----

## Chapter 1

### 1.1 Molecular electronics and thermopower

Since Moore's law was first proposed in 1965, thousands of studies have been carried out to seek ways to continue this historical trend. Over time, the length scale of electronic components, such as transistors, has become smaller and smaller, and is now approaching the *nano* or *molecular scale* [1]. The crucial challenges, both theoretical and experimental, in this area are the fabrication of devices at the *sub*-10 nm scale and the exploration of their properties.

A reduction in the size of electronic components was proposed in 1974, when Aviram and Ratner suggested the substitution of silicon chips by molecules [2]; their idea provided the foundation for the field of molecular electronics. Since then, the efforts of experts from many disciplines combining experiment and theory has vastly expanded the field. A significant achievement has been the development of computational and modelling tools to obtain theoretical results which closely match experimental measurements. Meanwhile, the latest experimental techniques, such as scanning tunnelling microscopy (STM) break junctions [4], allow the investigation of the electronic properties of a single molecule.

During the past couple of decades, the theory of molecular-scale electronics has further advanced, in part by comparing predictions of material-specific transport codes, such as SMEAGOL and GOLLUM [5, 6] with state-of-the-art experiments. Notable examples include studies of transport through long conjugated wires [7-10] graphene nanoribbons and graphene break junctions [11-25]. These studies have revealed the crucial role played by conformation [26, 27] and connectivity [28-30] in determining the electrical conductance of single molecules.

More recently, theories of phonon transport at the nanoscale [31, 32] have been generalised to describe phonon transport at the molecular scale [33-35]. These studies highlight the role of electrodes in controlling phonon scattering at interfaces and suggests that exploration of alternative electrode materials such as platinum, palladium or even iron [36,37] may be a fruitful route to controlling the flow of heat at the molecular scale. In a more exotic direction, the use of superconducting electrodes is now being explored, in which superconducting interference effects associated with Andreev scattering [38-42] coexist with quantum interference effects associated with frontier orbitals in molecular-scale junctions [43,44].

As well as explorations of electrical and thermal conductance, there has been much progress in understanding the thermoelectrical properties of single-molecule junctions [45-48], stimulated in part by reports of high Seebeck coefficients of order  $161 \mu\text{VK}^{-1}$  for PEDOT: PSS organic films [49]. In this regard, thermoelectricity in fullerenes and nanotubes has led to the observation that the sign of the Seebeck coefficient in fullerenes and nanotubes can be switched by pressure, strain and inter-molecular interactions [50-55]. Interestingly, many of the quantum interference effects observed and predicted in single-molecule junctions are now being scaled up into self-assembled monolayers [56-58], leading to new thin-film materials, whose room-temperature transport properties are controlled by quantum effects. These developments suggest that the field of single molecule electronics has a tremendous future for the design of new functional materials.

## 1.2 Thesis outline

In this thesis, I present the main equations and theoretical tools that constitute the foundation of these projects. In chapter 2, density functional theory as a method for solving the Schrödinger equation is reviewed. The Hohenberg-Kohn theorems and the Kohn-Sham ansatz are described. The functional forms of the exchange and correlation energy in the local density approximation and the generalized gradient approximation are explained. The SIESTA code is introduced along with some fine details of the calculations, such as the use of pseudopotentials and finite basis sets [59-62].

In Chapter 3, I discuss single electron charge transport through molecules by introducing quantum transport theory, with some examples of how to calculate the transmission coefficient for different systems using the Hamiltonian and Green's functions.

In Chapter 4 I investigate a series of alkane chains using different linker groups including amine (NH<sub>2</sub>), thiol (S), direct carbon contact (C), and thiomethyl (SMe). In this chapter, I nominated 8 molecules including 4 odd and 4 even number of -CH<sub>2</sub> units, each with 4 different anchor groups (4 x 8). So, in total, I investigate 32 alkane chains. I found that the conductance of alkane chains decreases with length regardless to the type of linker groups, however, conductance values differ by changing the terminal group; (Au-C) conductance values were the highest, while (Au-Amine) yielded the lowest conductance values. For instance, conductances of C<sub>4</sub>, C<sub>5</sub> and C<sub>6</sub> were -1, -1.75 and -2.1 with (Au-C) respectively. Similarly, -3, -3.5 and -4.0 are for the same chains with (Au-Amine) respectively. Furthermore, according to the DFT simulations investigation, one could classify the anchor groups based on their conductance order directed carbon > thiol > thiolmethyl > amine. The DFT conductance prediction of the 4 anchors is well-supported by many STM experimental measurements [63-76].

Chapter 5, is the second result chapter, where I investigated three even alkane chains **C<sub>6</sub>**, **C<sub>8</sub>** and **C<sub>10</sub>** terminated with thiomethyl anchors. Their conductances decrease with increasing length and were found to be  $\log_{10} G \approx -3.7, -4.2$  and  $-5.0$ .

Furthermore, I analyzed symmetric and asymmetric rings formed from alkane chains. For symmetric rings, I selected three rings, namely **C<sub>6</sub>C<sub>6</sub>**, **C<sub>8</sub>C<sub>8</sub>** and **C<sub>10</sub>C<sub>10</sub>** and found that the **C<sub>6</sub>C<sub>6</sub>** ring has the highest conductance compared to **C<sub>8</sub>C<sub>8</sub>** and **C<sub>10</sub>C<sub>10</sub>**. I found their conductances have a classical behaviour. In addition, for asymmetric rings, **C<sub>6</sub>C<sub>8</sub>**, **C<sub>6</sub>C<sub>10</sub>** and **C<sub>8</sub>C<sub>10</sub>**, their patterns are not so different from the symmetric rings. The **C<sub>6</sub>C<sub>8</sub>** ring has the smallest cavity, and comparing **C<sub>6</sub>C<sub>8</sub>** with **C<sub>6</sub>C<sub>10</sub>**, it was found that the latter has the largest conductance.

The most important and controversial prediction in this chapter is the validity of the Kirchhoff's law in the nano-scale structures. Surprisingly, the conductances of alkane chains were found to be higher than their corresponding ring conductances, which is in marked contrast with the behaviour of classical electrical conductors.

Since this study includes, symmetric and asymmetric rings. I formed three families, based on the common branch **C<sub>6</sub>**, **C<sub>8</sub>** and **C<sub>10</sub>**. Family-6 consists of **C<sub>6</sub>C<sub>6</sub>**, **C<sub>6</sub>C<sub>8</sub>** and **C<sub>6</sub>C<sub>10</sub>**, which possessed a non-classical trend. On the other hand, families-8 and -10, both follow a classical behaviour.

This chapter also covers the thermoelectric properties such as the Seebeck coefficients of the studied molecules, which are found to vary inversely with their conductances. To benchmark my theoretical models, I tested them against the STM measurements. I found that the DFT predictions and simulations are well supported by the STM measurements for the 9 alkane derivatives [77-82].

Finally, in chapter 6, I present the conclusions of this thesis and discuss future work.

## Bibliography

1. Leon, S. J., Bica, I. and Hohn, T. (1998). Linear algebra with applications (Vol. 6). Upper Saddle River, NJ: Prentice Hall.
2. Visions for a molecular future. (2013). *Nature Nanotechnology*, 8(6), pp.385–389.
3. Aviram, A. and Ratner, M.A. (1974). Molecular rectifiers. *Chemical Physics Letters*, 29(2), pp.277–283.
4. Lambert, C.J. (2015). Basic concepts of quantum interference and electron transport in single-molecule electronics. *Chemical Society Reviews*, 44(4), pp.875–888.
5. Gehring, P., Thijssen, J.M. and van der Zant, H.S.J. (2019). Single-molecule quantum-transport phenomena in break junctions. *Nature Reviews Physics*, [online] 1(6), pp.381–396. Available at: <https://www.nature.com/articles/s42254-019-0055-1> [Accessed 11 Jan. 2022].
6. Rocha, A.R., García-Suárez, V.M., Bailey, S., Lambert, C., Ferrer, J. and Sanvito, S. (2006). Spin and molecular electronics in atomically generated orbital landscapes. *Physical Review B*, 73(8).
7. Ferrer, J., Lambert, C.J., García-Suárez, V.M., Manrique, D.Z., Visontai, D., Oroszlany, L., Rodríguez-Ferradás, R., Grace, I., Bailey, S.W.D., Gillemot, K., Sadeghi, H. and Algharagholy, L.A. (2014). GOLLUM: a next-generation simulation tool for electron, thermal and spin transport. *New Journal of Physics*, 16(9), p.093029.
8. Ashwell, G.J., Urasinska, B., Wang, C., Bryce, M.R., Grace, I. and Lambert, C.J. (2006). Single-molecule electrical studies on a 7 nm long molecular wire. *Chemical Communications*, (45), p.4706.

9. Leary, E., Limburg, B., Alanazy, A., Sangtarash, S., Grace, I., Swada, K., Esdaile, L.J., Noori, M., González, M.T., Rubio-Bollinger, G., Sadeghi, H., Hodgson, A., AgraïtN., Higgins, S.J., Lambert, C.J., Anderson, H.L. and Nichols, R.J. (2018). Bias-Driven Conductance Increase with Length in Porphyrin Tapes. *Journal of the American Chemical Society*, 140(40), pp.12877–12883.
10. Algethami, N., Sadeghi, H., Sangtarash, S. and Lambert, C.J. (2018). The Conductance of Porphyrin-Based Molecular Nanowires Increases with Length. *Nano Letters*, 18(7), pp.4482–4486.
11. Li, X., Wu, Q., Bai, J., Hou, S., Jiang, W., Tang, C., Song, H., Huang, X., Zheng, J., Yang, Y., Liu, J., Hu, Y., Shi, J., Liu, Z., Lambert, C.J., Zhang, D. and Hong, W. (2020). Structure-Independent Conductance of Thiophene-Based Single-Stacking Junctions. *Angewandte Chemie*, 132(8), pp.3306–3312.
12. Zheng, X.H., Zhang, G.R., Zeng, Z., García-Suárez, V.M., Lambert, C.J. (2009) Effects of antidots on the transport properties of graphene nanoribbons *Physical Review B* 80 (7).
13. Oroszlány, L., Ferrer, J., Deák, A., Udvardi, L. and Szunyogh, L. (2019). Exchange interactions from a nonorthogonal basis set: From bulk ferromagnets to the magnetism in low-dimensional graphene systems. *Physical Review B*, 99(22).
14. Caneva, S., Hermans, M., Lee, M., García-Fuente, A., Watanabe, K., Taniguchi, T., Dekker, C., Ferrer, J., van der Zant, H.S.J. and Gehring, P. (2020). A Mechanically Tunable Quantum Dot in a Graphene Break Junction. *Nano Letters*, 20(7), pp.4924–4931.
15. García-Suárez, V.M., García-Fuente, A., Carrascal, D.J., Burzurí, E., Koole, M., van der Zant, H.S.J., El Abbassi, M., Calame, M. and Ferrer, J. (2018). *Spin*

- signatures in the electrical response of graphene nanogaps. *Nanoscale*, 10(38), pp.18169–18177.
16. Zheng, X.H., Zhang, G.R., Zeng, Z., García-Suárez, V.M. and Lambert, C.J. (2009). Effects of antidots on the transport properties of graphene nanoribbons. *Physical Review B*, 80(7).
17. Todd, K., Chou, H.-T., Amasha, S. and Goldhaber-Gordon, D. (2009). Quantum Dot Behavior in Graphene Nanoconstrictions. *Nano Letters*, 9(1), pp.416–421.
18. García-Suárez, V.M., García-Fuente, A., Carrascal, D.J., Burzurí, E., Koole, M., van der Zant, H.S.J., El Abbassi, M., Calame, M. and Ferrer, J. (2018). Spin signatures in the electrical response of graphene nanogaps. *Nanoscale*, 10(38), pp.18169–18177.
19. Burzurí, E., García-Fuente, A., García-Suárez, V., Senthil Kumar, K., Ruben, M., Ferrer, J. and van der Zant, H.S.J. (2018). Spin-state dependent conductance switching in single molecule-graphene junctions. *Nanoscale*, 10(17), pp.7905–7911.
20. Bailey, S., Visontai, D., Lambert, C.J., Bryce, M.R., Frampton, H. and Chappell, D. (2014). A study of planar anchor groups for graphene-based single-molecule electronics. *The Journal of Chemical Physics*, 140(5), p.054708.
21. Lambert, C.J. and Weaire, D.L. (1981). Theory of the arrangement of cells in a network. *Metallography*, 14(4), pp.307–318.
22. Limburg, B., Thomas, J.O., Holloway, G., Sadeghi, H., Sangtarash, S., Hou, I.C.-Y., Cremers, J., Narita, A., Müllen, K., Lambert, C.J., Briggs, G.A.D., Mol, J.A. and Anderson, H.L. (2018). Anchor Groups for Graphene-Porphyrin Single-Molecule Transistors. *Advanced Functional Materials*, 28(45), p.1803629.



23. El Abbassi, M., Sangtarash, S., Liu, X., Perrin, M.L., Braun, O., Lambert, C., van der Zant, H.S.J., Yitzchaik, S., Decurtins, S., Liu, S.-X., Sadeghi, H. and Calame, M. (2019). Robust graphene-based molecular devices. *Nature Nanotechnology*, 14(10), pp.957–961.
24. Sadeghi, H., Sangtarash, S. and Lambert, C. (2016). Hexagonal-boron nitride substrates for electroburnt graphene nanojunctions. *Physica E: Low-dimensional Systems and Nanostructures*, 82, pp.12–15.
25. Finch, C.M., Sirichantaropass, S., Bailey, S.W., Grace, I.M., García-Suárez, V.M. and Lambert, C.J. (2007). Conformation dependence of molecular conductance: chemistry versus geometry. *Journal of Physics: Condensed Matter*, 20(2), p.022203.
26. Jiang, F., Trupp, D.I., Algethami, N., Zheng, H., He, W., Alqorashi, A., Zhu, C., Tang, C., Li, R., Liu, J., Sadeghi, H., Shi, J., Davidson, R., Korb, M., Sobolev, A.N., Naher, M., Sangtarash, S., Low, P.J., Hong, W. and Lambert, C.J. (2019). Turning the Tap: Conformational Control of Quantum Interference to Modulate Single-Molecule Conductance. *Angewandte Chemie*, 131(52), pp.19163–19169.
27. Ismael, A.K., Grace, I. and Lambert, C.J. (2017). Connectivity dependence of Fano resonances in single molecules. *Physical Chemistry Chemical Physics*, 19(9), pp.6416–6421.
28. Sangtarash, S., Huang, C., Sadeghi, H., Sorohhov, G., Hauser, J., Wandlowski, T., Hong, W., Decurtins, S., Liu, S.-X. and Lambert, C.J. (2015). Searching the Hearts of Graphene-like Molecules for Simplicity, Sensitivity, and Logic. *Journal of the American Chemical Society*, 137(35), pp.11425–11431.

29. Lambert, C.J. and Liu, S.-X. (2018). A Magic Ratio Rule for Beginners: A Chemist's Guide to Quantum Interference in Molecules. *Chemistry - A European Journal*, 24(17), pp.4193–4201.
30. Kambili, A., Fagas, G., Fal'ko, V.I. and Lambert, C.J. (1999). Phonon-mediated thermal conductance of mesoscopic wires with rough edges. *Physical Review B*, 60(23), pp.15593–15596.
31. Sadeghi, H., Sangtarash, S. and Lambert, C.J. (2016). Cross-plane enhanced thermoelectricity and phonon suppression in graphene/MoS<sub>2</sub> van der Waals heterostructures. *2D Materials*, 4(1), p.015012.
32. Famili, M., Grace, I., Sadeghi, H. and Lambert, C.J. (2017). Suppression of Phonon Transport in Molecular Christmas Trees. *ChemPhysChem*, 18(10), pp.1234–1241.
33. Han, H., Zhang, Y., Wang, N., Samani, M.K., Ni, Y., Mijbil, Z.Y., Edwards, M., Xiong, S., Sääskilahti, K., Murugesan, M., Fu, Y., Ye, L., Sadeghi, H., Bailey, S., Kosevich, Y.A., Lambert, C.J., Liu, J. and Volz, S. (2016). Functionalization mediates heat transport in graphene nanoflakes. *Nature Communications*, 7(1).
34. Mosso, N., Sadeghi, H., Gemma, A., Sangtarash, S. and Lambert, C. (2019). Thermal transport through single molecule junctions. *Nano Letters*.
35. García-Suárez, V.M., Rocha, A.R., Bailey, S.W., Lambert, C.J., Sanvito, S. and Ferrer, J. (2005). Single-channel conductance of H<sub>2</sub> molecules attached to platinum or palladium electrodes. *Physical Review B*, 72(4).
36. García-Suárez, V.M., Newman, C.M., Lambert, C.J., Pruneda, J.M. and Ferrer, J. (2004). Optimized basis sets for the collinear and non-collinear phases of iron. *Journal of Physics: Condensed Matter*, 16(30), pp.5453–5459.

37. Lambert, C.J., Raimondi, R., Sweeney, V. and Volkov, A.F. (1997). Boundary conditions for quasiclassical equations in the theory of superconductivity. *Physical Review B*, 55(9), pp.6015–6021.
38. Fal'ko, V.I., Lambert, C.J. and Volkov, A.F. (1999). Andreev reflections and magnetoresistance in ferromagnet-superconductor mesoscopic structures. *Journal of Experimental and Theoretical Physics Letters*, 69(7), pp.532–538.
39. Hui, V.C. and Lambert, C.J. (1993). Andreev Scattering, Universal Conductance Fluctuations and Phase Periodic Transport. *Europhysics Letters (EPL)*, 23(3), pp.203–209.
40. Leadbeater, M. and Lambert, C.J. (1997). Superconductivity-induced phase-periodic transport in nanoscale structures. *Physical Review B*, 56(2), pp.826–831.
41. Lambert, C.J. and Martin, A. (1994). Quantum resonances of weakly linked, mesoscopic, superconducting dots. *Journal of Physics: Condensed Matter*, 6(16), pp.L221–L226.
42. Plaszkó, N.L., Rakyta, P., Cserti, J., Kormányos, A. and Lambert, C.J. (2020). Quantum Interference and Nonequilibrium Josephson Currents in Molecular Andreev Interferometers. *Nanomaterials*, 10(6), p.1033.
43. Rakyta, P., Alanazy, A., Kormányos, A., Tajkov, Z., Kukucska, G., Koltai, J., Sangtarash, S., Sadeghi, H., Cserti, J. and Lambert, C.J. (2019). Magic Number Theory of Superconducting Proximity Effects and Wigner Delay Times in Graphene-Like Molecules. *The Journal of Physical Chemistry C*, 123(11), pp.6812–6822.
44. Sadeghi, H., Sangtarash, S. and Lambert, C.J. (2015). Enhancing the thermoelectric figure of merit in engineered graphene nanoribbons. *Beilstein Journal of Nanotechnology*, 6, pp.1176–1182.

45. Noori, M., Sadeghi, H. and Lambert, C.J. (2017). High-performance thermoelectricity in edge-over-edge zinc-porphyrin molecular wires. *Nanoscale*, 9(16), pp.5299–5304.
46. Yzambart, G., Rincón-García, L., Al-Jobory, A.A., Ismael, A.K., Rubio-Bollinger, G., Lambert, C.J., Agraït, N. and Bryce, M.R. (2018). Thermoelectric Properties of 2,7-Dipyridylfluorene Derivatives in Single-Molecule Junctions. *The Journal of Physical Chemistry C*, 122(48), pp.27198–27204.
47. Wu, Q., Sadeghi, H., García-Suárez, V.M., Ferrer, J. and Lambert, C.J. (2017). Thermoelectricity in vertical graphene-C60-graphene architectures. *Scientific Reports*, 7(1).
48. Massonnet, N., Carella, A., Jaudouin, O., Rannou, P., Laval, G., Celle, C. and Simonato, J.-P. (2014). Improvement of the Seebeck coefficient of PEDOT:PSS by chemical reduction combined with a novel method for its transfer using free-standing thin films. *J. Mater. Chem. C*, 2(7), pp.1278–1283.
49. Rincón-García, L., Ismael, A.K., Evangeli, C., Grace, I., Rubio-Bollinger, G., Porfyraakis, K., Agraït, N. and Lambert, C.J. (2015). Molecular design and control of fullerene-based bi-thermoelectric materials. *Nature Materials*, 15(3), pp.289–293.
50. Algharagholy, L.A.A., Pope, T. and Lambert, C.J. (2018). Strain-induced bi-thermoelectricity in tapered carbon nanotubes. *Journal of Physics: Condensed Matter*, 30(10), p.105304.
51. La Rosa, A., Gillemot, K., Leary, E., Evangeli, C., González, M.T., Filippone, S., Rubio-Bollinger, G., Agraït, N., Lambert, C.J. and Martín, N. (2014). Does a Cyclopropane Ring Enhance the Electronic Communication in Dumbbell-Type C60 Dimers? *The Journal of Organic Chemistry*, 79(11), pp.4871–4877.

52. Sangtarash, S., Sadeghi, H. and Lambert, C.J. (2018). Connectivity-driven bi-thermoelectricity in heteroatom-substituted molecular junctions. *Physical Chemistry Chemical Physics*, 20(14), pp.9630–9637.
53. Lambert, C.J., Bailey, S.W.D. and Cserti, J. (2008). Oscillating chiral currents in nanotubes: A route to nanoscale magnetic test tubes. *Physical Review B*, 78(23).
54. Wu, Q., Sadeghi, H., García-Suárez, V.M., Ferrer, J. and Lambert, C.J. (2017). Thermoelectricity in vertical graphene-C60-graphene architectures. *Scientific Reports*, 7(1).
55. Jia, C., Famili, M., Carlotti, M., Liu, Y., Wang, P., Grace, I.M., Feng, Z., Wang, Y., Zhao, Z., Ding, M., Xu, X., Wang, C., Lee, S.-J., Huang, Y., Chiechi, R.C., Lambert, C.J. and Duan, X. (2018). Quantum interference mediated vertical molecular tunneling transistors. *Science Advances*, 4(10).
56. Famili, M., Jia, C., Liu, X., Wang, P., Grace, I.M., Guo, J., Liu, Y., Feng, Z., Wang, Y., Zhao, Z., Decurtins, S., Häner, R., Huang, Y., Liu, S.-X., Lambert, C.J. and Duan, X. (2019). Self-Assembled Molecular-Electronic Films Controlled by Room Temperature Quantum Interference. *Chem*, 5(2), pp.474–484.
57. Wang, X., Bennett, T.L.R., Ismael, A., Wilkinson, L.A., Hamill, J., White, A.J.P., Grace, I.M., Kolosov, O.V., Albrecht, T., Robinson, B.J., Long, N.J., Cohen, L.F. and Lambert, C.J. (2020). Scale-Up of Room-Temperature Constructive Quantum Interference from Single Molecules to Self-Assembled Molecular-Electronic Films. *Journal of the American Chemical Society*, 142(19), pp.8555–8560.
58. Hohenberg, P. and Kohn, W. (1964). Inhomogeneous Electron Gas. *Physical Review*, 136(3B), pp.B864–B871.
59. Kohn, W. and Sham, L.J. (1965). Self-Consistent Equations Including Exchange and Correlation Effects. *Physical Review*, 140(4A), pp.A1133–A1138.

60. Self-interaction correction to density-functional approximations for many-electron systems. J.P. Perdew, J. P. and A. Zunger, *Physical Review B*, 23(10), 5048. (1981).
61. Perdew, J.P., Burke, K. and Ernzerhof, M. (1996). Generalized Gradient Approximation Made Simple. *Physical Review Letters*, 77(18), pp.3865–3868.
62. Fang, G., Chang, X., Zhang, P., Diao, Y., Hinson, K. and Sun, Y. (2002). The SIESTA method for ab initio order-N materials simulation. *Journal of Physics: Condensed Matter*.
63. Davidson, R., Ismael, A. and Lambert, C., 2018. Conductance of ‘bare-bones’ tripod molecular wires. *RSC Advances*, 8(42), pp.23585-23590.
64. González, M., Ismael, A., Grace, I. and Lambert, C., 2021. Interference Controls Conductance in Phthalocyanine Molecular Junctions. *The Journal of Physical Chemistry C*, 125(27), pp.15035-15043.
65. Ismael, A. and Lambert, C., 2019. Single-molecule conductance oscillations in alkane rings. *Journal of Materials Chemistry C*, 7(22), pp.6578-6581.
66. Ismael, A., Alshehab, A., Grace, I. and Lambert, C., 2021. Correction: Molecular-scale thermoelectricity: as simple as ‘ABC’. *Nanoscale Advances*, 3(2), pp.619-619.
67. Ismael, A., Grace, I. and Lambert, C., 2017. Discriminating single-molecule sensing by crown-ether-based molecular junctions. *The Journal of Chemical Physics*, 146(6), p.064704.
68. Ismael, A., Nichols, R. and Lambert, C., 2019. Single molecule vs. large area design of molecular electronic devices incorporating an efficient 2-aminepyridine double anchoring group. *Nanoscale*, 11(34), pp.15871-15880.

69. Markin, A., Ismael, A., Davidson, R. and Lambert, C., 2020. Conductance Behavior of Tetraphenyl-Aza-BODIPYs. *The Journal of Physical Chemistry C*, 124(12), pp.6479-6485.
70. Naghibi, S., Ismael, A., Grace, I., Lambert, C. and Nichols, R., 2019. Synthetic Control of Quantum Interference by Regulating Charge on a Single Atom in Heteroaromatic Molecular Junctions. *The Journal of Physical Chemistry Letters*, 10(20), pp.6419-6424.
71. Wang, X., Ismael, A., Alshehab, A. and Lambert, C., 2021. Optimised power harvesting by controlling the pressure applied to molecular junctions. *Chemical Science*, 12(14), pp.5230-5235.
72. Wilkinson, L., Grace, I., Ismael, A. and Lambert, C., 2022. Assembly, structure and thermoelectric properties of 1,1'-dialkynylferrocene 'hinges'. *Chemical Science*, 13(28), pp.8380-8387.
73. Gantenbein, M., Ismael, A. and Lambert, C., 2017. Quantum interference and heteroaromaticity of para- and meta-linked bridged biphenyl units in single molecular conductance measurements. *Scientific Reports*, 7(1).
74. Herrer, I., Ismael, A., Grace, I., Lambert, C. and Nichols, R., 2018. Unconventional Single-Molecule Conductance Behavior for a New Heterocyclic Anchoring Group: Pyrazolyl. *The Journal of Physical Chemistry Letters*, 9(18), pp.5364-5372.
75. Ismael, A., Chen, Z., Lambert, C., Hong, W. and Zhang, Q., 2022. Highly Insulating Alkane Rings with Destructive  $\sigma$ -Interference. *Science China Chemistry*, 65.

76. Ismael, A., Grace, I. and Lambert, C., 2017. Connectivity dependence of Fano resonances in single molecules. *Physical Chemistry Chemical Physics*, 19(9), pp.6416-6421.
77. Bennett, T., Ismael, A. and Lambert, C., 2022. Multi-component self-assembled molecular-electronic films: towards new high-performance thermoelectric systems. *Chemical Science*, 13(18), pp.5176-5185.
78. Ismael, A. and Lambert, C., 2020. Molecular-scale thermoelectricity: a worst-case scenario. *Nanoscale Horizons*, 5(7), pp.1073-1080.
79. Ismael, A., Agraït, N. and Lambert, C., 2022. Exploring seebeck-coefficient fluctuations in endohedral-fullerene, single-molecule junctions. *Nanoscale Horizons*, 7(6), pp.616-625.
80. Ismael, A., Bennett, T., Wilkinson, L. and Lambert, C., 2020. Tuning the thermoelectrical properties of anthracene-based self-assembled monolayers. *Chemical Science*, 11(26), pp.6836-6841.
81. Ismael, A., Grace, I. and Lambert, C., 2018. Oscillating Seebeck coefficients in  $\pi$ -stacked molecular junctions. *RSC Advances*, 8(44), pp.24711-24715.
82. Ismael, A., Grace, I. and Lambert, C., 2015. Increasing the thermopower of crown-ether-bridged anthraquinones. *Nanoscale*, 7(41), pp.17338-17342.



## Chapter 2

### Density Functional Theory

This chapter introduces the density functional theory (DFT) formalism as well as the SIESTA DFT code, which is employed in all of the electronic structure computations in this thesis.

The initial step in determining the molecule's electron transport characteristics is to use DFT to obtain a mean-field Hamiltonian. However, since the Hamiltonian only pertains to the isolated molecule, it must still be linked to semi-infinite leads to form a molecular junction, as described in the next chapter.

#### 2.1 Introduction

It is necessary to have a reliable source of structural and electronic information in order to describe the behaviour of molecular electronic devices. In this chapter, I will give a brief summary of density functional theory (DFT) and the SIESTA (Spanish Initiative for Electronic Simulations with Thousands of Atoms) code [6], which I utilised extensively during my PhD studies as a theoretical tool for investigating both qualitatively and quantitatively the architectures of molecules, charge densities, and band structures. SIESTA is a collection of algorithms and a fully integrated software programme for performing DFT calculations on a large number of atoms (1000) in a matter of hours, days, or weeks. The fundamental principle of DFT is that every physical attribute of a complex system composed of several interacting particles can be represented as a function of the system's ground state density. The proof of the existence of such a functional was first presented by Hohenberg and Kohn [4] in 1964. However, the proof does not provide us any information on the shape of the functional. However, an ansatz proposed by Kohn and Sham [7] opened the door to applications for realistic physical systems. Since then, DFT has been a common tool in theoretical physics and

molecular chemistry. This chapter will give an overview of the principles of DFT and all of its numerical applications. The literature is quite broad and deals with the subject with considerably more detail [1-3,8]. I will begin by outlining the several alternative approaches to the many body issue, and then I will demonstrate the Hartree-Fock technique and the Hohenberg-Kohn theorems, followed by a demonstration of the Kohn-Sham ansatz. Next, I distil the most often used functional forms, which are critical in applied numerical analysis. I also focus on localised base sets, pseudo-atomic orbits defining the number space of the Hilbert computations in this thesis, and Basis Set Superposition Error Correction (BSSE) and Counterpoise Correction (CP).

## 2.2 The Schrödinger Equation and Variational Principle

The Schrödinger equation, which is time independent and non-relativistic, may be used to describe any non-relativistic multi-particle system:

$$\begin{aligned} H\psi_i(\vec{r}_1, \vec{r}_2, \dots, \vec{r}_N, \vec{R}_1, \vec{R}_2, \dots, \vec{R}_M) \\ = E_i\psi_i(\vec{r}_1, \vec{r}_2, \dots, \vec{r}_N, \vec{R}_1, \vec{R}_2, \dots, \vec{R}_M) \end{aligned} \quad (2.1)$$

In the above equation  $\psi_i$  is the wavefunction of the  $i^{th}$  molecular orbital of the system,  $r_i$  is the position of  $i$ -th electron,  $R_i$  is the position of  $i$ -th nucleus,  $E_i$  is the energy of the state and  $H$  is the Hamiltonian operator of a system consisting of  $N$ -electrons and  $M$ -nuclei that contains the interaction of particles with each other. The Hamiltonian operator of such a system can be written as a sum of five terms given by [4, 5, 7, 11, 13, 40, 41].

$$\begin{aligned}
H = & \overbrace{-\frac{\hbar^2}{2m_e} \sum_{i=1}^N \nabla_i^2}^{T_e} - \overbrace{\frac{\hbar^2}{2m_n} \sum_{n=1}^M \nabla_n^2}^{T_n} - \overbrace{\frac{1}{4\pi\epsilon_0} \sum_{i=1}^N \sum_{n=1}^M \frac{1}{|\vec{r}_i - \vec{R}_n|} Z_n e^2}^{U_{en}} \\
& + \overbrace{\frac{1}{8\pi\epsilon_0} \sum_{i=1}^N \sum_{i \neq j}^N \frac{e^2}{|\vec{r}_i - \vec{r}_j|}}^{U_{ee}} + \overbrace{\frac{1}{8\pi\epsilon_0} \sum_{n=1}^M \sum_{n \neq n'}^M \frac{1}{|\vec{R}_n - \vec{R}_{n'}|} Z_n Z_{n'} e^2}^{U_{nn}}
\end{aligned} \tag{2.2}$$

Where  $i$  and  $j$  denote the N-electrons while  $n$  and  $n'$  run over the M-nuclei in the system,  $m_e$  and  $m_n$  are the mass of electron and nucleus respectively,  $e$  and  $Z_e$  are the electron and nuclear charge respectively. The position of the electrons and nuclei are denoted as  $\vec{r}_i$  and  $\vec{R}_n$  respectively, and  $\nabla^2$  is the Laplacian operator, in Cartesian coordinates is defined as

$$\nabla_i^2 = \frac{\partial^2}{\partial x_i^2} + \frac{\partial^2}{\partial y_i^2} + \frac{\partial^2}{\partial z_i^2}$$

According to equation (2.2), the terms,  $T_e$  is the kinetic energy of electrons, while  $T_n$  is denoted as kinetic energy of nuclei in the system. Additionally, the last three terms describe the potential part of the Hamiltonian; the term  $U_{en}$  represents the attractive electrostatic interaction between nuclei and electrons in the system. The electron-electron ( $U_{ee}$ ) and nuclear-nuclear ( $U_{nn}$ ) are the repulsive part of the potential respectively [1, 6, 7, 11, 40]

We can separate the Hamiltonian (Equation 2.2) into two parts. The first part contains the kinetic terms of the nuclei and the repulsive electrostatic potential between the nuclei and the attractive potential felt by the electrons due to the positively charged nuclei. This part is system specific and will determine the geometric properties of the physical problem. The second part of the Hamiltonian contains terms which only depend on the electrons. This part

is universal in all problems. Hence, we can rewrite the Hamiltonian for the electronic degrees of freedom as:

$$H = \overbrace{\sum_i V_{ext}(r_i)}^{\text{nuclei-electron interaction}} - \overbrace{\frac{\hbar^2}{2m_n} \sum_i \nabla_i^2}^{\text{kinetic term}} + \overbrace{\frac{1}{8\pi\epsilon_0} \sum_{i \neq j} \frac{e^2}{|\vec{r}_i - \vec{r}_j|}}^{\text{electron-electron interaction}} \quad (2.3)$$

Where  $V_{ext}$  contains the system-specific nuclei terms from Eq. 2.2. Working with Hartree atomic units are convenient. This means that in the following, we adopt the convention that the length scale is set by the hydrogen atom's Bohr radius,  $a_0$ , the energy scale is set by the hydrogen atom's ground state, the mass scale is set by the electron mass,  $m_e$ , the charge scale is set by the electron's elementary charge,  $e$ , the angular momentum scale is set by the reduced Planck's constant,  $\hbar$ , and the electric force scale is set by  $\frac{1}{4\pi\epsilon_0}$ .

We can compute any physical quantities we are interested in after solving the Schrödinger equation 2.1 and obtaining the wave function,  $\psi$ . However, even on a contemporary supercomputer, diagonalization of the general issue is essentially unfeasible for small system sizes—merely a handful of atoms.

In fact, solving the full Hamiltonian represented by (2.2) is impossible for a system consisting of a large number of electrons and nucleons except the hydrogen atom. Therefore, we should find some mathematical approximations to reduce the degree of freedom of a system. One of the important approximations is Born-Oppenheimer approximation that will be discussing in detail in the following section.

### 2.3 Born-Oppenheimer approximation

We know already the solution of Schrödinger equation represented in 2.1 with Hamiltonian shown in 2.2 is a wavefunction of all the electrons and nucleons. Since we know finding this wavefunction for a complicated system is impossible. Born and Oppenheimer, however, have

shown it is possible to get that wavefunction as solution of many-body Hamiltonian 2.2 by dividing the Hamiltonian into independent effective electron and nucleon parts which can be solved independently. Since we know that the mass of nucleons is about 2000 times larger than mass of electrons. Therefore, relaxation of the electrons is faster than the nucleons into their ground states. So, we can consider nucleons as fixed within the relaxation time of the electrons. Moreover, the wavefunctions of nucleons could be assumed to be independent of the electron's positions. In this case, we can write the solution of 2.1 could be written as the product of an independent nucleon wavefunction  $\chi$  and an electron wavefunction  $\phi$

$$\psi(r_i, R_I) = \chi(R_I) \phi(r_i, R_I) \quad (2.4)$$

By compensating 2.5 and 2.3 in 2.1

$$\begin{aligned} & \chi(R_I) \sum_{i=1}^N \left( -\frac{\hbar^2}{2m_i} \nabla_i^2 \right) \phi(r_i, R_I) + \sum_{I=1}^M \left( -\frac{\hbar^2}{2M_I} \nabla_I^2 \right) \chi(R_I) \phi(r_i, R_I) + \\ & \chi(R_I) \frac{1}{4\pi\epsilon_0} \frac{1}{2} \sum_{i \neq j}^N \frac{e^2}{|r_i - r_j|} \phi(r_i, R_I) + \frac{1}{4\pi\epsilon_0} \frac{1}{2} \sum_{I \neq J}^M \frac{e^2 Z_I Z_J}{|R_I - R_J|} \chi(R_I) \phi(r_i, R_I) - \\ & \frac{1}{4\pi\epsilon_0} \sum_{iI=1}^{NM} \frac{e^2 Z_I}{|r_i - R_I|} \chi(R_I) \phi(r_i, R_I) = E \chi(R_I) \phi(r_i, R_I) \end{aligned} \quad (2.5)$$

The second term in 2.6 can be expanded using the product rule of a differential operator

$$\nabla_I^2 [\chi(R_I) \phi(r_i, R_I)] = \chi(R_I) \nabla_I^2 \phi(r_i, R_I) + 2 \nabla_I \chi(R_I) \nabla_I \phi(r_i, R_I) + \phi(r_i, R_I) \nabla_I^2 \chi(R_I) \quad (2.6)$$

From the equation 2.7, we see that the first term, the variation of the electronic wavefunction as a function of the nucleon position, equals zero due to the nucleons are considered to be stationary within the relaxation time of the electrons. For the second term, it is the electron-phonon interaction which can be zero if we assume that we have a low temperature. Of course, we have only one term in the equation 2.7. By substituting 2.7, only one term, in the full Schrödinger equation 2.6.

If we are going to introduce a new term, an effective Hamiltonian  $H_e$  that describes only the electron's motion by assuming the nuclei are stationary.

$$H_e = \sum_{i=1}^N \left( -\frac{\hbar^2}{2m_i} \nabla_i^2 \right) + \frac{1}{4\pi\epsilon_0} \frac{1}{2} \sum_{i \neq j}^N \frac{e^2}{|r_i - r_j|} - \frac{1}{4\pi\epsilon_0} \sum_{il=1}^{NM} \frac{e^2 Z_I}{|r_i - R_J|} \quad (2.7)$$

$$\{H_e \phi(r_i, R_I) + \sum_{I=1}^M \phi(r_i, R_I) \left( -\frac{\hbar^2}{2M_I} \nabla_I^2 \right) + \frac{1}{4\pi\epsilon_0} \frac{1}{2} \sum_{I \neq J}^M \frac{e^2 Z_I Z_J}{|R_I - R_J|} \phi(r_i, R_I) \} \chi(R_I) = E \chi(R_I) \phi(r_i, R_I) \quad (2.8)$$

And an effective Schrödinger equation could be written as following

$$H_e \phi = E_e \phi \quad (2.9)$$

Similarly, we introduce the nucleon Hamiltonian  $H_N$  that has only kinetic and interaction terms of the nucleon

$$H_N = \sum_{I=1}^M \left( -\frac{\hbar^2}{2M_I} \nabla_I^2 \right) - \frac{1}{4\pi\epsilon_0} \frac{1}{2} \sum_{I \neq J}^M \frac{e^2 Z_I Z_J}{|R_I - R_J|} \quad (2.10)$$

And a nucleon Schrödinger equation could be written as following

$$H_N \chi = E_N \chi \quad (2.11)$$

The total energy of the system is simply the sum of the two energies

$$E = E_e + E_N \quad (2.12)$$

It is clear that the Born-Oppenheimer approximation allows to us to separate the full Hamiltonian of the system which has M nuclei and N electrons into two Hamiltonian, the effective(electron)Hamiltonian represented by the equation 2.8 and the nucleon Hamiltonian shown in the equation 2.11. By using the DFT, we solve first the electron Hamiltonian, after that we deal the nucleon Hamiltonian as equation of motion classically. Right now, I am going to show some methods and approximations mathematically how to use the DFT to calculate the electron (effective) Hamiltonian.

## 2.4 The Hohenberg-Kohn Theorems

P. Hohenberg and W. Kohn demonstrated in 1964 [4] that there is a relationship between the ground state energy and the density,  $\rho(r)$ , of an interacting electron system. The Hohenberg-Kohn theorems are two simple but strong statements:

a) The external potential,  $V_{ext}$ , is a density-specific functional ( $r$ ). Given that  $V_{ext}$  fixes the system's Hamiltonian,  $H$ , it is obvious that the complete many-body ground state is a unique functional of  $\rho(r)$ .

b) The ground state,  $E_{HK}$ , is a ground state density  $\rho(r)$ .

It is a straightforward matter of reduction ad absurdum to demonstrate the validity of the first theorem presented above. Assume we have two external potentials,  $V_{ext}^1$  and  $V_{ext}^2$ , that vary by a constant. Assume that the two external potentials provide the same ground-state density  $\rho(r)$ . Each system's Hamiltonians are designated by  $H^{(1)}$  and  $H^{(2)}$  and, since they vary, they will have distinct ground-state wavefunctions,  $\psi^{(1)}$  and  $\psi^{(2)}$ . We have  $\psi^{(2)}$  since it is not a ground state of  $H^{(1)}$ , we have:

$$E^{(1)} = \langle \psi^{(1)} | H^{(1)} | \psi^{(1)} \rangle \langle \psi^{(2)} | H^{(1)} | \psi^{(2)} \rangle \quad (2.13)$$

Similarly:

$$E^{(2)} = \langle \psi^{(2)} | H^{(2)} | \psi^{(2)} \rangle \langle \psi^{(1)} | H^{(1)} | \psi^{(1)} \rangle \quad (2.14)$$

The simplified assumption is that our ground states are non-degenerate. The problem has been

formulated to incorporate degeneracies in the literature [13, 42]. We can rewrite equation 2.15:

$$\begin{aligned}\langle \psi^{(2)} | H^{(1)} | \psi^{(2)} \rangle &= \langle \psi | H^{(2)} | \psi^{(2)} \rangle \langle \psi^{(2)} | H^{(1)} - H^{(2)} | \psi^{(2)} \rangle \\ &= E^{(2)} + \int dr \left( V_{ext}^{(1)}(r) - V_{ext}^{(2)}(r) \right) \rho_o(r)\end{aligned}\tag{2.15}$$

Also, equation 2.16:

$$\langle \psi^{(2)} | H^{(1)} | \psi^{(2)} \rangle = E^{(2)} + \int dr \left( V_{ext}^{(1)}(r) - V_{ext}^{(2)}(r) \right) \rho_o(r)\tag{2.16}$$

When we combine equations 2.16 and 2.17, we get the following contradiction:

$$E^{(1)} + E^{(2)} < E^{(1)} + E^{(2)}$$

Two or more potentials may vary by no more than a constant and can produce the same ground-state density, hence it is impossible for there to be two such potentials.

The second theorem is just as easy to prove as the first. Consider the following equation for the system's total energy,  $E$ :

$$E(\rho) = T(\rho) + E_{int}(\rho) + \int dr V_{ext}(\rho)(r)\tag{2.17}$$

The kinetic term,  $T$  and internal interaction of the electrons,  $E_{int}$ , are, by definition, universal.

Consider a system with a ground-state density of  $\rho_o$ , an external potential of  $V_{ext}$ , and a wavefunction of  $\psi_o$ . According to the first theorem,  $\rho_o$  determines the Hamiltonian, therefore for any density and wave function,  $\psi$ , other than the ground state, we get:



$$E_o = \langle \psi_0 | H | \psi_0 \rangle < \langle \psi | H | \psi \rangle = E \quad (2.18)$$

This reduces the functional density of the ground,  $\rho_o$ , equation 2.19. As a result, if we know the functional:  $T(\rho) + E_{int}(\rho)$ , we can extract the ground-state of the system and compute all ground-state attributes by minimising equation 2.19.

## 2.5 The Kohn-Sham Theorems

We have already shown that by acquiring the ground-state density, we can calculate the ground-state energy, and it is theoretically possible to compute the ground-state energy by getting the ground-state density. The precise form of the functional indicated in equation 2.10, however, is unknown. The kinetic term as well as the internal energy of the interacting electrons cannot be represented as a function of density in general. The solution was introduced by Kohn and Sham in 1965 [7].

The original Hamiltonian can be substituted, according to Kohn and Sham, with an effective Hamiltonian of non-interacting particles, with a real external potential having the same ground-state density as the original system. Because this is not a defined recipe, it is merely an ansatz, but a non-interacting problem is far easier to resolve. Contrary to equation 2.10, the functional energy of the ansatz Kohn-Sham will have the formula:

$$E_{KS}(\rho) = T_{KS}(\rho) + \int dr V_{ext}(r) \rho(r) + E_H(\rho) + E_{xc}(\rho) \quad (2.19)$$

$T_{KS}$  is the non-interacting system's kinetic energy. The kinetic energy of the interacting system was employed in equation 2.19.  $T$  the distinction is known as the exchange correlation functional,  $E_{xc}$ , equation 2.22.

The Hartree functional,  $E_H$ , represents the electron-electron interaction using the Hartree-Fock method and has the following form:

$$E_H(\rho) = \frac{1}{2} \int \frac{\rho(r)\rho(r')}{|r - r'|} dr dr' \quad (2.20)$$

This is a roughly  $E_{int}$  version, as previously defined. Again,  $E_{xc}$  refers to the difference. As a result, the exchange correlation functional,  $E_{xc}$ , represents the difference between the exact and approximation solutions to the kinetic energy term and the electron-electron interaction term. Its definition is as follows:

$$E_{xc}(\rho) = (E_{int}(\rho) - E_H(\rho)) + (T(\rho) - T_{KS}(\rho)) \quad (2.21)$$

In practice, the first three functionals of equation 2.22 are easily defined and account for the majority of the contribution to ground-state energy. In comparison, the exchange correlation functional makes a minor contribution. Despite decades of investigation, there is no exact remedy. The next part discusses several excellent approximations that have been developed.

## 2.6 The Exchange Correlation Functionals

Several modifications on the exchange and correlation energy have been published in the literature. The first successful form was the Local Density Approximation (LDA) [29, 30], That depends on the density only, and hence is functional locally. Then the next step was the Generalized Gradient Approximation (GGA) [18-21], Including the density derivative, it also includes neighbourhood information and is thus semi-local. One of the most commonly used approximations in density functional theory is LDA and GGA.

LDA and GGA can't be considered the only possible functionals. Some of these functionals are tailored to fit specific needs of basis sets used in solving the Kohn-Sham equations, equation 2.12 and a large category is the so-called hybrid functionals (e.g. B3LYP [43], HSE [35] and Meta hybrid GGA [34, 36]), which combine the LDA and GGA forms.

One of the most recent and universal features, the Van der Waals density functional (vdW-DF) [37], contains non-local terms and has proven to be very accurate in systems where dispersion forces are important [38, 39].

Following sections will provide a brief introduction to the Local Density Approximation and the Generalized Gradient Approximation.

### **2.6.1 Local Density Approximation (LDA)**

The exchange correlation functional in LDA simply depends on the local density. This approximation can be expected to produce satisfactory results for systems where the density does not change too rapidly.

In some ways, the LDA is the most basic representation of the exchange and correlation energy. It is a basic yet powerful functional, and it is known to be correct for graphene and carbon nanotubes, as well as where the electron density is not changing rapidly. For example, for atoms that have d and f-type orbits, a bigger inaccuracy is expected. But LDA has numerous drawbacks: the band gap in semiconductors and insulators is sometimes underestimated with a significant inaccuracy, for example. So, it is advisable to try to improve the functionality.

### **2.6.2 Generalized Gradient Approximation (GGA)**

When derivatives are included in the functional form of the exchange and correlation energies the GGA is obtained. In this condition there is no closed form for the functional exchange, so analytical solutions have to have been used to calculate the correspondence contributions. Just

as in the case of the LDA there exist many parameterizations for the exchange and correlation energies in GG [17- 20].

For the approximation of exchange-correlation energies in the DFT, LDA and GGA are two of the most widely utilized approximations. Several functionalities, beyond LDA and GGA, are also provided. Tests are performed on diverse materials to test functional properties for a wide range of systems and then statistical comparisons are performed to establish valid data.

## **2.7 Pseudopotentials**

I have demonstrated how to transform a huge interacting problem into an effective non-interacting problem using the Kohn Sham formalism and an exchange-correlation functional. This greatly simplifies the situation from a physical point of view. When molecules with a significant number of atoms are involved, however, the calculation becomes too massive and computationally intensive to use. By introducing pseudopotentials, the number of core electrons in an atom can be reduced. Pseudopotentials were first introduced by Fermi in 1934 [14, 15] and since then methods have evolved from creating not so realistic empirical pseudopotentials [16, 22] to more realistic ab-initio pseudopotentials [24, 27].

Electrons can be classified into two types: core and valence. Valence electrons occupy the outermost shells of an atom while core electrons are those occupying the innermost shells. As long as core electrons are restricted around the nucleus, the only valence electron states overlap when atoms are brought together. This makes it possible to remove the core electron and replace it with a pseudopotential that allows the valence electrons to still be screened as if the core electrons are still present. This dramatically lowers the number of electrons in a system and reduces the time and stored properties of molecules that contain a significant number of electrons.

## **2.8 SIESTA**

For the purpose of this thesis, all DFT calculations were performed using the SIESTA (Spanish Initiative for Electronic Simulations) package. It is used for obtaining the relaxed geometry of the given structures as well as to perform calculations to explore their electronic characteristics. SIESTA is a self-consistent density functional theory code that enables efficient calculations to be performed using norm-conserving pseudo-potentials and linear combination of atomic orbital (LCAO) basis sets [46]. Additional theoretical information regarding the SIESTA code and what it enables can be found in [47, 48]. DFT simulations can be performed in two distinct modes, namely a standard self-consistent field diagonalisation technique used for solving the Kohn-Sham equations and a second technique in which a modified energy functional is directly minimised [49]. The following sections will present a description of specific components of SIESTA as well the process by which they are implemented in the code.

## **2.9 Conclusion**

In summary, density functional theory (DFT), as a method for solving the Schrödinger equation has been reviewed, and the Hohenberg-Kohn theorems and the Kohn-Sham ansatz have been explained. In addition, the functional forms of the exchange and correlation energy in the local density approximation and the generalized gradient approximation are illustrated. Finally, the SIESTA code was introduced, along with some fine details of the calculations, such as the use of pseudopotentials.

## Bibliography

1. Gross, E. K., Runge, E., and Heinonen, O. H (1991). Many Particle Theory. Taylor & Francis (1991).
2. Probert, M. (2011). Electronic Structure: Basic Theory and Practical Methods, by Richard M. Martin: Scope: graduate level textbook. Level: theoretical materials scientists/condensed matter physicists/computational chemists.
3. Gross, E.K. and R.M. Dreizler. (1995). *Density functional theory*. Vol. 337: Springer.
4. Hohenberg, P., and Kohn, W. (1964). Inhomogeneous electron gas. *Physical review*, 136(3B), B864.
5. Born, M., and Oppenheimer, R. (1927). On the quantum theory of molecules. *Annalen der Physik*, 84:20.
6. Soler, J. M., Artacho, E., Gale, J. D., García, A., Junquera, J., Ordejón, P., and Sánchez-Portal, D. (2002). The SIESTA method for ab initio order-N materials simulation. *Journal of Physics: Condensed Matter*, 14(11), 2745.
7. Kohn, W., and Sham, L. J. (1965). Self-consistent equations including exchange and correlation effects. *Physical review*, 140(4A), A1133.
8. Parr, R. G., and Weitao, Y. (1989). Chemical potential derivatives. In *Density-Functional Theory of Atoms and Molecules*. Oxford University Press.
9. Boys, S. F., and Bernardi, F. J. M. P. (1970). The calculation of small molecular interactions by the differences of separate total energies. Some procedures with reduced errors. *Molecular Physics*, 19(4), 553-566.
10. Haynes, P. D., Skylaris, C. K., Mostofi, A. A., and Payne, M. C. (2006). Elimination of basis set superposition error in linear-scaling density-functional calculations with local orbitals optimised in situ. *Chemical physics letters*, 422(4-6), 345-349.

11. Levy, M., and Perdew, J. P. (1985). The constrained search formulation of density functional theory. In *Density functional methods in physics* (pp. 11-30). Springer, Boston, MA.
12. Levy, M. (1979). Universal variational functionals of electron densities, first-order density matrices, and natural spin-orbitals and solution of the v-representability problem. *Proceedings of the National Academy of Sciences*, 76(12), 6062-6065.
13. Levy, M. (1982). Electron densities in search of Hamiltonians. *Physical Review A*, 26(3), 1200.
14. Fermi, E. (1934). Sopra lo spostamento per pressione delle righe elevate delle serie spettrali. *Il Nuovo Cimento (1924-1942)*, 11(3), 157-166.
15. Fermi, E. (1936). Motion of neutrons in hydrogenous substances. *Ricerca Scientifica*, 7(2), 13-52.
16. Animalu, A. O. E., and Heine, V. (1965). The screened model potential for 25 elements. *Philosophical Magazine*, 12(120), 1249-1270.
17. Boese, A. D., Jansen, G., Torheyden, M., Höfener, S., and Klopper, W. (2011). Effects of counterpoise correction and basis set extrapolation on the MP2 geometries of hydrogen bonded dimers of ammonia, water, and hydrogen fluoride. *Physical Chemistry Chemical Physics*, 13(3), 1230-1238.
18. Becke, A. D. (1988). Density-functional exchange-energy approximation with correct asymptotic behavior. *Physical review A*, 38(6), 3098.
19. Hammer, B. H. L. B., Hansen, L. B., and Norskov, J. K. (1999). Improved adsorption energetics within density-functional theory using revised Perdew-Burke-Ernzerhof functionals. *Physical review B*, 59(11), 7413.

20. Perdew, J. P., Burke, K., and Ernzerhof, M. (1996). Generalized gradient approximation made simple. *Physical review letters*, 77(18), 3865.
21. Perdew, J. P., and Wang, Y. (1992). Accurate and simple analytic representation of the electron-gas correlation energy. *Physical review B*, 45(23), 13244.
22. Ashcroft, N. W. (1966). Electron-ion pseudopotentials in metals. *Physics Letters*, 23(1), 48-50.
23. Lieb, E. H. (1982). Density functionals for coulomb systems. Physics as Natural Philosophy: Essays in Honor of Laszlo Tisza on His 75th Birthday. A. Shimony and H. Feshbach (MIT, Cambridge, MA), 111.
24. Lieb, E. H. (1982). Density functionals for coulomb systems. Physics as Natural Philosophy: Essays in Honor of Laszlo Tisza on His 75th Birthday. A. Shimony and H. Feshbach (MIT, Cambridge, MA), 111.
25. Zunger, A., and Cohen, M. L. (1978). First-principles nonlocal-pseudopotential approach in the density-functional formalism: Development and application to atoms. *Physical Review B*, 18(10), 5449.
26. Zunger, A., and Cohen, M. L. (1978). First-principles nonlocal-pseudopotential approach in the density-functional formalism: Development and application to atoms. *Physical Review B*, 18(10), 5449.
27. Hamann, D. R., Schlüter, M., and Chiang, C. (1979). Norm-conserving pseudopotentials. *Physical Review Letters*, 43(20), 1494.
28. Bachelet, G. B., and Schlüter, M. (1982). Relativistic norm-conserving pseudopotentials. *Physical Review B*, 25(4), 2103.
29. Ceperley, D. M., and Alder, B. J. (1980). Ground state of the electron gas by a stochastic method. *Physical review letters*, 45(7), 566.



30. Langreth, D. C., and Perdew, J. P. (1977). Exchange-correlation energy of a metallic surface: Wave-vector analysis. *Physical Review B*, 15(6), 2884.
31. Senent, M. L., and Wilson, S. (2001). Intramolecular basis set superposition errors. *International journal of quantum chemistry*, 82(6), 282-292.
32. Mierzwicki, K., and Latajka, Z. (2003). Basis set superposition error in N-body clusters. *Chemical physics letters*, 380(5-6), 654-664.
33. Sankey, O. F., and Niklewski, D. J. (1989). Ab initio multicenter tight-binding model for molecular-dynamics simulations and other applications in covalent systems. *Physical Review B*, 40(6), 3979.
34. Zhao, Y., and Truhlar, D. G. (2008). The M06 suite of density functionals for main group thermochemistry, thermochemical kinetics, noncovalent interactions, excited states, and transition elements: two new functionals and systematic testing of four M06-class functionals and 12 other functionals. *Theoretical chemistry accounts*, 120(1), 215-241.
35. Heyd, J., Scuseria, G. E., and Ernzerhof, M. (2003). Hybrid functionals based on a screened Coulomb potential. *The Journal of chemical physics*, 118(18), 8207-8215.
36. Zhao, Y., and Truhlar, D. G. (2011). Applications and validations of the Minnesota density functionals. *Chemical Physics Letters*, 502(1-3), 1-13.
37. Dion, M., Rydberg, H., Schröder, E., Langreth, D. C., and Lundqvist, B. I. (2004). Van der Waals density functional for general geometries. *Physical review letters*, 92(24), 246401.
38. Klimeš, J., Bowler, D. R., and Michaelides, A. (2011). Van der Waals density functionals applied to solids. *Physical Review B*, 83(19), 195131.
39. Visontai, D. (2011). Quantum and Classical Dynamics of Molecule Size Systems. *Physics Department 2013, Lancaster University*.

40. Martin, R. M. (2020). *Electronic structure: basic theory and practical methods*. Cambridge university press.
41. Griffiths, D. J. (2005). *Introduction to quantum mechanics*. Pearson Prentice Hall.
42. Levy, M. (1985). Density Functional Methods in Physics. *The inhomogeneous electron gas*, 32-94.
43. Lee, C., Yang, W., and Parr, R. G. (1988). Development of the Colle-Salvetti correlation-energy formula into a functional of the electron density. *Physical review B*, 37(2), 785.
44. Ceperley, D. M., and Alder, B. J. (1980). Ground state of the electron gas by a stochastic method. *Physical review letters*, 45(7), 566.
45. Daza, M. C., Dobado, J. A., Molina, J. M., Salvador, P., Duran, M., and Villaveces, J. L. (1999). Basis set superposition error-counterpoise corrected potential energy surfaces. Application to hydrogen peroxide... X (X= F<sup>-</sup>, Cl<sup>-</sup>, Br<sup>-</sup>, Li<sup>+</sup>, Na<sup>+</sup>) complexes. *The Journal of chemical physics*, 110(24), 11806-11813.
46. Sánchez-Portal, D., Ordejón, P., Artacho, E., & Soler, J. M. (1997). Density-functional method for very large systems with LCAO basis sets. *International journal of quantum chemistry*, 65(5), 453-461.
47. Artacho, E., Cela, J. M., Gale, J. D., Martin, R. M., & Soler, J. M. (2011). SIESTA 3.1. *Fundacion General Universidad Autonoma de Madrid, Madrid*.
48. Ordejón, P., Drabold, D. A., Grumbach, M. P., & Martin, R. M. (1993). Unconstrained minimization approach for electronic computations that scales linearly with system size. *Physical Review B*, 48(19), 14646.
49. Kleinman, L., & Bylander, D. M. (1982). Efficacious form for model pseudopotentials. *Physical Review Letters*, 48(20), 1425.

## Chapter 3

### Theory of Quantum Transpor

Chapter 2 discussed density functional theory, which is a method for determining the electrical structure of an isolated molecule. The next step is to connect this isolated molecule to semi-infinite leads and compute the transmission coefficient across a system. My methodology is based on the Green's function scattering formalism, discussed in this chapter and used throughout the thesis.

By combining scattering theory and Green's functions, we describe the electric and thermoelectric characteristics of nanoscale systems sandwiched between a number of macroscopic sized electrodes.

#### 3.1 Introduction

This chapter begins with a brief overview of the Landauer formula . After that, as an example, I discuss a one-dimensional tight-binding chain, along with its retarded Green's function. Thereafter, I show that the Green's function and Dyson's equation are directly related to the transmission coefficient of scattering region by breaking the periodicity at a single connection. Using these methods, we will calculate the transmission coefficients of mesoscopic conductors having arbitrarily complex geometries. The fundamental assumption underlying this approach, is that the system is described by a time-independent mean-field Hamiltonian and that inelastic scattering within the scattering region is negligible, so that the energy  $E$  of an electron passing through the scattering region is conserved.

### 3.2 Landauer formula and thermoelectric coefficient

Seebeck, Peltier and Thompson developed the relationship between heat, current, temperature and voltage at the turn of the 19<sup>th</sup> century [1]. The Seebeck effect explains the production of electrical current as a result of a temperature difference, while the Thompson and Peltier effects explain the cooling or heating of a current-carrying conductor [2]. A deeper mechanism can be imagined where a temperature difference is  $\Delta T$  and a voltage difference  $\Delta V$  occurs in the system that causes heat and charge fluctuations. For heat ( $Q$ ) and charge ( $I$ ) currents in the linear response regime, the common Landauer-Büttiker formulas can be generalised to determine the thermoelectric coefficients of a device with two terminals. The system is composed of a scattering region that is connected to two leads, which are themselves connected to a pair of electron reservoirs. These left ( $L$ ) and right ( $R$ ) reservoirs are assigned chemical potentials  $\mu_L$  and  $\mu_R$ , temperatures  $T_L$  and  $T_R$ .

The electron current ( $I$ ) and heat current ( $Q$ ) [3-5] caused by electrons can be expressed as follows:

$$I = \frac{2e}{h} \int_{-\infty}^{\infty} dE T(E) [f_L(E) - f_R(E)] \quad (3.1)$$

$$Q = \frac{2}{h} \int_{-\infty}^{\infty} dE (E - E_F) T(E) [f_L(E) - f_R(E)] \quad (3.2)$$

Here,  $T(E)$  is the transmission coefficient,  $f_{L,R}(E)$  is the Fermi –Dirac distribution and takes

this formula  $f_L(E) = \frac{1}{e^{\frac{E-\mu_L}{k_B T}} + 1}$ ,  $f_R(E) = \frac{1}{e^{\frac{E-\mu_R}{k_B T}} + 1}$ , (chemical potential)  $\mu_L = E_F + e V_b/2$

and  $\mu_R = E_F - e V_b/2$ .

In addition,  $T$  is the temperature,  $k_B$  is Boltzmann's constant and  $e$  is the charge of an electron.

Applying Taylor expansion of  $f_{L,R}(\mu, T)$  at  $\mu = E_F, T = \frac{T_L + T_R}{2}$  and in the case of small temperature difference and bias with respect to the first order only.

$$f_L(\mu_L, T_L) = f(E_F, T) + \frac{\partial f(E_F, T)}{\partial \mu} (\mu_L - E_F) + \frac{\partial f(E_F, T)}{\partial T} (T_L - T) \quad (3.3)$$

$$f_R(\mu_R, T_R) = f(E_F, T) + \frac{\partial f(E_F, T)}{\partial \mu} (\mu_R - E_F) + \frac{\partial f(E_F, T)}{\partial T} (T_R - T) \quad (3.4)$$

Using the last two equations

$$f_L - f_R = \frac{\partial f(E_F, T)}{\partial \mu} (\mu_L - \mu_R) + \frac{\partial f(E_F, T)}{\partial T} (T_L - T_R) \quad (3.5)$$

$$= - \left( \frac{df(E)}{dE} \right)_{\mu=E_F, T} (e \Delta V) - \left( \frac{df(E)}{dE} \right)_{\mu=E_F, T} \frac{E - E_F}{T_0} (\Delta T)$$

Next, I am going to compensate the equation (3.5) in the equations (3.1) and (3.2).

$$I = \frac{2e}{h} \int_{-\infty}^{\infty} dE T(E) \left[ - \left( \frac{df(E)}{dE} \right)_{\mu=E_F, T} ((e \Delta V) + \frac{E - E_F}{T} (\Delta T)) \right] \quad (3.6)$$

$$Q = \frac{2}{h} \int_{-\infty}^{\infty} dE (E - E_F) T(E) \left[ - \left( \frac{df(E)}{dE} \right)_{\mu=E_F, T} ((e \Delta V) + \frac{E - E_F}{T} (\Delta T)) \right] \quad (3.7)$$

Let me introduce a new term  $L_n$  :

$$L_n = \int_{-\infty}^{\infty} (E - E_F)^n T(E) \left( - \frac{\partial f(E, T)}{\partial E} \right) dE \quad (3.8)$$

Now, equations (3.6) and (3.7) could be written as following

$$I = \frac{2e}{h} \left[ \frac{L_1}{T} (\Delta T) + e L_0 (\Delta V) \right] \quad (3.9)$$

$$Q = \frac{2}{h} \left[ \frac{L_2}{T} (\Delta T) + e L_1 (\Delta V) \right] \quad (3.10)$$

Now, I can express equations (3.9) and (3.10) in a matrix as following:

$$\begin{pmatrix} I \\ Q \end{pmatrix} = \frac{2}{h} \begin{pmatrix} e^2 L_0 & \frac{e}{T} L_1 \\ e L_1 & \frac{1}{T} L_2 \end{pmatrix} \begin{pmatrix} \Delta V \\ \Delta T \end{pmatrix} \quad (3.11)$$

Again, it is considered that Fermi level of the whole system in the equilibrium, therefore,  $\mu =$

$$E_F, T = \frac{T_L + T_R}{2}$$

Now, I am going to discuss special cases of equation (3.11). First, in case of  $\Delta T = 0$ , then,

$$G = \left( \frac{2e^2}{h} \right) L_0 \quad (G = (I/V) \text{ is electrical conductance and } h \text{ is the Plank's constant}) \quad (3.12)$$

$$= \left( \frac{2e^2}{h} \right) \int_{-\infty}^{\infty} T(E) \left( -\frac{\partial f(E,T)}{\partial E} \right) dE \quad (3.13)$$

Secondly, when  $T$  goes to zero ( $T \rightarrow 0$ )

$$\lim_{T \rightarrow 0} \left( -\frac{\partial f(E,T)}{\partial E} \right) = \delta(E - E_F) \quad (3.14)$$

From equations (3.12 and 3.14)

$$G = \left( \frac{2e^2}{h} \right) \int_{-\infty}^{\infty} T(E) \delta(E - E_F) dE \quad (3.15)$$

By using the mathematical delta function formula

$$\int_{-\infty}^{\infty} f(x) \delta(x - a) dx = f(a) \quad (3.16)$$

From equations (3.15 and 3.16), I obtain the Landauer formula

$$G = G_0 T(E_F) \quad (3.17)$$

Where  $G_0$  is the quantum of conductance  $G_0 = \frac{2e^2}{h}$

A third special case of equation (3.11) occurs when total electron current  $I = 0$ , which yields an expression for Seebeck coefficient  $S = -(\frac{\Delta V}{\Delta T})_{I=0}$

$$S = -(\frac{\Delta V}{\Delta T})_{I=0} = \frac{1}{eT} \frac{L_1}{L_0} \quad (3.18)$$

I can rewrite equation (3.11) again in terms of  $G$  and  $S$

$$\begin{pmatrix} I \\ Q \end{pmatrix} = \begin{pmatrix} G & GS \\ GST & K \end{pmatrix} \begin{pmatrix} \Delta V \\ \Delta T \end{pmatrix} \quad (3.19)$$

$$\begin{pmatrix} \Delta V \\ Q \end{pmatrix} = \begin{pmatrix} 1/G & -S \\ \Pi & K_e \end{pmatrix} \begin{pmatrix} I \\ \Delta T \end{pmatrix} \quad (3.20)$$

Where

$$\Pi = \frac{1}{e} \frac{L_1}{L_0} = ST \quad (\Pi \text{ is Peltier coefficient}) \quad (3.21)$$

$$K_e = k - S^2 GT = \frac{2}{hT} (L_2 - \frac{(L_1)^2}{L_0}) \quad (K_e \text{ is thermal conductance due to electrons}) \quad (3.22)$$

$$\text{The thermoelectric figure of merit is } ZT_e = S^2 \frac{GT}{K_e} = \frac{(L_1)^2}{L_0 L_2 - (L_1)^2} \quad (3.23)$$

### 3.3 Green's function for the double-infinite chain in one- dimension

In this section, my goal is to find the Green's function for the double-infinite chain system as shown in Figure 3.1. In this system, I have a double-infinite chain with  $(\varepsilon_0)$  represents the site energy of each atom in the lead. Also,  $(-\gamma)$  represents the coupling between atoms in the lead.

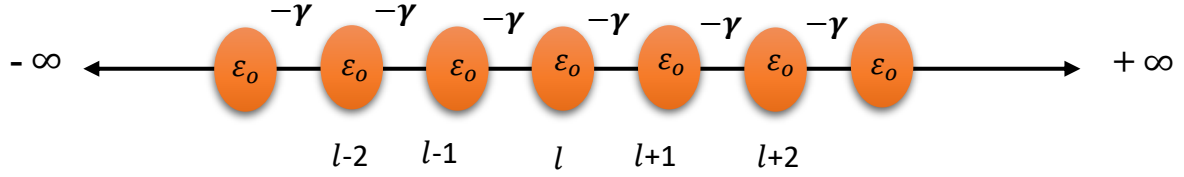


Figure 3. 1. Double-infinite chain in one- dimension on-site energies  $\varepsilon_0$  and couplings  $-\gamma$ .

We know that the Schrödinger equation can be written

$$H |\varphi\rangle = E |\varphi\rangle \quad (3.24)$$

Whereas the Green's function equation

$$(E - H)G = 1 \quad (3.25)$$

The equation (3.25) could be written

$$E G_{ij} - \sum_{l=-\infty}^{\infty} H_{il} G_{lj} = \delta_{ij} \quad (3.26)$$

I will compensate in the equation (3.26) in two cases ( $l \neq j$  and  $l = j$ )

$$\varepsilon_0 G_{lj} - \gamma G_{l+1,j} - \gamma G_{l-1,j} - E G_{lj} = 0 \quad (3.27)$$

$$\varepsilon_0 G_{ll} - \gamma G_{l+1,l} - \gamma G_{l-1,l} - E G_{ll} = -1 \quad (3.28)$$

Guess



$$G_{lj} = \begin{cases} \phi_l = A e^{ikl} & l \geq j \\ \phi_l = B e^{-ikl} & l \leq j \end{cases} \quad (3.29)$$

The retarded Greens function,  $G_{lj}$ , describes the response of a system at a certain point  $l$  to a source at a certain point  $j$ . An excitation of this type will result in two waves that travel outward from the point of excitation as shown in Figure 3.3.

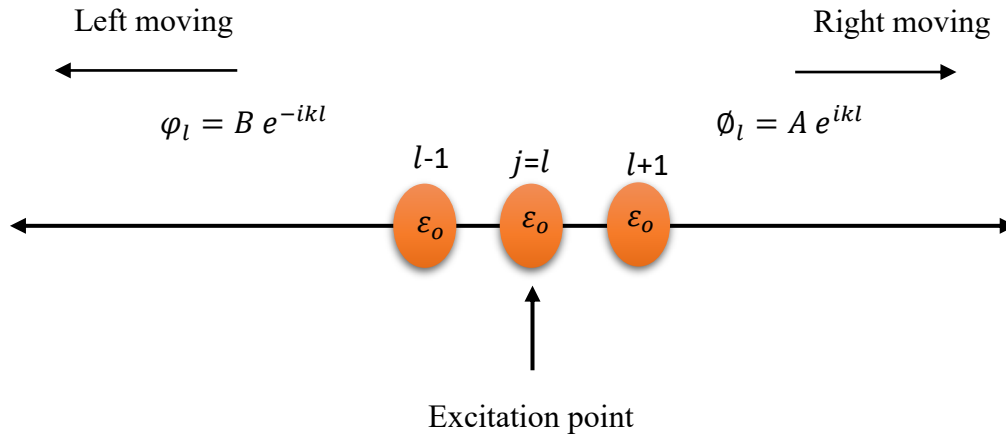


Figure 3. 2. The structure of retarded Green's function of an infinite one-dimensional chain.

The excitation at  $l = j$  causes wave to propagate left and right with amplitudes  $B$  and  $A$  respectively.

The Green's function must be continuous at  $l = j$  (see Figure 3.2)

$$A e^{ikj} = B e^{-ikj}$$

$$A = C e^{-ikj} \quad \text{and} \quad B = C e^{ikj} \quad (3.30)$$

From the last equations

$$G_{lj} = \begin{cases} C e^{ik(l-j)} & l \geq j \\ C e^{ik(j-l)} & l \leq j \end{cases} \quad (3.31)$$

Substituting (3.31) in the equation (3.28)

$$\varepsilon_0 C - \gamma C e^{ik} - \gamma C e^{-ik} - E C = -1 \quad (3.32)$$

$$C = \frac{1}{2 i \gamma \sin(k)} = \frac{1}{i \hbar v} \quad (3.33)$$

$$G_{lj} = \frac{e^{ik|l-j|}}{i \hbar v} \quad (\text{Green's function for the double-infinite chain-}) \quad (3.34)$$

$$G_{lj} = \frac{e^{ik|l-j|}}{i \hbar v} + A e^{ikl} + B e^{-ikl} \quad (\text{general solution}) \quad (3.35)$$

### 3.4 Green's functions for the semi-infinite chain in one- dimension

Here, this system is the similar with the previous one, except that one lead is infinite in one direction and it is finite for the opposite side as shown in Figure 3.3.

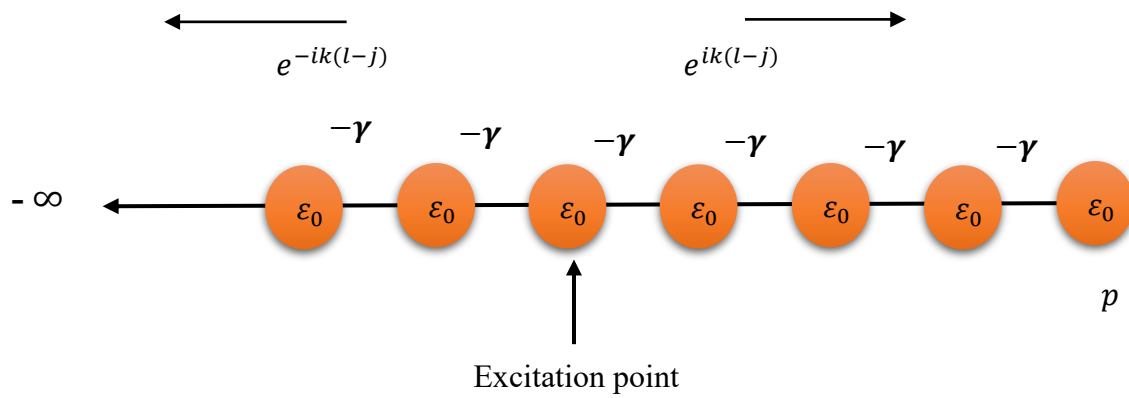


Figure 3. 3. Semi-infinite chain in one- dimension with on-site energies  $\varepsilon_0$  and couplings  $-\gamma$  .

Based on equation (3.35) for the current system

$$G_{lj} = \frac{e^{ik|l-j|}}{i \hbar v} + A e^{-ikl} \quad (3.36)$$

From the figure, I can extract the boundary condition for this system

I will consider the number of atoms is P

$$G_{p+1,j} = 0 \quad (3.37)$$

From the last two equations

$$A = -\frac{e^{-ikJ}}{i h v} e^{2ik(P+1)} \quad (3.38)$$

Plugging (3.38) in the equation (3.36)

$$G_{lj} = \frac{e^{ik(l-J)} - e^{-ik(l+J)} e^{2ik(P+1)}}{i h v} \quad (\text{Green's functions for the semi-infinite system}) \quad (3.39)$$

Now, in case of  $l = p$

$$G_{pj} = \frac{e^{ik(p-J)} [1 - e^{2ik(P+1)}]}{i h v} \quad (3.40)$$

Now, when  $l = p = j$

$$G_{pp} = -\frac{e^{ik}}{\gamma} \quad (\text{Surface Green's function}) \quad (3.41)$$

### 3.5 Dyson's equation and Green's function for a scattering system

In this section, I will prove the Dyson's equations based on the idea of the Green's function that I have discussed before. In this system, as presented in Figures 3.4 and 3.5, I have a double-infinite chain with  $(\varepsilon_L, \varepsilon_R)$  represent the site energy of each atom in the left and right leads respectively where  $(\varepsilon_0)$  is a site energy for each atom in the scattering region (SR). Also,  $(-\gamma)$  represents the coupling between atoms for both leads whereas  $(-\alpha)$  and  $(-\beta)$  are the coupling between the left and right leads with S.R respectively. These transport calculations following the derivation of Lambert, mentioned in [6-7].

For only the scatterer area, I can calculate the Green's function easily, since the Hamiltonian of the scatterer is finite with total number of atoms is  $(N)$ .

Where  $h_B$  represents the Hamiltonian of the SR

$$g_B = (E - h_B)^{-1} \quad (3.42)$$

However, if we are interested in finding the Green's function for the whole system (two leads and the SR), I cannot use the equation (3.42), because the Hamiltonian representing the whole scattering system is not finite. In other words, the Hamiltonian for this system is infinite matrix. In this case, I should find another approach that avoiding us in dealing with the infinite matrix.

I am going to deal with this system in two cases, one of them is before the perturbation  $\alpha = \beta = 0$  (as shown in Figure 3.4) and the second case is after the perturbation  $\alpha$  and  $\beta \neq 0$  (as shown in Figure 3.5).

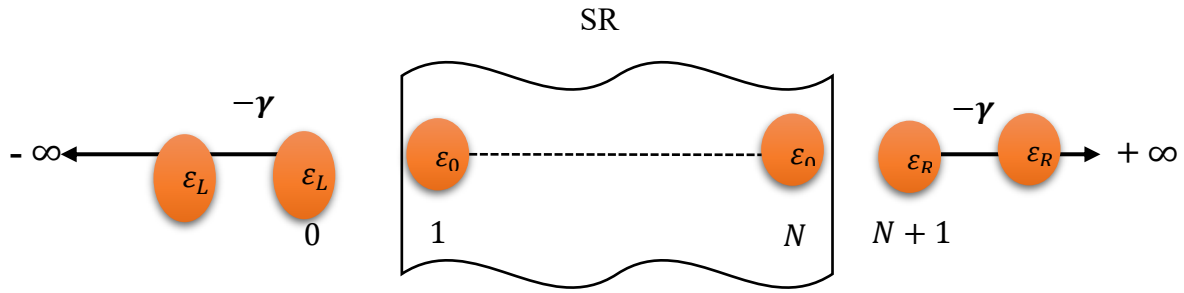


Figure 3. 4. A one-dimensional scatterer connected to one-dimensional leads before perturbation  $\alpha = \beta = 0$ .

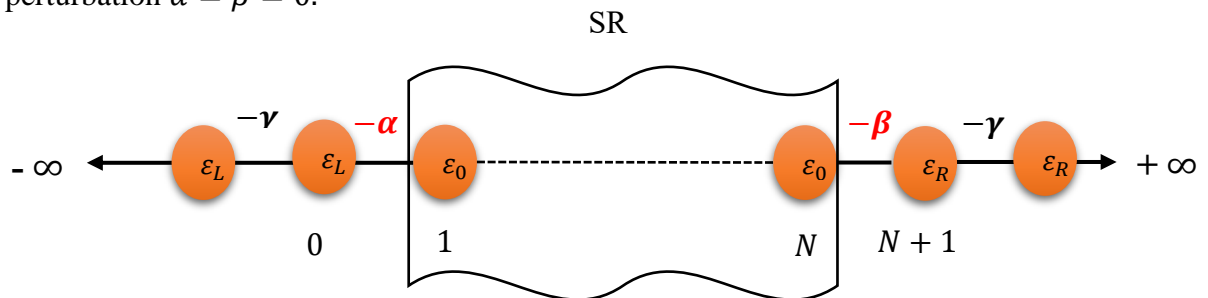


Figure 3. 5. A one-dimensional scatterer connected to one-dimensional leads after perturbation  $\alpha$  and  $\beta \neq 0$ .

Before the perturbation, the Hamiltonian could be written as following:

$$H_o = \begin{pmatrix} H \text{ for the semi-infinite lead in the left} & 0 & \cdot \\ & 0 & h_B \\ \cdot & 0 & H \text{ for the semi-infinite lead in the right} \end{pmatrix} \quad (3.43)$$

Similarly, before the perturbation, the Green's function could be written as following

$$g_o = \begin{pmatrix} g \text{ for the semi-infinite lead in the left} & 0 & \cdot \\ & 0 & g_B \\ \cdot & 0 & g \text{ for the semi-infinite lead in the right} \end{pmatrix} \quad (3.44)$$

After the perturbation ( $\alpha$  and  $\beta \neq 0$ )

$$H_1 = \begin{pmatrix} 0 & \dots & \cdot \\ & -\alpha & \\ \vdots & -\alpha \boxed{h_1} -\beta & \vdots \\ \cdot & \dots & 0 \end{pmatrix}$$

So, it is clear that the total Hamiltonian H

$$H = H_o + H_1 \quad (3.45)$$

The total Green's function (Whole system includes left and right leads and the S.R) could be written G

$$(E - H)G = 1$$

$$(E - H_o - H_1)G = 1 \quad (3.46)$$

$$\text{The solution for the equation (3.46) is } G = g + g H_1 G \quad (3.47)$$

By multiplying (3.47) by  $(E - H_o)$  in both sides and multiplying by  $g^{-1}$

$$G = (g^{-1} - H_1)^{-1} \quad (3.48)$$

$$G = (g^{-1} - h_1)^{-1} \quad (\text{Dyson's equation}) \quad (3.49)$$

$$= \begin{pmatrix} G_{00} & G_{01} & G_{0N} & G_{0N+1} \\ G_{10} & G_{11} & G_{1N} & G_{1N+1} \\ \cdot & \cdot & \cdot & \cdot \\ G_{N+1,0} & \cdot & \cdot & G_{N+1,N+1} \end{pmatrix} = \begin{pmatrix} G_{AA} & G_{AB} \\ G_{BA} & G_{BB} \end{pmatrix} \quad (3.50)$$

I can see from the Dyson's equation; we have converted from the dealing with infinite matrix into finite matrix.

Let A represents the leads and B represents the SR

Where  $g_A$  represents the Green's function for the semi-infinite leads before the perturbation and  $g_B$  represents the Green's function for the SR before the perturbation.

$$g = \begin{pmatrix} g_A & 0 \\ 0 & g_B \end{pmatrix} \quad (3.51)$$

$$g_B = \begin{pmatrix} g_{11} & g_{1N} \\ g_{N1} & g_{NN} \end{pmatrix} = (E - h_B)^{-1} \quad (3.52)$$

$$g_A = \begin{pmatrix} g_{00} & g_{0,N+1} \\ g_{N+1,0} & g_{N+1,N+1} \end{pmatrix} = \begin{pmatrix} -\frac{e^{ik}}{\gamma} & 0 \\ 0 & -\frac{e^{ik}}{\gamma} \end{pmatrix} \quad (3.53)$$

$$h_1 = \begin{pmatrix} H_{AA} & H_{AB} \\ H_{BA} & H_{BB} \end{pmatrix} = \begin{pmatrix} 0 & 0 & -\alpha & 0 \\ 0 & 0 & 0 & -\beta \\ -\alpha & 0 & 0 & 0 \\ 0 & -\beta & 0 & 0 \end{pmatrix} \quad (3.54)$$

From the Dyson's equation (3.49) and equations (3.52-3.54)

$$(g^{-1} - h_1) G = 1 = \begin{pmatrix} 1 & 0 \\ 0 & 1 \end{pmatrix}$$

$$= \begin{pmatrix} g_A^{-1} G_{AA} - H_{AB} G_{BA} & g_A^{-1} G_{AB} - H_{AB} G_{BB} \\ -H_{BA} G_{AA} + g_B^{-1} G_{BA} & -H_{BA} G_{AB} + g_B^{-1} G_{BB} \end{pmatrix} = \begin{pmatrix} 1 & 0 \\ 0 & 1 \end{pmatrix} \quad (3.55)$$

From the equation (3.55)

$$G_{AA} = g_A + g_A H_{AB} G_{BA} \quad (3.56)$$

$$G_{BB} = g_B + g_B H_{BA} G_{AB} \quad (3.57)$$

$$G_{AB} = g_A H_{AB} G_{BB} \quad (3.58)$$

$$G_{BA} = g_B H_{BA} G_{AA} \quad (3.59)$$

From the equations (3.56-3.59) I will end up with the following questions

$$G_{AA} = (g_A^{-1} - \Sigma_{AA})^{-1} \quad (3.60)$$

$$\text{Where } \Sigma_{AA} = H_{AB} g_B H_{BA} \quad \text{self-energy} \quad (3.61)$$

$$G_{BB} = (g_B^{-1} - \Sigma_{BB})^{-1} \quad (3.62)$$

$$\text{Where } \Sigma_{BB} = H_{BA} g_A H_{AB} \quad \text{self-energy} \quad (3.63)$$

In the next section, I will take some applications related to Green's function and Dyson's equations.

### 3.6 Green's functions and Dyson's equation applications

In this section, I introduce two examples about Green's functions and Dyson's equation applications. For the first example, destructive quantum interference (DQI), low conductance, is shown in transmission coefficient plots while the second example, constructive quantum interference (CQI), high conductance, is presented.

#### 3.6.1 A dangling system

In this system, I have a double-infinite chain and one dangling atom with site energy( $\varepsilon_1$ ), whereas ( $\varepsilon_0$ ) represents the site energy of each atom in the lead. Also, ( $-\gamma$ ) represents the

coupling between atoms in the lead and  $(-\alpha)$  is the coupling between the dangling atom and an atom in the lead.

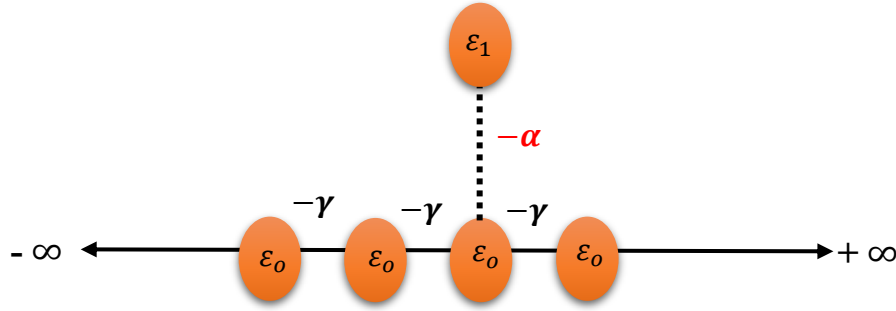


Figure 3. 6. A dangling system.

First, let A represents the leads and B represents the SR where  $g_A$  represents the Green's function for the double-infinite leads before the perturbation and  $g_B$  represents the Green's function for the SR before the perturbation.

As I have studied this system before and I found that

$$g_A = g_{00(l=j=0)} = \frac{1}{i\hbar v} \quad (3.64)$$

$g_B$  represents the Green's function for the SR before perturbation

$$(E - H_B)^{-1} g_B = 1 \quad (3.65)$$

$$g_B = (E - H_B)^{-1} = \frac{1}{E - \epsilon_1} \quad (3.66)$$

After the perturbation( $\alpha \neq 0$ )

$$h_1 = \begin{pmatrix} H_{AA} & H_{AB} \\ H_{BA} & H_{BB} \end{pmatrix} = \begin{pmatrix} 0 & -\alpha \\ -\alpha & 0 \end{pmatrix} \quad (3.67)$$

$$\text{Self-energy } \Sigma_{BB} = H_{BA} g_A H_{AB} \quad (3.68)$$



$$\Sigma_{BB} = \frac{\alpha^2}{i \hbar v} \quad (3.69)$$

$$G_{BB} = (g_B^{-1} - \Sigma_{BB})^{-1} = \left( (E - \epsilon_1) - \frac{\alpha^2}{i \hbar v} \right)^{-1} \quad (3.70)$$

$$G_{AA} = G_{AA} = g_A + g_A H_{AB} G_{BA} \quad (3.71)$$

$$G_{AA} = G_{00} = \frac{1}{i \hbar v} + \left( \frac{\alpha}{i \hbar v} \right)^2 \left( \frac{1}{(E - \epsilon_1) - \frac{\alpha^2}{i \hbar v}} \right) \quad (3.72)$$

The transmission amplitude ( $t$ )

$$t = (i \hbar v) G_{00} = 1 + \frac{1}{i \hbar v} \frac{\alpha^2}{(E - \epsilon_1) - \frac{\alpha^2}{i \hbar v}} \quad (3.73)$$

The transmission coefficient ( $T$ )

$$T = |t|^2 = \frac{1}{1 + \frac{\alpha^4}{(\hbar v)^2 (E - \epsilon_1)^2}} \quad (3.74)$$

Note that if  $E = \epsilon_1$ , then  $T(E) = 0$ . Ie an anti-resonance occurs at  $E = \epsilon_1$ . This is known as destructive quantum interference (DQI) and is shown in Fig. 3.7.

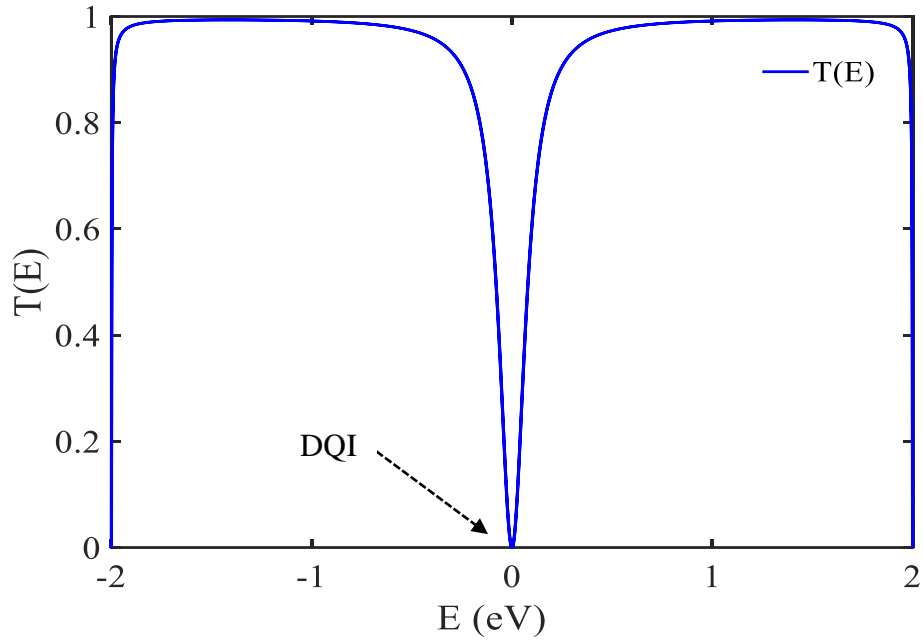


Figure 3. 7. Transmission coefficients of dangling system against electron energy  $E$ . In this system  $\alpha=0.6$ ,  $\gamma=1$  and  $\varepsilon_1=0$ .

Figure 3.7 shows that  $\varepsilon_1$  value is responsible for the position of (DQI).

### 3.6.2 A scattering system with only one atom

As a further example, consider the simple system, shown in the Figure 3.8, in which there is only one atom in the scattering region (SR) with site energy ( $\varepsilon_0$ ), whereas ( $\varepsilon_L$ ) and ( $\varepsilon_R$ ) are site energies for the atoms in the left and right leads respectively. In addition, ( $-\gamma$ ) is the coupling between neighbouring atoms, whereas ( $-\alpha$ ) and ( $-\beta$ ) are the coupling between the left and right leads with S.R respectively.

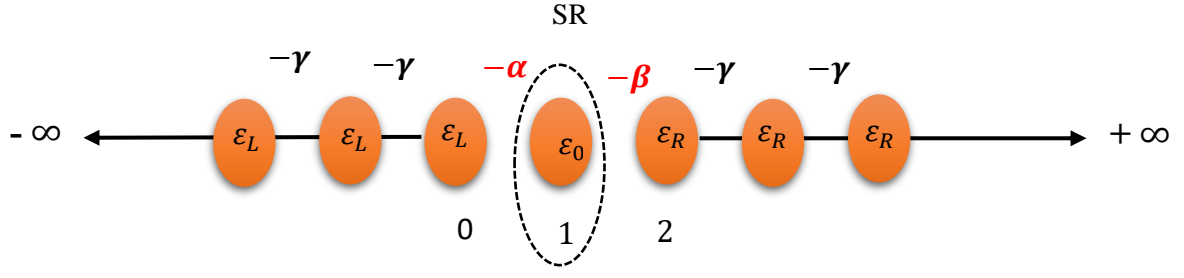


Figure 3. 8. Open system with only one atom in the SR before the perturbations  $\alpha, \beta$ .

If sub-system A represents the leads and sub-system B represents the SR, then,  $g_A$  represents the Green's function for the semi-infinite leads before the perturbation (ie when  $\alpha = \beta = 0$ ) and  $g_B$  represents the Green's function for the SR before the perturbation.

$$g_A = \begin{pmatrix} \frac{-e^{ik}}{\gamma} & 0 \\ 0 & \frac{-e^{ik}}{\gamma} \end{pmatrix} \quad (3.75)$$

Here, for simplicity, I will consider that  $\gamma_L = \gamma_R = \gamma$

$H_B$ (represents the Hamiltonian of the SR)

$$g_B = (E - H_B)^{-1} = \frac{1}{E - \varepsilon_0} \quad (3.76)$$

Before the perturbation, the Hamiltonian could be written as following

$$H_o = \begin{pmatrix} \varepsilon_0 & 0 & 0 \\ 0 & \varepsilon_0 & 0 \\ 0 & 0 & \varepsilon_0 \end{pmatrix} \quad (3.77)$$

After the perturbation as shown in the Figure 3.9, the Hamiltonian could be written as following.

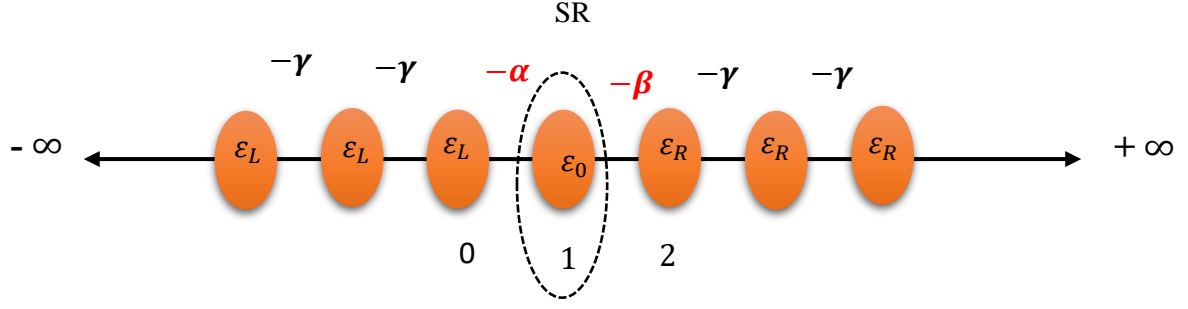


Figure 3. 9. Open system with only one atom in the SR after the perturbation.

After the perturbation( $\alpha \neq 0$ )

$$h_1 = \begin{pmatrix} H_{AA} & H_{AB} \\ H_{BA} & H_{BB} \end{pmatrix} = \begin{pmatrix} \varepsilon_0 & 0 & -\alpha \\ 0 & \varepsilon_0 & -\beta \\ -\alpha & -\beta & \varepsilon_0 \end{pmatrix} \quad (3.78)$$

$$H_{AA} = \begin{pmatrix} \varepsilon_0 & 0 \\ 0 & \varepsilon_0 \end{pmatrix} \quad (3.79)$$

$$H_{BB} = \varepsilon_0, \quad H_{BA} = (-\alpha \quad -\beta) \text{ and } H_{AB} = \begin{pmatrix} -\alpha \\ -\beta \end{pmatrix}$$

$$\text{Self-energy for this system } \Sigma_{AA} = H_{AB} g_B H_{BA} \quad (3.80)$$

$$\Sigma_{AA} = \frac{1}{E - \varepsilon_0} \begin{pmatrix} \alpha^2 & \alpha\beta \\ \alpha\beta & \beta^2 \end{pmatrix} \quad (3.81)$$

$$G_{AA} = (g_A^{-1} - \Sigma_{AA})^{-1} \quad (3.82)$$

$$\text{Let } D = \frac{1}{E - \varepsilon_0}$$

$$G_{AA} = \frac{1}{\gamma^2 e^{-2ik} + \gamma D e^{-ik} (\alpha^2 + \beta^2)} \begin{pmatrix} -\gamma e^{-ik} - D\beta^2 & D\alpha\beta \\ D\alpha\beta & -\gamma e^{-ik} - D\alpha^2 \end{pmatrix} \quad (3.83)$$

$$G_{AA} = \begin{pmatrix} G_{00} & G_{02} \\ G_{20} & G_{22} \end{pmatrix} \quad (3.84)$$

$$T = |t|^2 = |i \hbar v|^2 |G_{02}|^2$$

$$T = \frac{4 (\gamma \alpha \beta)^2 \sin^2(k)}{\left[ \frac{\gamma^2}{D} \cos(2k) + \gamma(\alpha^2 + \beta^2) \cos(k) \right]^2 + \left[ \frac{\gamma^2}{D} \sin(2k) + \gamma(\alpha^2 + \beta^2) \sin(k) \right]^2} \quad (3.85)$$

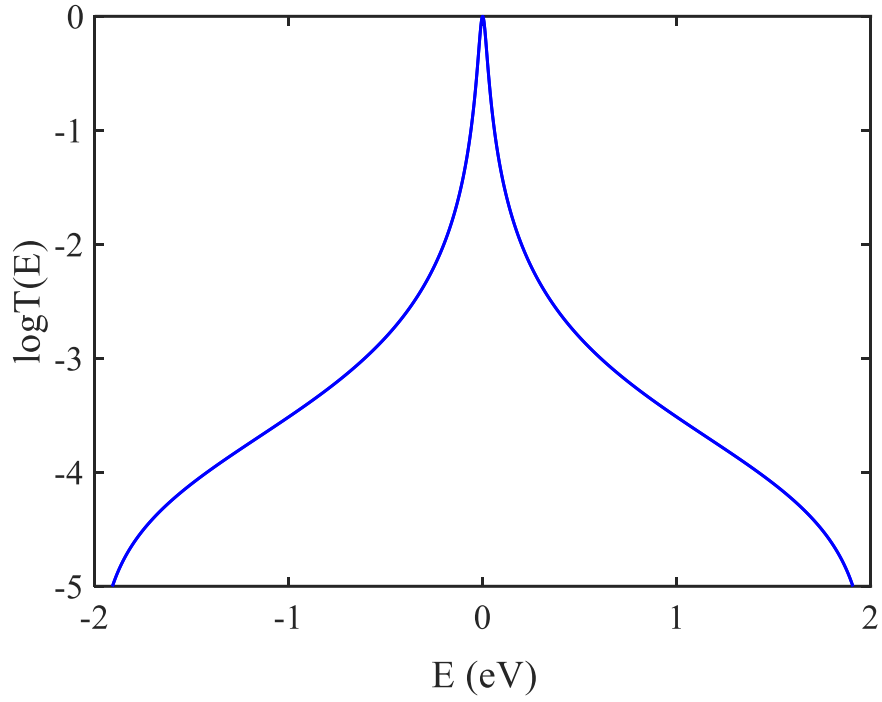


Figure 3. 10. Transmission coefficient versus energy  $E$  for only one atom in the SR.

As shown in Fig. 3.10, the transmission coefficient now possess a resonance at  $E = 0$ , which is a signature of constructive quantum interference (CQI).

### 3.6.3 Breit-Wigner resonance

By playing with the maths and using some trigonometric identities, the equation (3.85) could be written as following:

$$T(E) = \frac{4 \Gamma_L \Gamma_R}{(E - \sigma)^2 + (\Gamma_L + \Gamma_R)^2} \quad (3.86)$$

In this case equation (3.86) reduces to the well-known Breit-Wigner formula [8].

Where  $\Gamma_L = \frac{\alpha^2 \sin(k)}{\gamma}$  ,  $\Gamma_R = \frac{\beta^2 \sin(k)}{\gamma}$  ,  $\sigma = \sigma_L + \sigma_R$  ,  $\sigma_L = \frac{\alpha^2 \cos(k)}{\gamma}$  and  $\sigma_R = \frac{\beta^2 \cos(k)}{\gamma}$

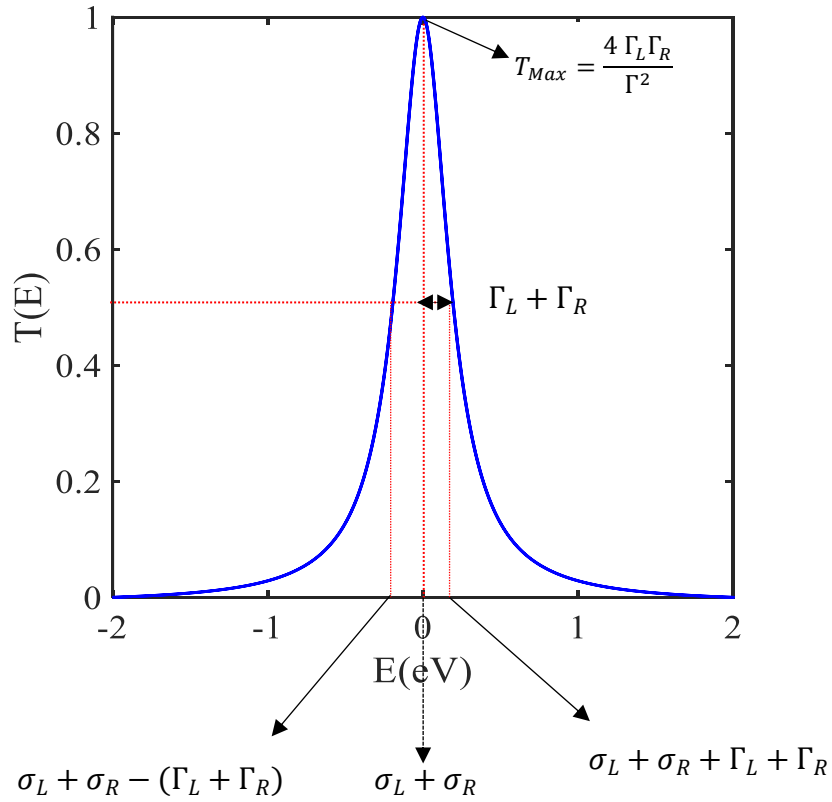


Figure 3.11. Breit-Wigner peak in one transmission spectra  $T(E)$ . The longer dashed red vertical line shows the on-resonance position  $E = \sigma_L + \sigma_R$  while the two shorter dashed red lines represent the position  $E = \sigma_L + \sigma_R - (\Gamma_L + \Gamma_R)$  and  $E = \sigma_L + \sigma_R + \Gamma_L + \Gamma_R$  at half

maximum value (left to right). In consequence, the corresponding half width of half maximum value is  $\Gamma_L + \Gamma_R$ .

Some features of the equation (3.86) are as follows:

1. The maximum transmission coefficient could be found by taking the first derivative for the equation (3.86) and equalizes it to zero when  $E = \sigma_L + \sigma_R$ .

$$T_{Max} = \frac{4 \Gamma_L \Gamma_R}{\Gamma^2}$$

2. When  $\Gamma_L \ll \Gamma_R$ , transmission coefficient on resonance is approximately equal to

$$T \approx \frac{4 \Gamma_L}{\Gamma_R}$$

### 3.7 Conclusion

In conclusion, I have discussed single electron charge transport through molecules by introducing quantum transport theory. The theoretical basis for calculating electronic and heat transport was described, including Green's function methods for obtaining the transmission coefficient of semi-infinite leads connected to a scattering region. Therefore, the transmission coefficient has been computed using Green's functions, Dyson's equation and scattering theory for some simple systems. In addition, the Landauer-Büttiker formula can be used to determine thermoelectric coefficients, such as Seebeck coefficient  $S$ , for a two-terminal device. I have also proved that systems showing constructive quantum interference (CQI), their transmission coefficient equations could be converted to the Breit-Wigner formula.

## Bibliography

1. Lambert, C. J. (2021). Quantum Transport in Nanostructures and Molecules. IoP publishing.
2. Finch, C. M. (2008). *An understanding of the electrical characteristics of organic molecular devices* (Doctoral dissertation, Lancaster University).
3. Lambert, C.J., Sadeghi, H. and Al-Galiby, Q.H. (2016). Quantum-interference-enhanced thermoelectricity in single molecules and molecular films. *Comptes Rendus Physique*, 17(10), pp.1084–1095.
4. M. Buttiker, “Conductance Formula,” vol. 31, no. 10, pp. 6207–6215, 1985
5. Galperin, M., Nitzan, A., & Ratner, M. A. (2007). Heat conduction in molecular transport junctions. *Physical Review B*, 75(15).
6. Sanvito, S. (1999). Giant Magnetoresistance and Quantum Transport in Magnetic Hybrid Nanostructures. (Doctoral dissertation, Lancaster University).
7. Visontai, D. (2011). Quantum and Classical Dynamics of Molecule Size Systems. Physics Department 2013, Lancaster University.
8. Sparks, R.E., García-Suárez, V.M., Manrique, D.Zs. and Lambert, C.J. (2011). Quantum interference in single molecule electronic systems. *Physical Review B*, 83(7).



## Chapter 4

### Further investigations of anchoring groups on linear alkane chains

#### 4.1 Introduction

This chapter provides thorough and vigorous theoretical investigations about series of alkane chains using different anchor groups including amine ( $\text{NH}_2$ ), thiol (S), direct carbon contact (C), and thiomethyl (SMe). However, I will discuss briefly the alkane chains conductance with (Au-SMe) in this chapter because this anchor will be investigated deeply in chapter 5.

Here, I shall demonstrate the impact of using different terminal groups on the conductance of alkane molecules. This study includes eight molecules with four different anchor groups. Thus, I am going to investigate 32 alkane linear chains.

At the end of anchor group calculations, I shall test my theoretical predictions against experimental measurements that gathered from the literature.

#### 4.2 Motivation

Oil and natural gas are the most important sources for alkanes. Oil contains liquid alkanes while higher alkanes (solid)s, occur as residues from oil distillation (tar), such as asphalt lakes known as the Pitch Lake [1]. Cycloalkanes with one ring have the general formula  $\text{C}_n\text{H}_{2n}$  compared with the general formula  $\text{C}_n\text{H}_{(2n+2)}$  for acyclic alkanes. Cycloalkanes have two fewer hydrogen atoms than alkanes, because another carbon–carbon bond is needed to form the ring [2].

In today's world, alkane chains have been used in many applications, such as sensors that could be used in safety and security fields globally. Here, in this chapter, I am focusing on studying the conductance of alkane chains with different anchor groups.

### 4.3 Optimised DFT Structures of Isolated Molecules

In this chapter, I am going to investigate different type of alkane linear chains. Mainly, I divide the chains into two types, odd and even groups, according to their number of  $-CH_2$  units. Each group consists of four molecules based on their molecular length. For the odd group, I choose the following: **C3**, **C5**, **C7** and **C9**, while for the even group **C4**, **C6**, **C8** and **C10**. For both odd and even groups, 4 different anchor groups have been employed including amine, thiol, direct carbon contact and thiomethyl. Therefore, in total I am going to investigate 32 alkane chains. (Note: the last anchor thiomethyl is going to be investigated in more detail in chapter 5).

#### 4.3.1 Geometries of the isolated alkane chains terminated with an amine anchor

The optimum geometries of the isolated molecules were obtained by relaxing the molecules until all forces on the atoms were less than  $0.01 \text{ eV} / \text{\AA}$ . Eight alkane chains with different lengths are going to be explored (4 odd and 4 even). The 8 chains are all terminated with two amine anchors ( $NH_2$ ), as shown in Figure 4.1. The odd numbered molecules are as follows: **C3**, **C5**, **C7** and **C9**, as shown in left panel of Figure 4.1, while the even molecules are: **C4**, **C6**, **C8** and **C10**, as shown in the right panel of Figure 4.1 (top to bottom respectively).

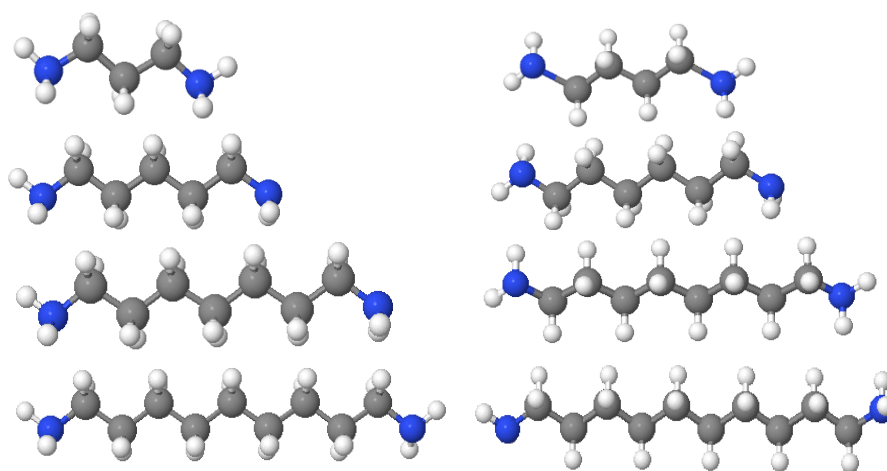


Figure 4. 1. Alkane chains: Fully relaxed isolated molecules, of different length 3-10 carbon atoms. (Left panel) shows the odd chains **C3**, **C5**, **C7** and **C9** while (right panel) represents the even ones **C4**, **C6**, **C8** and **C10**, both chains are terminated with amine anchors.

#### 4.4 Frontier orbitals for the studied molecules

Tables 4.1-4.3 show the theoretical frontier orbitals of the 8 isolated molecules. The plots below show iso-surfaces of the HOMO and LUMO along with their energies for the alkane chains, **C<sub>3</sub>** to **C<sub>10</sub>** in the gas phase. Local density approximation (LDA) was chosen to be the exchange correlation functional.

Table 4. 1. Comparison between the Frontier molecular orbitals of alkane chain, including C<sub>3</sub>, C<sub>4</sub> and C<sub>5</sub> in the gas phase.




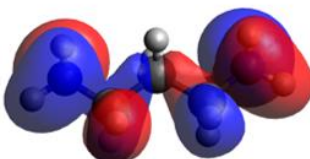
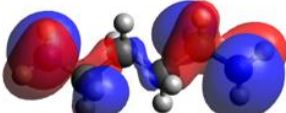
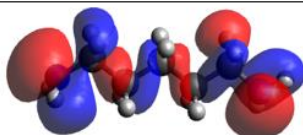
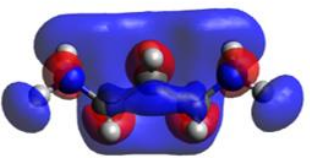
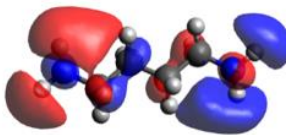
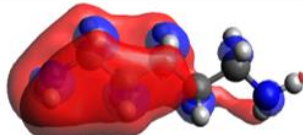
Chains	C <sub>3</sub>	C <sub>4</sub>	C <sub>5</sub>
Mol.			
HOMO			
eV	-4.5	-4.6	-4.5
LUMO			
eV	2.1	2.1	2.0

Table 4. 2. Comparison between the frontier molecular orbitals of alkane chain, including **C<sub>9</sub>** and **C<sub>10</sub>** in the gas phase.




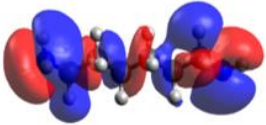
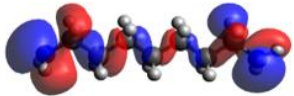
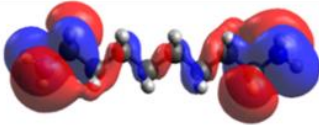
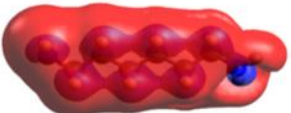
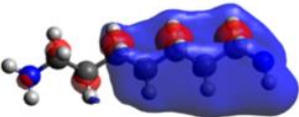


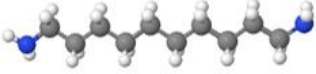
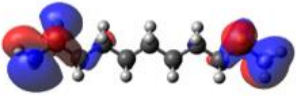
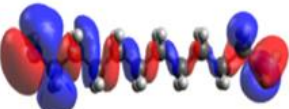


Chains	C <sub>6</sub>	C <sub>7</sub>	C <sub>8</sub>
Mol.			
HOMO eV	 -4.63	 -4.7	 -4.66
LUMO eV	 1.9	 1.9	 2.0

Table 4. 3. Comparison between the frontier molecular orbitals of alkane chain, including **C<sub>9</sub>** and **C<sub>10</sub>** in the gas phase.

Chains	C <sub>9</sub>	C <sub>10</sub>
Mol.		
HOMO		
eV	-4.7	-4.65
LUMO		
eV	2.0	1.96

## 4.5 Binding energy of linear chains on gold

To calculate the optimum binding distance of the alkane molecules with amine as anchor groups binding to the gold (111) surfaces, DFT and the counterpoise method were used, which removes basis set superposition errors (BSSE). The binding distance was defined as the distance between the gold surface and the terminal end group/atom of the molecule. The ground state energy of the total system was calculated using SIESTA and is denoted  $E_{AB}^{AB}$ . The energy of each monomer was then calculated in a fixed basis, which is achieved through the use of ghost atoms in SIESTA. Hence the energy of the individual molecule in the presence of the fixed basis is defined as  $E_A^{AB}$  and for the isolated gold as  $E_B^{AB}$ . The binding energy (B.E) is then calculated using the following equation:

$$\text{Binding Energy} = E_{AB}^{AB} - E_A^{AB} - E_B^{AB} \quad (4.1)$$

Figure 4.2, shows the binding energy of an alkane chain (i.e:  $C_6$ ). The amine anchor possesses a weak bond to an under-coordinated gold-electrode atom compared to other anchors such as thiol. The equilibrium distance (i.e. the minimum of the binding energy curve), for  $NH_2$  anchor is found to be approximately 3 Å, with binding energy of approximately -0.15 eV.

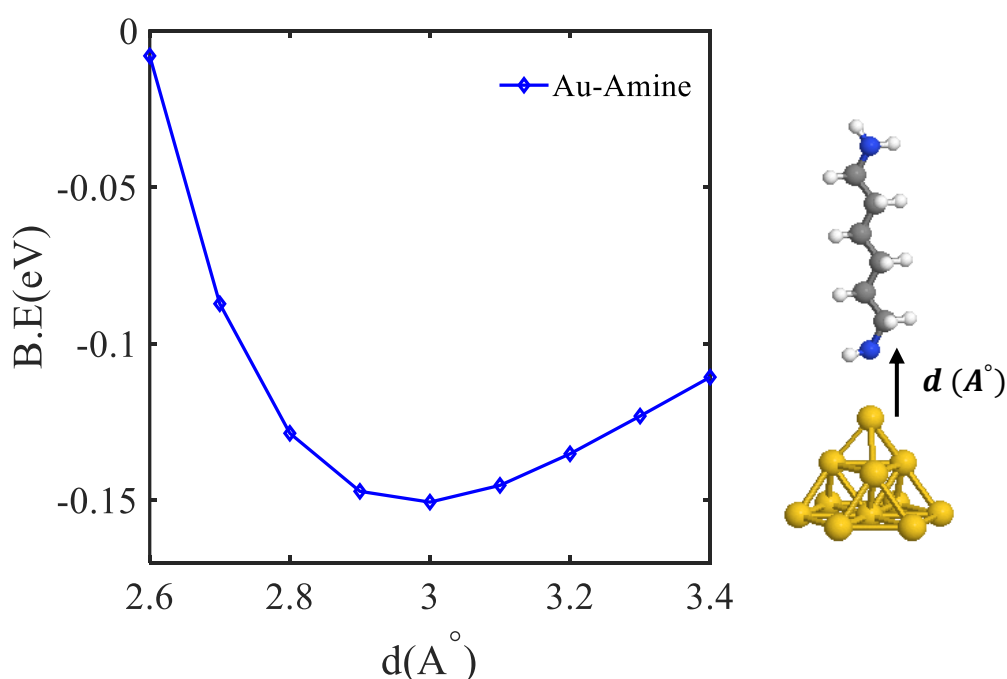


Figure 4. 2. An example of alkane molecule terminated with an amine anchor on a gold tip : (Left) Binding energy of C<sub>6</sub> alkane molecule to gold as a function of molecule-contact distance. The equilibrium distance (i.e. the minimum of the binding energy curve) is found to be approximately 3 Å, for Au-Amine. (Right) its idealised ad-atom configuration at the Au lead interface Au-Amine. Key: C = grey, H = white, N = blue, Au = dark yellow.

#### 4.6 DFT Calculations

Using the density functional code SIESTA [3] (for more detail see section 2.7 in chapter 2), the optimum geometries of the isolated molecules were obtained by relaxing the molecules until all forces on the atoms were less than 0.01 eV / Å. A double-zeta plus polarization orbital basis set, norm-conserving pseudopotentials, an energy cut-off of 250 Rydbergs defined the real space grid were used and the local density approximation (LDA) was chosen to be the exchange correlation functional. I also computed results using GGA and found that the resulting transmission functions were comparable with those obtained using LDA [4-10]. (for more detail see chapter 2).

After relaxing each molecular junction with lengths varying from  $n = 3$  to  $n = 10$ , I calculated the electrical conductance using the Gollum quantum transport code [11]. From the ground state Hamiltonian, the transmission coefficient, the room temperature electrical conductance  $G$  was obtained, as described in the sections below.

#### 4.7 Optimised DFT Structures of Compounds in their Junctions

Some examples of optimised DFT structures for alkane chains are shown in the section 4.3.1, while Figure 4.3 illustrates them in their junctions.



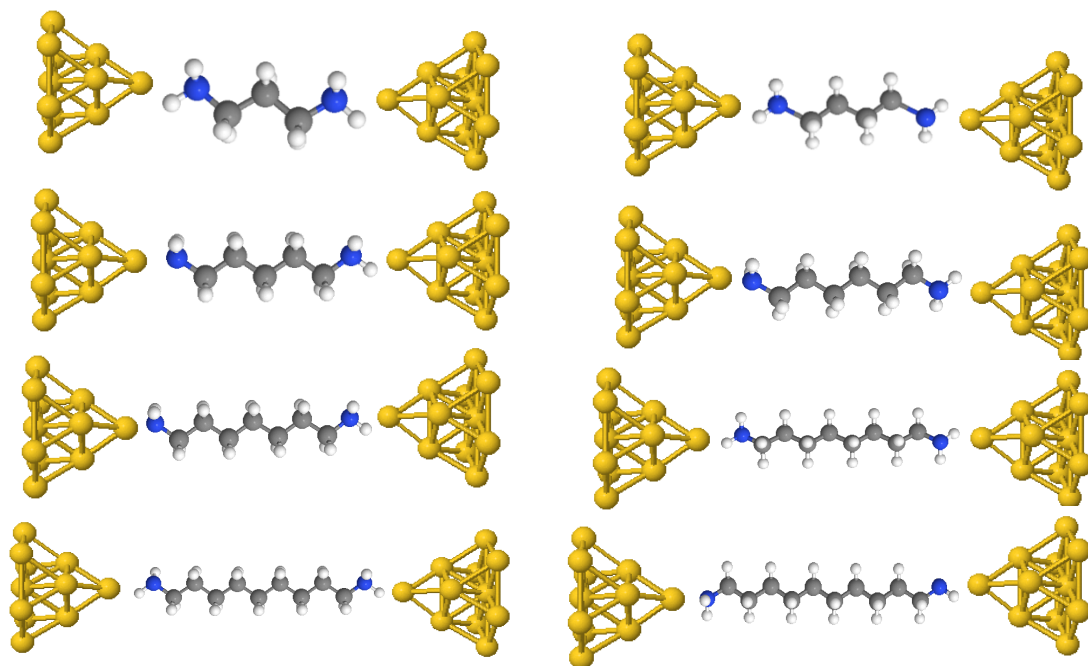


Figure 4. 3. Examples of fully relaxed alkane derivatives in Au|molecule|Au junctions. (Left panel) shows odd number of linear chains **C<sub>3</sub>**, **C<sub>5</sub>**, **C<sub>7</sub>** and **C<sub>9</sub>** (top to bottom) connected to gold electrodes via amine anchor groups. (Right panel) shows even number of linear chains **C<sub>4</sub>**, **C<sub>6</sub>**, **C<sub>8</sub>** and **C<sub>10</sub>** (top to bottom) with the same anchor groups.

## 4.8 Transport calculations

Here, the GOLLUM transport code is used to calculate the transmission coefficients  $T(E)$  for alkane chains with terminal groups (Amine) binding to the gold (111) surfaces. I will investigate the transmission coefficients  $T(E)$ , in more detail and I shall compare the conductance against some experimental measurements.

### 4.8.1 Transmission coefficient of alkane chains with Amine as terminal group

Previous published studies [12-28], predict the Fermi energy is near the middle of the HOMO-LUMO gap regardless to the type of the anchor group. In this theoretical investigation, I choose the DFT-predicted Fermi level (black-dashed line of Figure 4.4) to compare with experimental

measurements. The transmission coefficients of the alkane chains with (Au-Amine) of different lengths ( $n=3-10$ ) are shown in Figures (4.4 and 4.5).

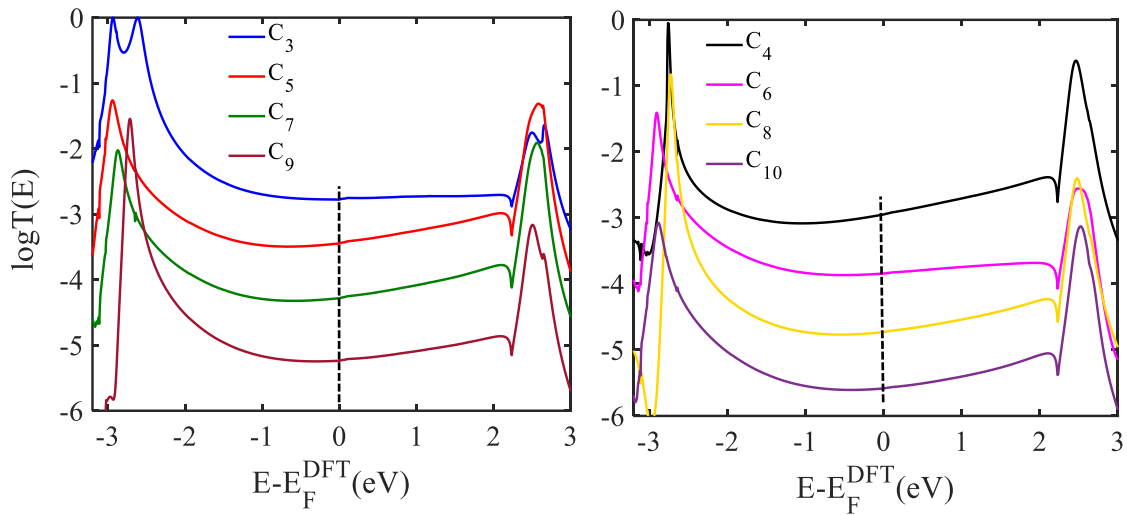


Figure 4. 4. Transmission coefficient curves of alkane chains . (Left panel) and (right panel) represent transmission coefficients  $T(E)$  of alkane chains with odd (left) and even (right) number of carbon atoms against electron energy  $E$ .

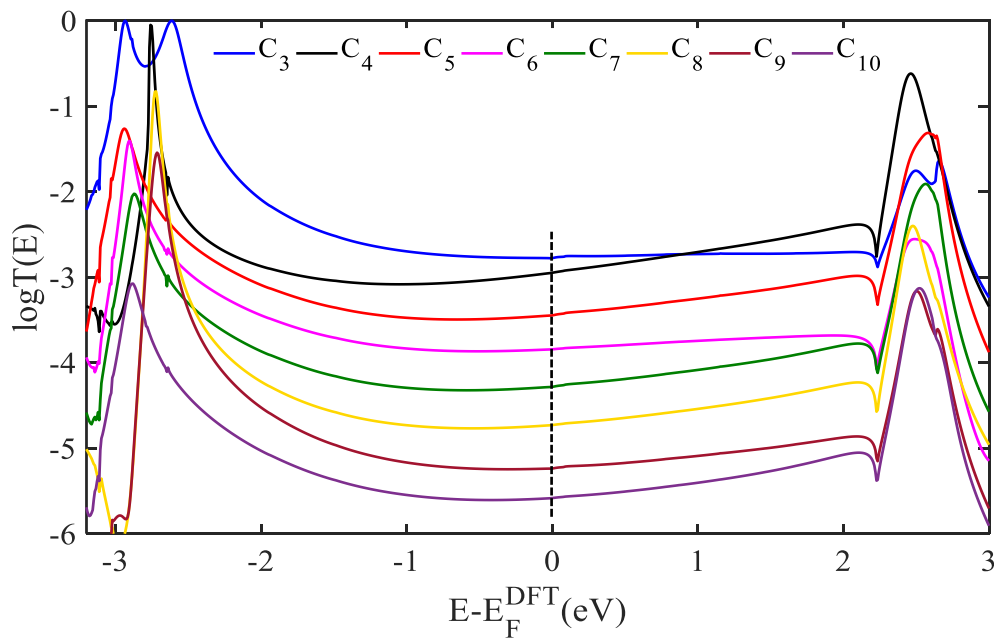


Figure 4. 5. Transmission coefficient curves of alkane chains with (Au-Amine) for both odd and even number of carbon atoms of linear chains against electron energy  $E$ .

Figures 4.4 and 4.5, illustrate the relationship between transmission coefficient and the length of alkane chains. As expected, the conductance decreases exponentially with increasing the length of the chain from 3 to 10  $-CH_2$  units. The amount of the decreasing in the conductance value (ie the decay constant) is approximately constant and as follows -3.0, -4.0, -4.9 and -5.7 for even chains  $C_4$ ,  $C_6$ ,  $C_8$  and  $C_{10}$  respectively. Similarly, -2.72, -3.5, -4.30 and -5.31 for odd chains  $C_3$ ,  $C_5$ ,  $C_7$  and  $C_9$  respectively. Figure 4.6 shows a conductance comparison between odd and even alkane chains (green and purple lines).

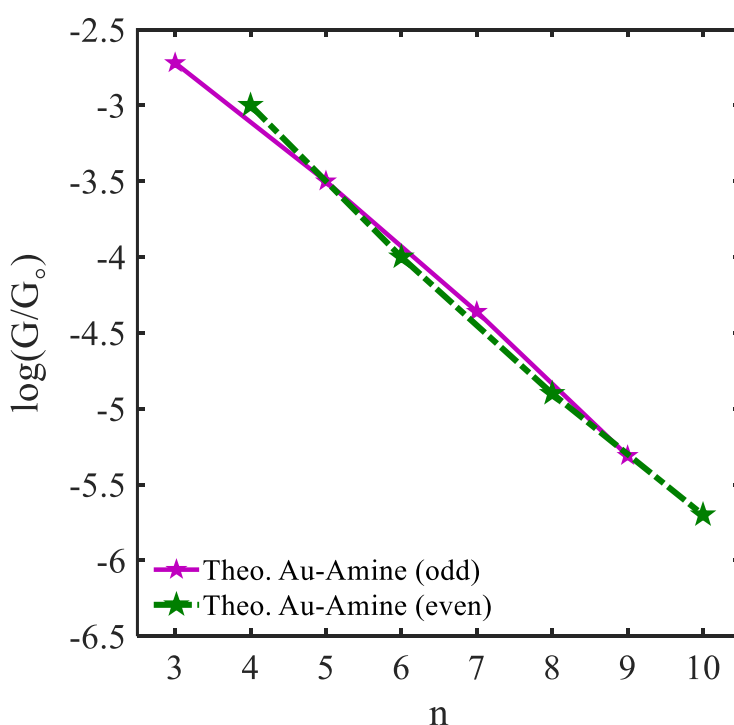


Figure 4. 6. Length dependence of the conductance of a single-molecule Au| linear chains |Au junction with Au-Amine covalent bonds connecting the ends of the alkane to gold electrodes. The purple line and the green dashed line show the DFT conductances for odd and even number of  $-CH_2$  units respectively.

#### 4.8.2 Comparison between theory and experiment of amine anchor

To test my simulations, I shall check the DFT calculations against STM measurements. For this comparison, I found two different sets of measurements for the studied molecules (group-

1 [15] and group-2 [16]). For some reason, the two experimental groups managed to measure only the even chains as shown in Table 4.4.

Table 4. 3. Conductances of two STM measurements and DFT simulations of linear alkane chains terminated with  $\text{NH}_2$  anchors. Simulations are taken at the DFT-predicted Fermi ( $E - E_F = 0 \text{ eV}$ ).

Chains	DFT conductance $\log(G/G_0)$	STM conductance $\log(G/G_0)$ group-1	STM conductance $\log(G/G_0)$ group-2
<b>C<sub>3</sub></b>	-2.72	==	==
<b>C<sub>4</sub></b>	-3.0	-2.69	-3.04
<b>C<sub>5</sub></b>	-3.5	==	==
<b>C<sub>6</sub></b>	-4	-3.52	-4
<b>C<sub>7</sub></b>	-4.30	==	==
<b>C<sub>8</sub></b>	-4.9	-4	-5
<b>C<sub>9</sub></b>	-5.31	==	==
<b>C<sub>10</sub></b>	-5.7	-5	-6

== No experimental value is available.

To have a better understanding of this comparison, I plot these results as shown in Figure 4.7. This Figure shows that my simulations accurately predict the conductance trend of these alkane chains. It also illustrates how the experimental measurements vary from one STM device to another (blue- against red-line). This difference is understandable due to many parameters for instance, solvent, temperature and so on. My simulations results (black-line), agree well with group-2 than group-1.

To obtain the decay constant, the slope of each line is taken and the DFT-slope is compared with the STM-slopes. The DFT-line possesses a slope of approximately -0.42, and STM-slopes are -0.37 and -0.49 (group-1 and group-2 respectively).

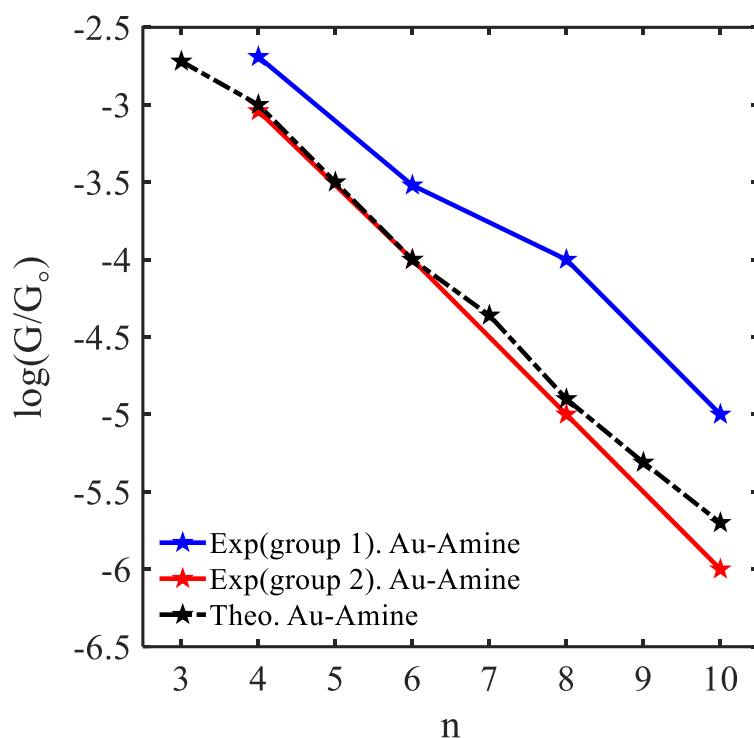


Figure 4. 7. STM measreaments versus DFT simulation of alkane chains terimenated with  $\text{NH}_2$  anchor. Two set of measurements from different experimental group (blue- and red-line), and DFT calculations (black-line).

#### 4.9 Studied alkane chains with thiol as terminal group

I shall repeat the same calculations that have been described in above sections (amine anchor). For the thiol anchor, the hydrogen atoms from both ends have removed when attached to the Au electrodes. In the following sections, I will study linear alkane chains consisting of 8 molecules based on the molecular length and terminated with SH.

##### 4.9.1 Geometries of the isolated alkane chains terminated with a thiol anchor

The 8 chains are all terminated with two thiol anchors (SH), as shown in Figure 4.9. The odd number of molecules are as follows: **C<sub>3</sub>**, **C<sub>5</sub>**, **C<sub>7</sub>** and **C<sub>9</sub>**, as shown in left panel of Figure 4.9, while the even molecules are: **C<sub>4</sub>**, **C<sub>6</sub>**, **C<sub>8</sub>** and **C<sub>10</sub>**, as shown in the right panel of Figure 4.9 (top to bottom respectively).

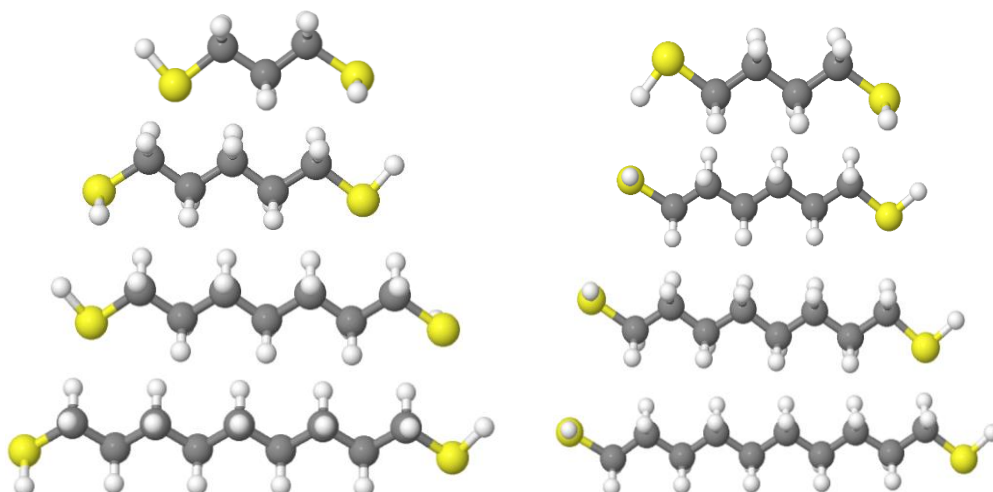


Figure 4. 8. Alkane chains: Fully relaxed isolated molecules, of different length 3-10 carbon atoms. (Left panel) shows the odd chains **C<sub>3</sub>**, **C<sub>5</sub>**, **C<sub>7</sub>** and **C<sub>9</sub>** while (right panel) represents the even ones **C<sub>4</sub>**, **C<sub>6</sub>**, **C<sub>8</sub>** and **C<sub>10</sub>**, both chains are terminated with thiol anchors.

#### 4.10 Frontier orbitals for studied molecules

The plots below show iso-surfaces of the HOMO and LUMO along with their energies of the alkane chains, including **C<sub>3</sub>** to **C<sub>10</sub>** in the gas phase as shown in Tables 4.5-4.7.

Table 4. 4. Comparison between the frontier molecular orbitals of alkane chain, including C<sub>3</sub>, C<sub>4</sub> and C<sub>5</sub> in the gas phase.

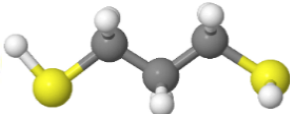

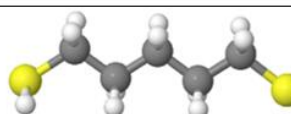
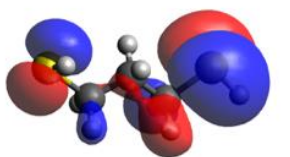
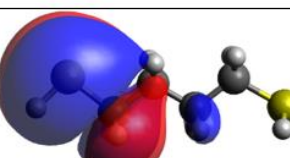
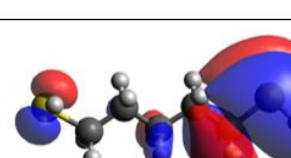
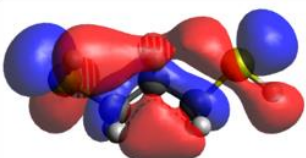
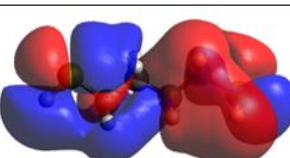
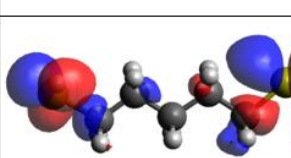
Chains	C <sub>3</sub>	C <sub>4</sub>	C <sub>5</sub>
Mol.			
HOMO			
eV	-4.8	-4.80	-4.7
LUMO			
eV	0.26	0.45	0.49

Table 4. 5. Comparison between the frontier molecular orbitals of alkane chain, including C<sub>6</sub>, C<sub>7</sub> and C<sub>8</sub> in the gas phase.

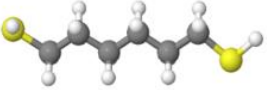
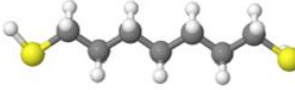
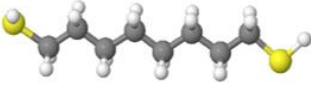
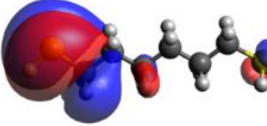
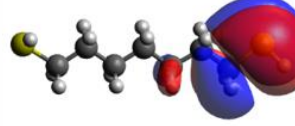
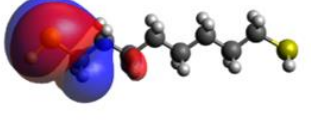
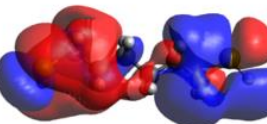
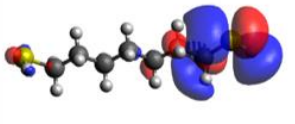
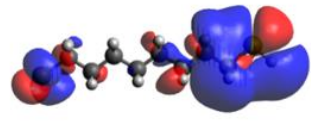
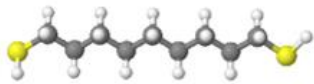

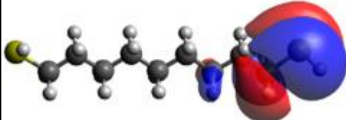
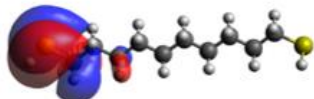
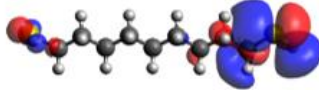
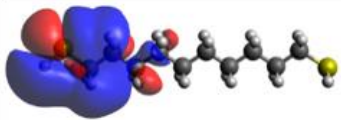
Chains	C <sub>6</sub>	C <sub>7</sub>	C <sub>8</sub>
Mol.			
HOMO			
eV	-4.75	-4.70	-4.72
LUMO			
eV	0.50	0.54	0.56



Table 4. 6. Comparison between the frontier molecular orbitals of alkane chain, including **C<sub>9</sub>** and **C<sub>10</sub>** in the gas phase.

Chains	C <sub>9</sub>	C <sub>10</sub>
Mol.		
HOMO		
eV	-4.7	-4.71
LUMO		
eV	0.56	0.57

#### 4.11 Binding energy of linear chain on gold

Figure 4.9, shows the binding energy of an alkane chain (i.e:  $C_4$ ). The thiol anchor possesses a strong bond to under-coordinated gold electrode compared to other anchors such as amine. The equilibrium distance (i.e. the minimum of the binding energy curve), for thioether anchor is found to be approximately 2.4 Å, with binding energy of approximately -2.0 eV.

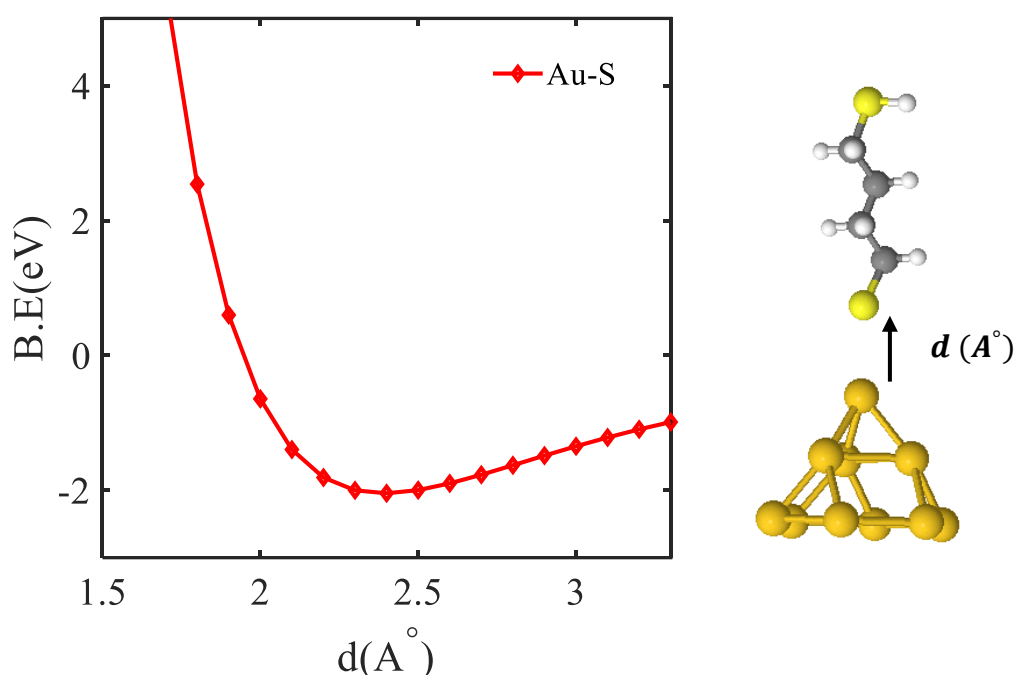


Figure 4. 9. An example of alkane molecule terminated with a thiol anchor on a gold tip :( Left) Binding energy of  $C_4$  alkane molecule to gold as a function of molecule-contact distance. The equilibrium distance (i.e. the minimum of the binding energy curve) is found to be approximately 2.4 Å, for Au-S. (Right) its idealised ad-atom configuration at the Au lead interface Au-thiol. Key: C = grey, H = white, S = light yellow, Au = dark yellow.

#### 4.12 Optimised DFT Structures of Compounds in their Junctions

Here are a few examples of optimised DFT structures of the alkane chains, in their junctions as shown in the Figure 4.10.

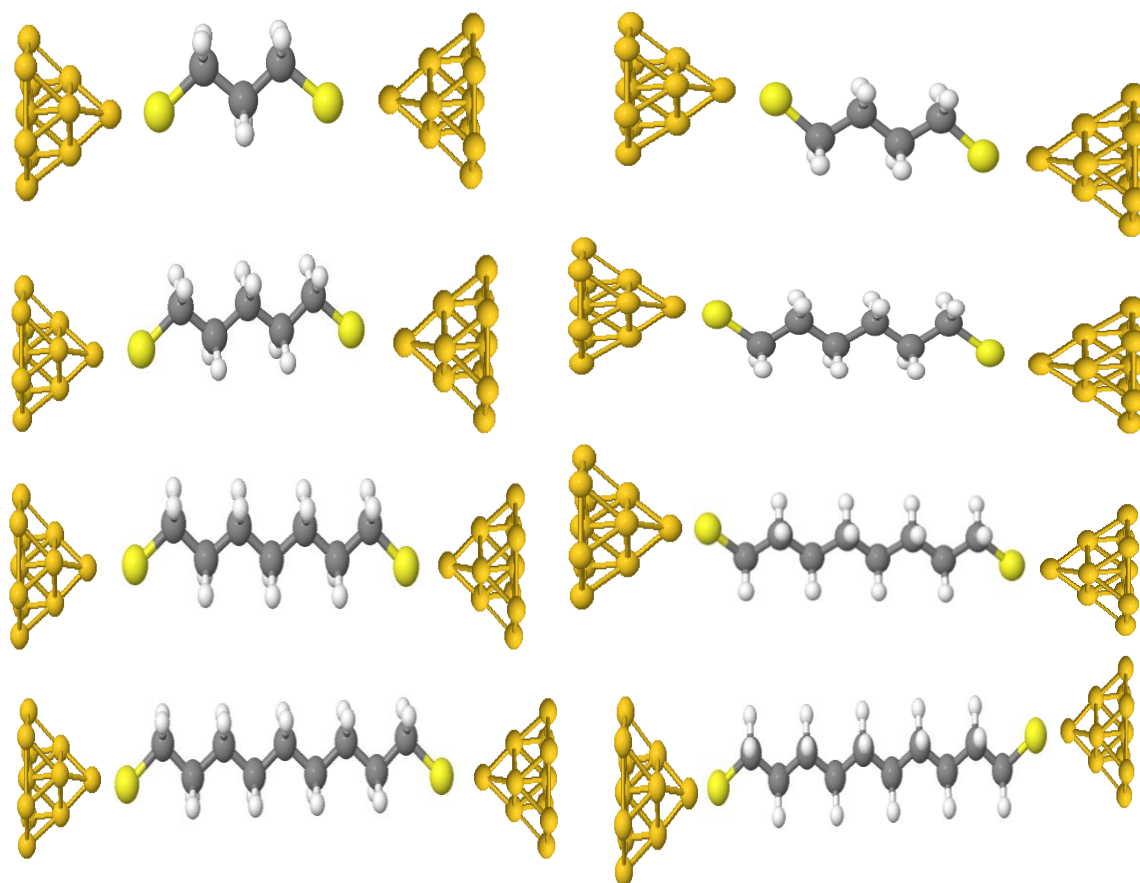


Figure 4. 10. Examples of fully relaxed alkane derivatives in Au|molecule|Au junctions.

(Left panel) shows odd number of linear chains  $C_3$ ,  $C_5$ ,  $C_7$  and  $C_9$  (top to bottom) connected to gold electrodes via thiol anchor groups. (Right panel) shows even number of linear chains  $C_4$ ,  $C_6$ ,  $C_8$  and  $C_{10}$  (top to bottom) with the same anchor groups.

#### 4.13 Transmission coefficient of alkane chains with Thiol as terminal group

The Fermi energy is predicted to be approximately HOMO dominated due to the presence of thiol anchor group [12-14]. In this study, I choose the DFT-predicted Fermi level (black-dashed line of Figure 4.11) to compare with the experimental results. The transmission coefficients of the alkane chains with (Au-S) of different lengths ( $n=3-10$ ) are shown in

Figures 4.11 and 4.12.

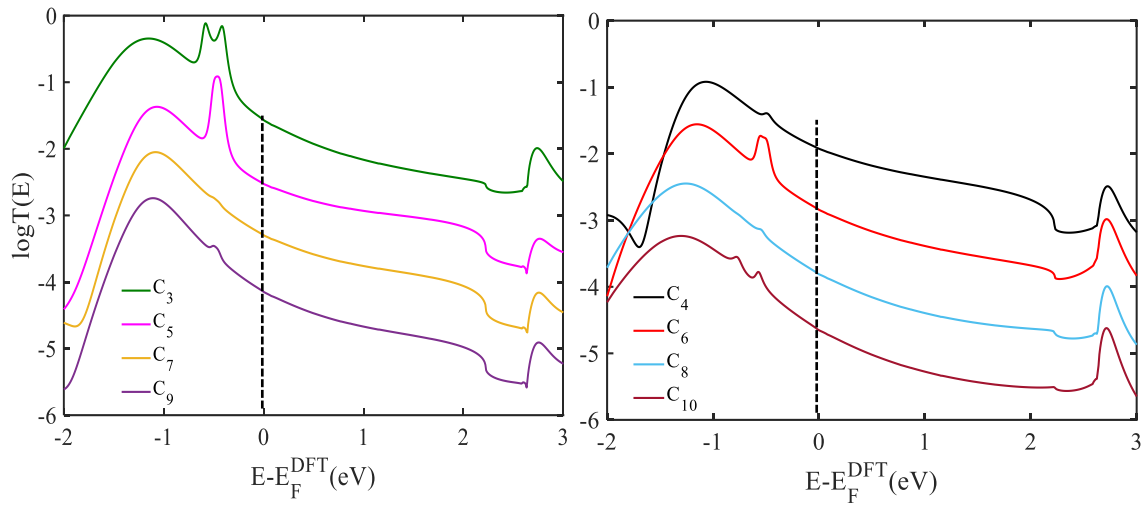


Figure 4. 11. Transmission coefficients curves of alkanes chains with (Au-S) . (Left panel) and (right panel) represent transmission coefficients  $T(E)$  of alkane chains with odd (left) and even (right) number of carbon atoms against electron energy  $E$ .

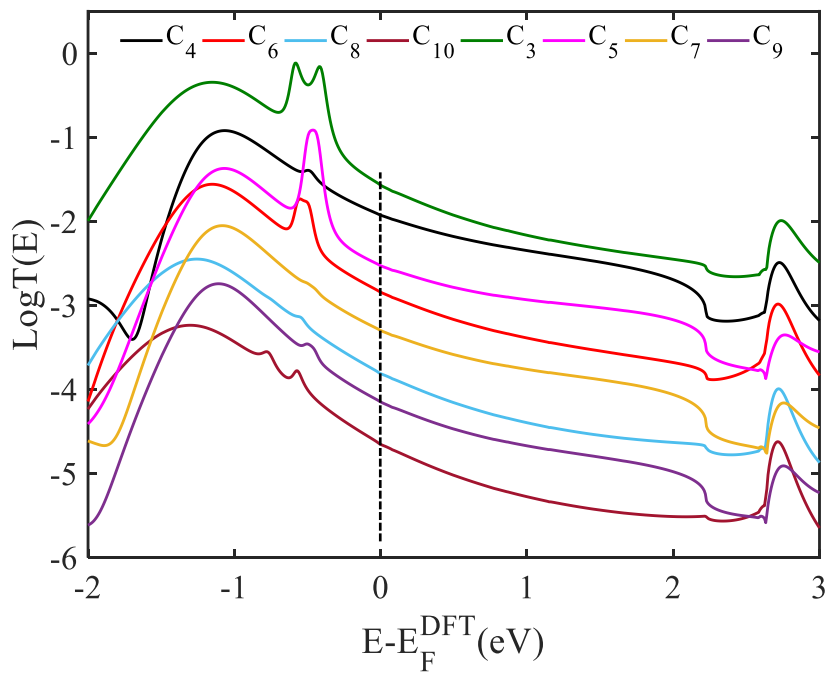


Figure 4. 12. Transmission coefficients of alkanes chains with (Au-S) for both odd and even number of carbon atoms of linear chains against electron energy  $E$ .

Figures 4.11 and 4.12, illustrate the relationship between transmission coefficient and the length of alkane chains. Again, as expected, the conductance decreases exponentially with increasing length of the chain from 3 to 10  $-CH_2$  units. The amount of the decreasing in the conductance value is approximately constant and as follows -2, -3, -3.8 and -4.65 for even chains  $C_4$ ,  $C_6$ ,  $C_8$  and  $C_{10}$  respectively. Similarly, -1.57, -2.54, -3.3 and -4.14 for odd chains  $C_3$ ,  $C_5$ ,  $C_7$  and  $C_9$  respectively, as shown in Figure 4.13.

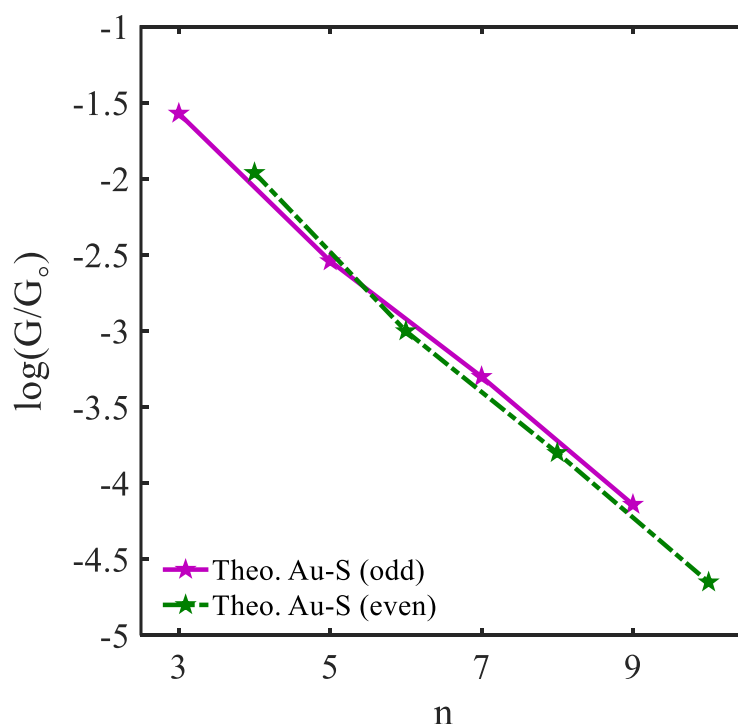


Figure 4. 13. Length dependence of the conductance of a single-molecule Au| linear chains |Au junction with Au-S covalent bonds connecting the ends of the alkane to gold electrodes. The purple line and the green dashed line show the DFT conductances of odd and even number of  $-CH_2$  units respectively.

#### 4.13.1 Comparison between theory and experiment of thiol anchor

To benchmark my simulations, I am going to compare the DFT calculations with STM measurements. For this purpose, I found a set of measurements for the studied molecules [13].

Again, the experimental measurements are available only the even chains **C<sub>6</sub>**, **C<sub>8</sub>** and **C<sub>10</sub>** as shown in Figure 4.14.

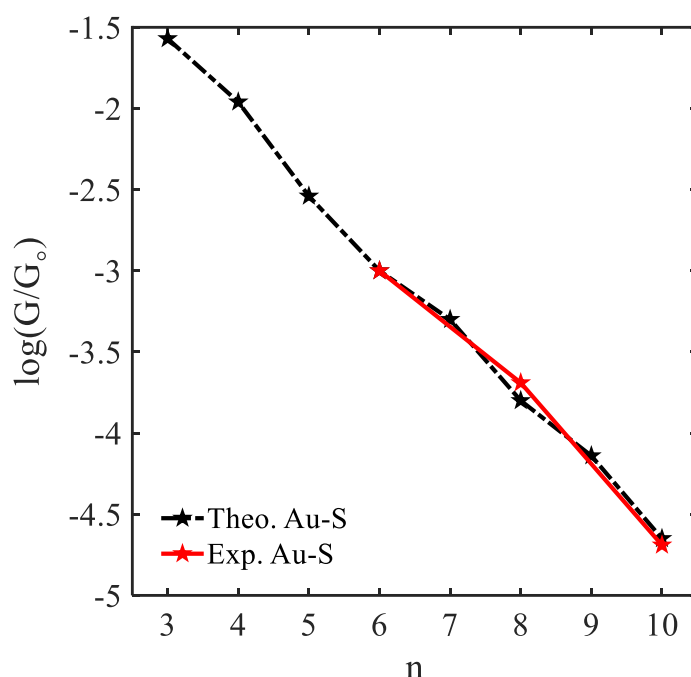


Figure 4. 14. STM measurements versus DFT simulation of alkane chains terminated with thiol anchor. The black dashed line shows the DFT calculations whereas the red line represents experimental measurements of **C<sub>6</sub>**, **C<sub>8</sub>** and **C<sub>10</sub>**

Figure 4.14 shows my simulations accurately predict the conductance trends of these alkane chains. At the chosen DFT Fermi energy, excellent agreement between the DFT predictions and STM measurements of **C<sub>6</sub>**, **C<sub>8</sub>** and **C<sub>10</sub>** chains is obtained.

Up to this point, I have explored two anchors amine and thiol. For comparison purposes, the DFT simulations of the two anchors are shown in the left panel of Figure 4.15, while STM measurements are shown in the right panels. The STM results support these simulation predictions.

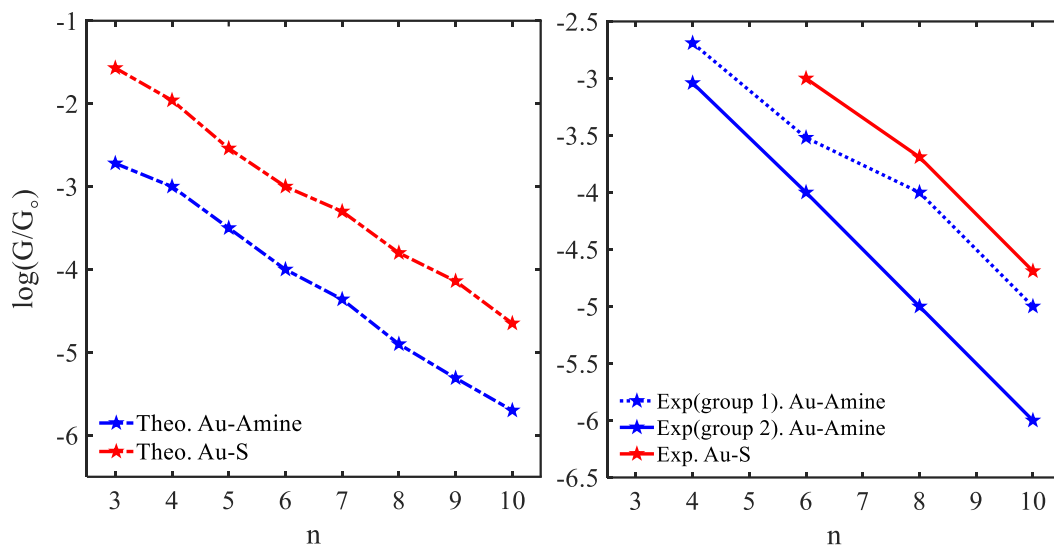


Figure 4. 15. Chain-length dependence of the single-junction Au |alkane linear chain | Au conductance for two different terminal groups. (Left panel) and (right panel) represent logarithmic conductances of DFT and STM (left to right), as a function of length for two different terminal groups Au- Amine (theoretical blue-dashed line of left panel and experimental blue and blue-dot lines of right panel) and Au-S (theoretical red-dashed line of left panel and experimental red line of right panel).

#### 4.14 Alkane chains with carbon as a terminal group

Up to this point, I have investigated 2 linker groups including amine and thiol. The next linker to be explored in this study is the direct carbon anchor.

##### 4.14.1 Geometries of the isolated alkane chains terminated directly with a carbon anchor

Again 8 alkane chains with different length are going to be discovered (4 odd and 4 even). The 8 chains are all terminated with two carbon anchors ( $CH_3$ ), as shown in Figure 4.16. The odd number of molecules are as follows:  $C_3$ ,  $C_5$ ,  $C_7$  and  $C_9$ , as shown in left panel of Figure 4.16, while the even molecules are:  $C_4$ ,  $C_6$ ,  $C_8$  and  $C_{10}$ , as shown in the right panel of Figure 4.16 (top to bottom respectively).

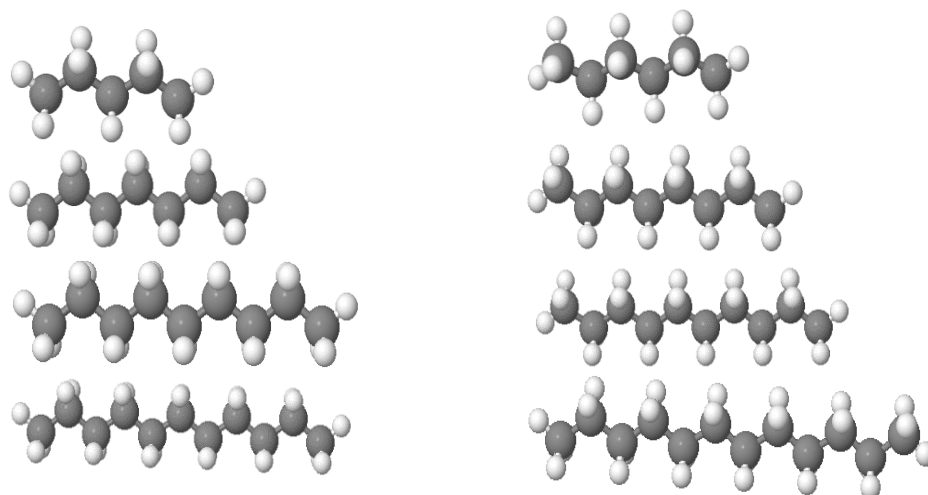


Figure 4. 16. Alkane chains: Fully relaxed isolated molecules, of different length 3-10 carbon atoms. (Left panel) shows the odd chains **C<sub>3</sub>**, **C<sub>5</sub>**, **C<sub>7</sub>** and **C<sub>9</sub>** while (right panel) represents the even ones **C<sub>4</sub>**, **C<sub>6</sub>**, **C<sub>8</sub>** and **C<sub>10</sub>**, both chains are terminated with carbon anchors ( $CH_3$ ).

#### 4.15 Frontier orbitals for the studied molecules

The plots below show iso-surfaces of the HOMO and LUMO along with their energies of the alkane chains, including **C<sub>3</sub>** to **C<sub>10</sub>** in the gas phase as shown in Tables 4.8- 4.10.



Table 4. 7. Comparison between the frontier molecular orbitals of alkane chain, including C<sub>3</sub>, C<sub>4</sub> and C<sub>5</sub> in the gas phase.


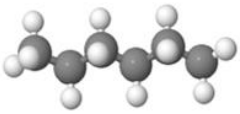

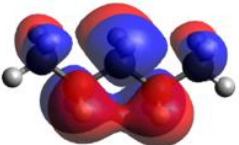
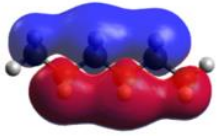
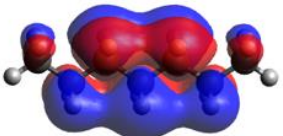
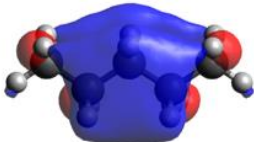
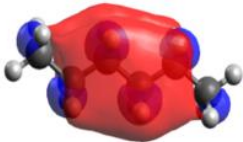
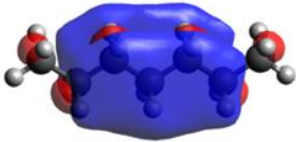
Chains	C <sub>3</sub>	C <sub>4</sub>	C <sub>5</sub>
Mol.			
HOMO			
eV	-7.2	-7.19	-7.2
LUMO			
eV	2.1	2.1	2.0

Table 4. 9. Comparison between the frontier molecular orbitals of alkane chain, including C<sub>3</sub>, C<sub>4</sub> and C<sub>5</sub> in the gas phase.




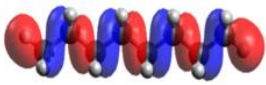
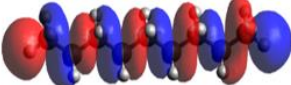
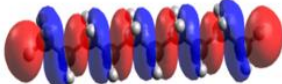
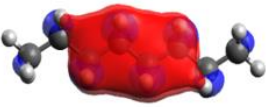
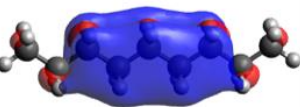
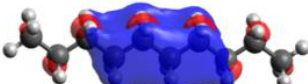

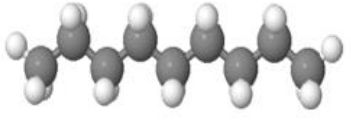
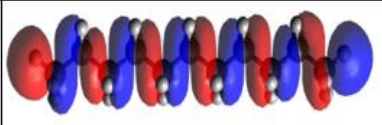
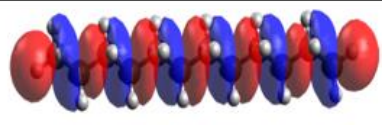
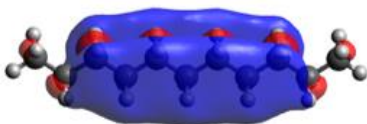
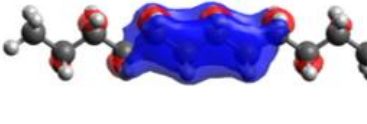
Chains	C <sub>6</sub>	C <sub>7</sub>	C <sub>8</sub>
Mol.			
HOMO			
eV	-7.14	-7.1	-7.0
LUMO			
eV	2.0	2.1	2.0

Table 4. 9. Comparison between the frontier molecular orbitals of alkane chain, including **C<sub>9</sub>** and **C<sub>10</sub>** in the gas phase.

Chains	C <sub>9</sub>	C <sub>10</sub>
Mol.		
HOMO		
eV	-7.0	-6.9
LUMO		
eV	1.98	1.9

#### 4.16 Binding energy of linear chain on gold

The counterpoise method is employed again to calculate the binding energy of alkane linear chains (as shown in Figure 4.18) in the presence of Au-C bond; ie. I just repeat the same procedure that described in the section 4.7 and using the equation (4.1). Figure 4.17 shows the binding energy of an alkane chain. This curve has a strong binding to an under-coordinated gold apex atom; the Au-C covalent binding energy is approximately -1.8 eV.

Figure 4.17, shows the binding energy of an alkane chain (i.e: C<sub>5</sub>). The carbon direct anchor also possesses a strong bond to under-coordinated gold electrode compared to other anchors such as amine. The equilibrium distance (i.e. the minimum of the binding energy curve), for carbon direct anchor is found to be approximately 2.3 Å, with binding energy of approximately -1.8 eV.

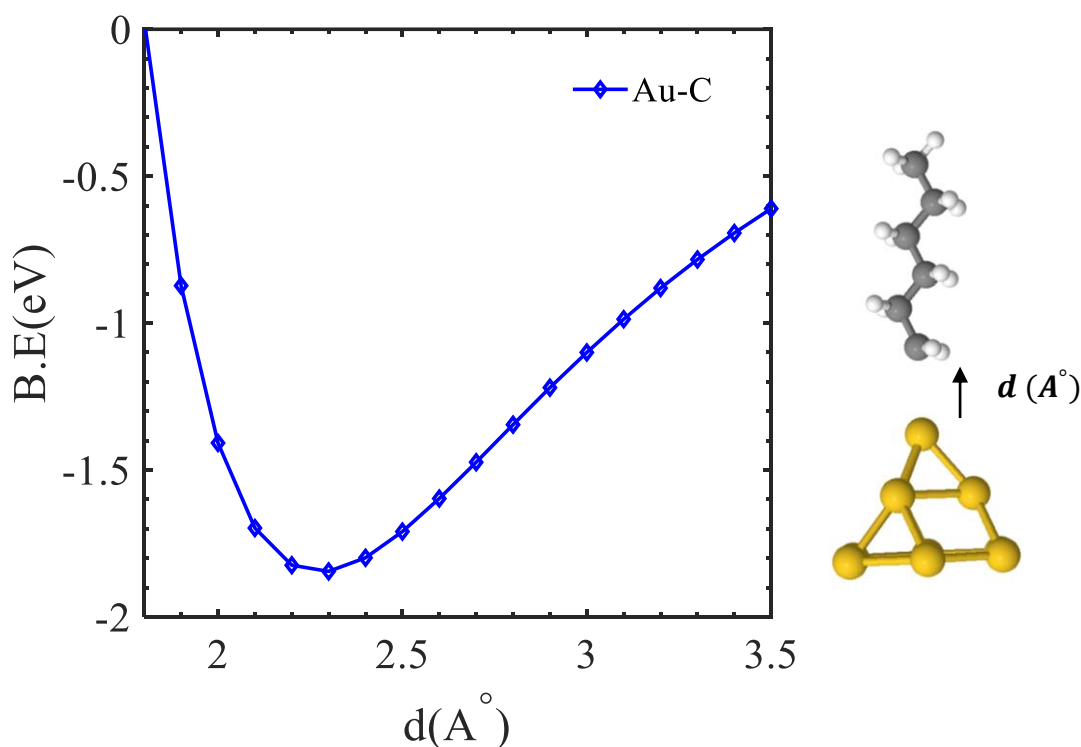


Figure 4. 17. An example of alkane molecule terminated with a carbon on a gold tip :( Left) Binding energy of C alkane molecule to gold as a function of molecule-contact distance. The equilibrium distance (i.e. the minimum of the binding energy curve) is found to be

approximately 2.3 Å, for Au-C. (Right) its idealised ad-atom configuration at the Au lead interface Au-thiol. Key: C = grey, H = white, Au = dark yellow.

#### 4.17 Optimised DFT Structures of Compounds in their Junctions

Figure 4.18 shows some examples of optimised DFT structures of alkane direct anchor chains in Au-Au junctions. It is worth mentioning, that one of the 3 hydrogen atoms of the methyl group has removed to form a direct carbon gold bond.

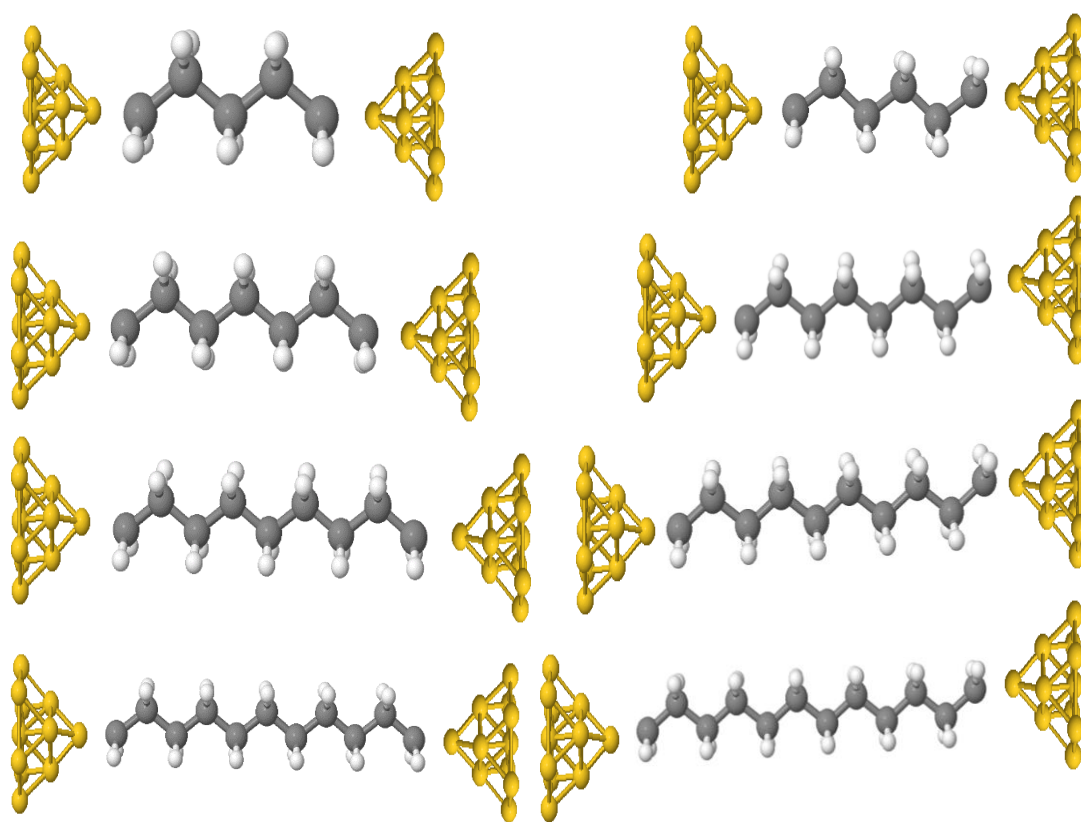


Figure 4. 18. Examples of fully relaxed alkane derivatives in Au|molecule|Au junctions. (Left panel) shows odd number of linear chains **C<sub>3</sub>**, **C<sub>5</sub>**, **C<sub>7</sub>** and **C<sub>9</sub>** (top to bottom) connected to gold electrodes via direct carbon anchor groups. (Right panel) shows even number of linear chains **C<sub>4</sub>**, **C<sub>6</sub>**, **C<sub>8</sub>** and **C<sub>10</sub>** (top to bottom) with the same anchor groups.

#### 4.18 Transmission coefficient of alkane chains with carbon as terminal group

For the direct carbon-gold bond, the Fermi energy is predicted to be HOMO dominated due to the presence of the (Au-C) anchor group. In this study, again I choose the DFT-predicted Fermi level (black-dashed line of Figure 4.19) to compare with the experimental results.

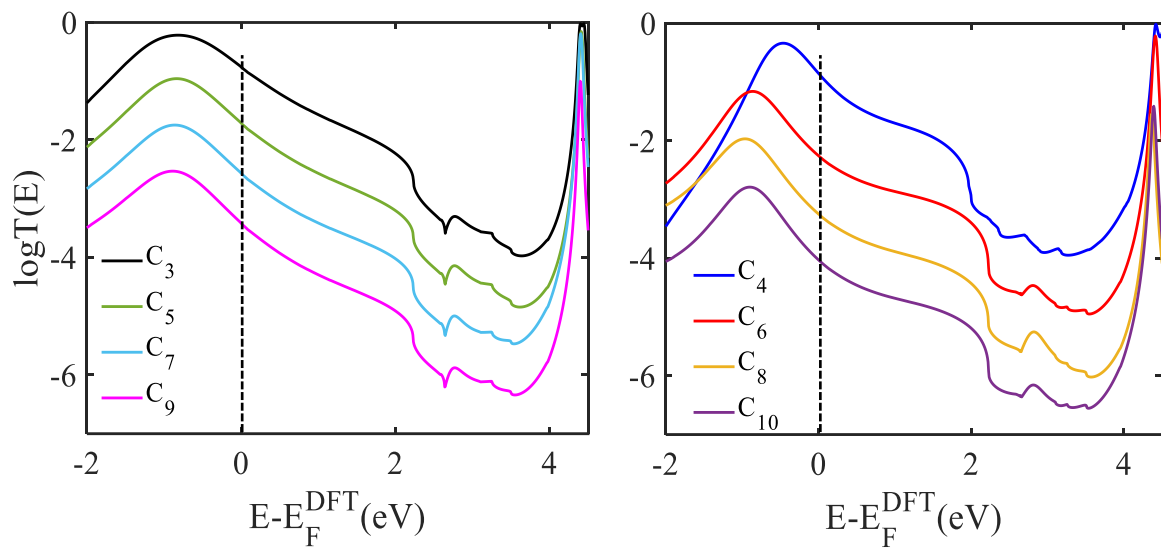


Figure 4. 19. Transmission coefficients curves of alkanes chains with (C-Au) . (Left panel) and (right panel) represent transmission coefficients  $T(E)$  of alkane chains with odd (left) and even (right) number of carbon atoms against electron energy  $E$ .

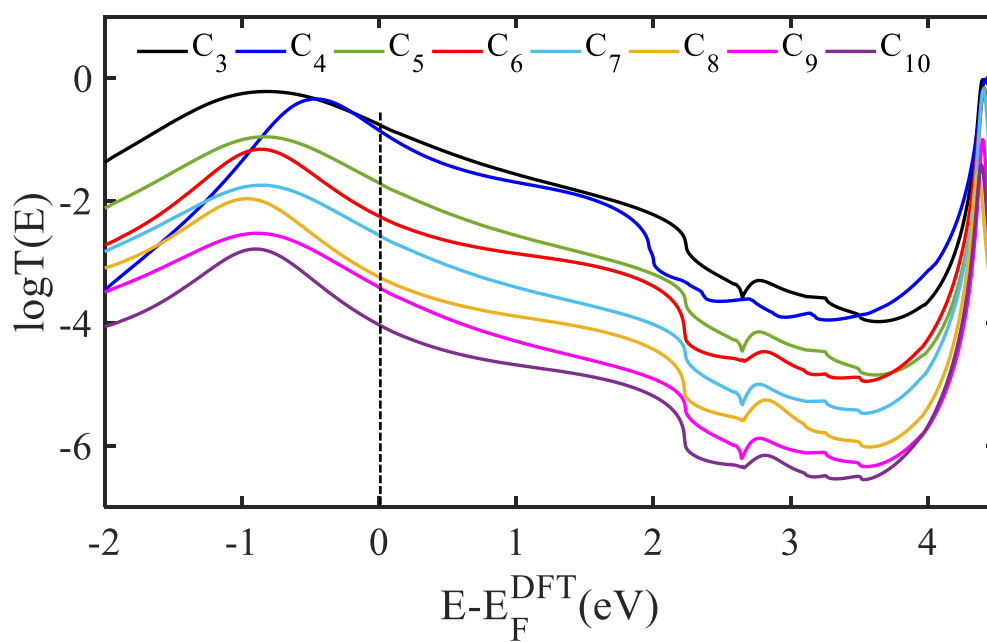


Figure 4. 20. Transmission coefficients of alkanes chains with (C-Au) for both odd and even carbon atoms of linear chains against electron energy  $E$ .

Figures 4.19 and 4.20, determine the relationship between transmission coefficient and the length of alkane chains. Meaning, the conductance decreases exponentially with increasing the length of the chain from 3 to 10  $-CH_2$  units. The rate of the decrease in the conductance is approximately constant and as follows -1, -2.1, -3.1 and -4.0 for even chains  $C_4$ ,  $C_6$ ,  $C_8$  and  $C_{10}$  respectively. Similarly, -0.75, -1.75, -2.56 and -3.40 for odd chains  $C_3$ ,  $C_5$ ,  $C_7$  and  $C_9$  respectively.

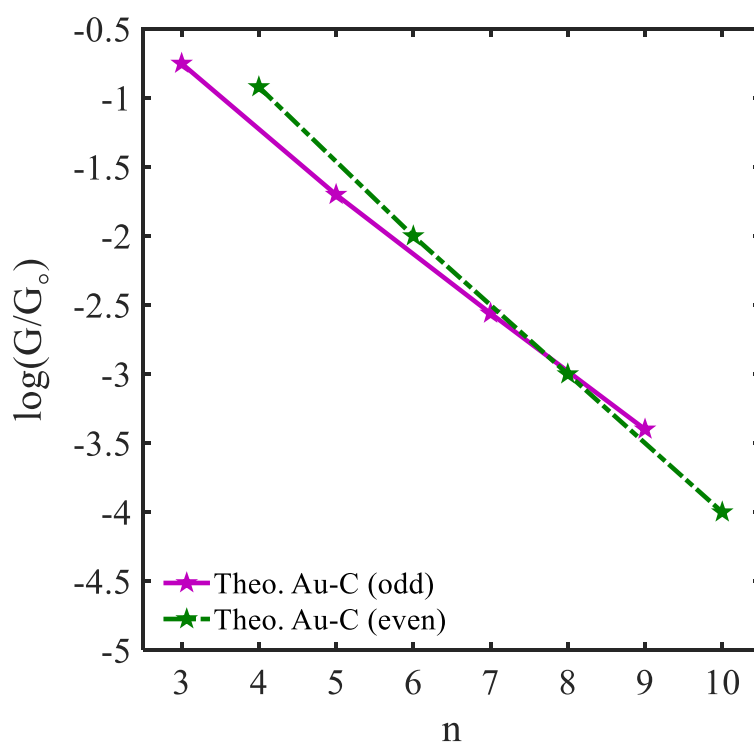


Figure 4. 21. Length dependence of the conductance of a single-molecule Au| linear chains |Au junction with C-Au covalent bonds connecting the ends of the alkane to gold electrodes. The purple line and the green dashed line show the DFT conductances of odd and even number of  $-CH_2$  units respectively.

#### 4.18.1 Comparison between theory and experiment of carbon anchor

As demonstrated with amine and thiol anchors, I shall examine the DFT calculations against STM measurements. For the comparison purpose, I have found a set of experimental measurements that includes 3 even linear chains **C<sub>4</sub>**, **C<sub>6</sub>** and **C<sub>8</sub>** [17] as shown in Figure 4.22.

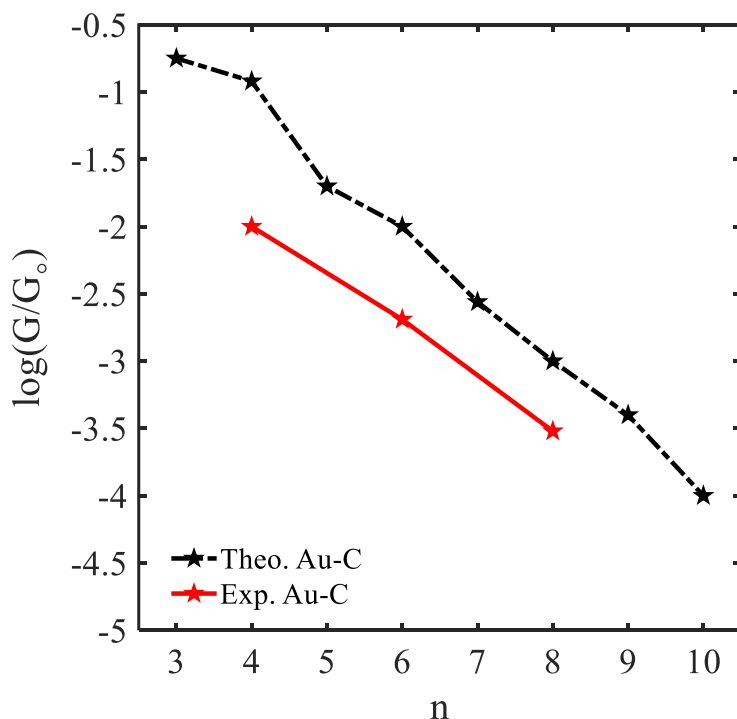


Figure 4. 22. STM measreaments versus DFT simulation of alkane chains terimenated with carbon anchor. The black dashed line shows the DFT calculations where the red line represents experimental measurements.

Figure 4.22, demonstrates the accuracy of the DFT predictions for the slope, although the theoretical conductance values are higher than the measured ones.



#### 4.19 Transmission coefficient of alkane chains with Thiomethyl as terminal group

Following the same procedure described in sections 4.3 - 4.18 (amine, thiol and direct carbon anchors). I shall briefly investigate the thiomethyl anchor by employing only 3 linear chains and I am going to investigate this anchor in more detail in chapter 5 (sections 5.3-5.8), as I will use these linear chains to test the Kirchhoff's law.

Here, I increase the length of the chain by adding two  $-CH_2$  units to form 3 molecules and as follows: **C<sub>6</sub>**, **C<sub>8</sub>** and **C<sub>10</sub>**. The three chains are terminated with two thiomethyl anchors (SMe) as shown in Figure 4.23.

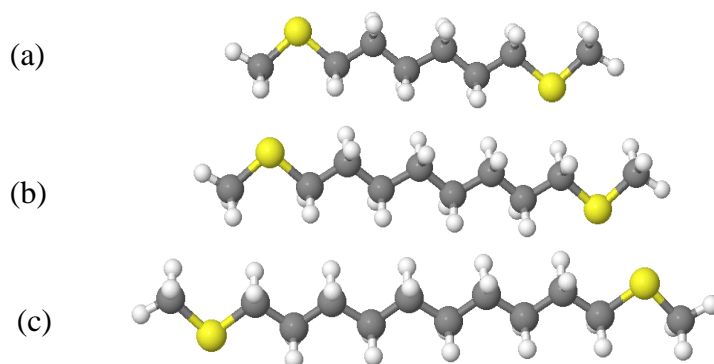


Figure 4. 23. Alkane chains: Fully relaxed isolated molecules, of different length of carbon atoms, mainly even chains **C<sub>4</sub>**, **C<sub>6</sub>**, **C<sub>8</sub>** and **C<sub>10</sub>**, and all are terminated with SMe anchors.

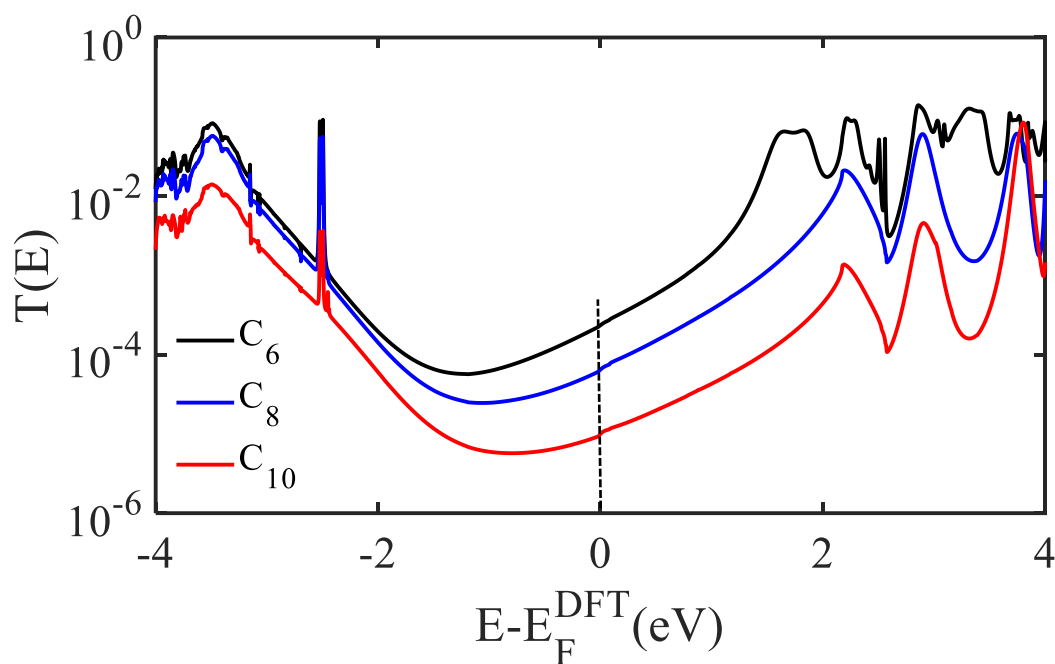


Figure 4. 24. Transmission coefficient curves of alkanes chains . Transmission coefficient  $T(E)$  curves of even alkane chains against electron energy  $E$ .

The same message of the other anchors was found; ie an exponential decrease in conductance with increasing length is obtained. In the next section, I would like to finish this thorough investigation of alkane chains with different 4 terminal groups, by making a comparison between DFT predictions and STM measurements.

#### 4.20 STM versus DFT Conductance of four different terminal groups

In this section, I shall compare the conductance  $G$  of 4 different linear chains based on the terminal group. Each chain of these possesses different length. In DFT simulations the molecular length varies from 3 to 8  $-CH_2$  units, with 4 linker groups including  $NH_2$ , C, S and SMe. Similarly, for STM measurements except the molecular length is usually shorter mainly 3 or 4 chains for each anchor.

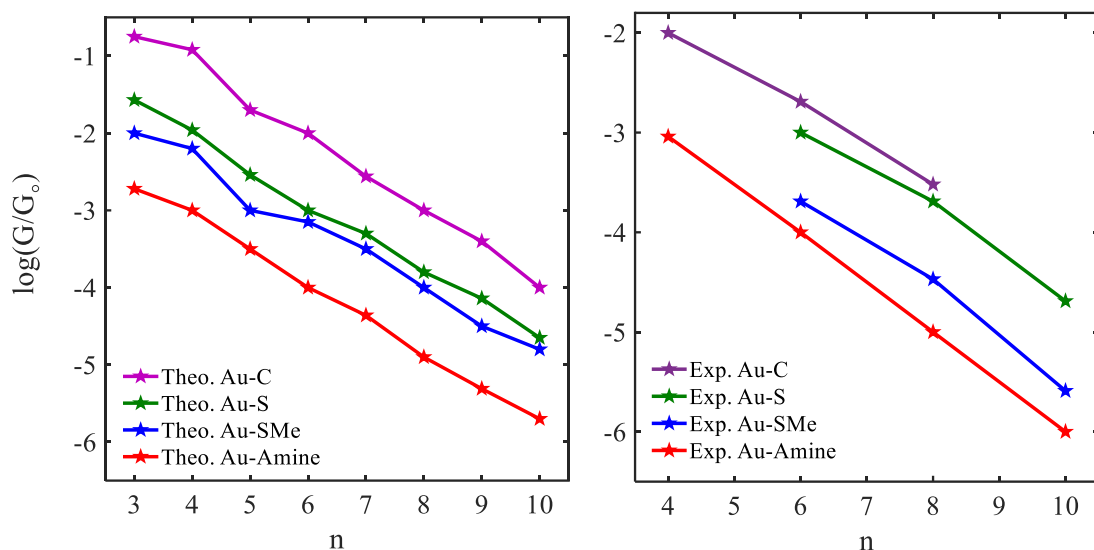


Figure 4. 25. Chain-length conductance dependence of Au |alkane linear chain | Au junctions for four different terminal groups. Logarithmic conductance of DFT and STM (left to right), as a function of the chain length of four different terminal groups Au- C (purple line), Au-S (green line), Au-SMe (blue line) and Au-Amine (red line).

The DFT simulations predict that the conductances follow the order  $C > S > SMe > NH_2$  (left panel). The DFT prediction order for the 4 anchors is well supported by STM measurements (right panel), as shown in Figure 4.25. In general, the theoretical conductances are slightly higher than the measured ones, in agreement with literature values.

#### 4.21 Exponential decay $\beta$ calculations

Formula 4.2 uses to calculate the  $\beta$  factor of linear alkane chains [29]. The conductance  $G$  was observed to decay exponentially with length ( $n$ ).

$$\frac{G}{G_0} = A e^{-\beta n} \quad (4.2)$$

Solving (4.2) with respect to  $\beta$

$$-\beta = \log \left( \frac{G_{n+1}}{G_0} \right) - \log \left( \frac{G_n}{G_0} \right) \quad (4.3)$$

Where  $n$  is number of methylene  $-CH_2$  units,  $\beta$  is decay constant per  $-CH_2$  unit and  $A$  is a constant will be discussed in detail later. In addition,  $G_n$  and  $G_{n+1}$  represent logarithmic conductance for each two neighbouring points (see Figure 4.25).

Table 4.11 shows  $\beta$  values for the 4 different linker groups that employ in this study.  $\beta$  represents the efficiency of electron transport along alkane chains and is regarded as an important parameter [29].

Table 4. 11.  $\beta$  values for different alkane chain length  $C_3$  to  $C_{10}$  terminated with four different anchor groups.

$\beta_{Anchor}$	$\beta_C$	$\beta_S$	$\beta_{SMe}$	$\beta_{NH_2}$
Range	0.5– 0.54	0.4–0.42	0.4	0.4–0.5

In the above table,  $\beta_C$ ,  $\beta_S$ ,  $\beta_{SMe}$  and  $\beta_{NH_2}$  represent  $\beta$  values for alkane chains terminated with C, S, SMe and amine respectively.

Table 4.11, demonstrates that  $\beta$  factors vary slightly from one anchor to another. For example, the direct carbon anchor possesses the  $\beta$  and it varies from 0.5 to 0.54. All in all, one could tell that  $\beta$  factor range from 0.4 to 0.54 per -CH<sub>2</sub> unit for the 4 anchors.

On the other hand,  $A$  constant simply represents Y-intercept values which could be used to calculate the distance between two desired lines by taking the difference between their constants (see Figure 4.25).

Table 4.12 represents  $A$  values for the 4 different linker groups that were used in this study.

Table 4. 12.  $A$  constant values for different alkane chain length C<sub>3</sub> to C<sub>10</sub> terminated with four different anchor groups.

$A_{Anchor}$	$A_C$	$A_S$	$A_{SMe}$	$A_{NH_2}$	order
Theo.	5.8	0.5	0.18	0.05	$A_C > A_S > A_{SMe} > A_{NH_2}$

In the above table,  $A_C$ ,  $A_S$ ,  $A_{SMe}$  and  $A_{NH_2}$  represent  $A$  values for alkane chains terminated with C, S, SMe and amine respectively.

Table 4.12 demonstrates  $A$  constant varies from one anchor to another. For example, the amine anchor possesses the lowest  $A$  with value 0.05. The second lowest  $A$  is the thiomethyl anchor with 0.018 followed by the thiol with 0.5. On the other hand, the direct carbon anchor shows the highest  $A$  with 5.8. Additionally, Table 4.12 shows that the order of  $A$  constant is taking the same order of  $G$  ( $G_C > G_S > G_{SMe} > G_{NH_2}$ ).

#### 4.21.1 Comparison between theory and experiment of $\beta$ factor

In sections above, theory simulations have been checked against experimental measurements of the 4 studied anchors in different molecular lengths. Here, I shall examine the predicted  $\beta$  and  $A$  values to the measured ones.

Table 4. 13. DFT prediction and STM measurement  $\beta$  factor comparison of different molecular alkane chain lengths for 4 different anchor groups including thiol, thiomethyl, direct carbon and amine. The experimental molecular lengths for direct carbon are: **C4**, **C6** and **C8**, thiol **C6**, **C8** and **C10**, thiomethyl **C6**, **C8** and **C10** and amine **C4**, **C6**, **C8** and **C10**, while for theory **C3** to **C10**.

$\beta_{Anchor}$	$\beta_C$	$\beta_S$	$\beta_{SMe}$	$\beta_{NH_2}$
Theo.	0.5– 0.54	0.4–0.42	0.4	0.4–0.5
Exp.	0.35–0.4 [31]	0.34–0.5 [29]	0.4–0.56[our]	0.48–0.5[29]

Table 4.13 reveals that the theoretical  $\beta$  factors are generally higher than the experimental ones, however, one could notice there is an excellent agreement between the DFT predictions and the STM measured  $\beta$  factors.

Additionally,  $A$  constants have been compared with some experimental results with the same anchors shown in Table 4.14.

Table 4. 14. DFT prediction and STM measurement  $A$  constants comparison of different molecular alkane chain lengths for 4 different anchor groups including thiol, thiomethyl, direct carbon and amine. The experimental molecular lengths for direct carbon are: **C4**, **C6**

and C<sub>8</sub>, thiol C<sub>6</sub>, C<sub>8</sub> and C<sub>10</sub>, thiomethyl C<sub>6</sub>, C<sub>8</sub> and C<sub>10</sub> and amine C<sub>4</sub>, C<sub>6</sub>, C<sub>8</sub> and C<sub>10</sub>, while for theory C<sub>3</sub> to C<sub>10</sub>.

$A_{Anchor}$	$A_C$	$A_S$	$A_{SMe}$	$A_{NH_2}$	order
Theo.	5.8	0.5	0.18	0.05	$A_C > A_S > A_{SMe} > A_{NH_2}$
Exp.	0.35[31]	0.4[29]	0.16[our]	0.08[29]	$A_C \approx A_S > A_{SMe} > A_{NH_2}$

Based on Table 4.14, the  $A$  constant values follow the same order experimentally and theoretically. However, there is a significant gap in  $A_C$  values theoretically and experimentally while DFT predictions and STM measurements agree exceptionally well on the remaining  $A$  constants.

#### 4.21 Conclusion

In summary, I have studied the frontier orbitals of different moleculars starting from C<sub>3</sub> to C<sub>8</sub>, with four different anchors including thiol, thiomethyl, direct carbon and amine, so, in total 32 linear chains have been investigated. The iso-surface plots show different behaviours of localised and delocalised weights of the HOMO and LUMO orbitals for the different linkers. These 4 linkers bind to gold metal differently, meaning that some bind more strongly than others; for instance thiol binds 7 times more strongly than thioether.

The conductance varies from one anchor to another and the order is C > S > SMe > NH<sub>2</sub>. The DFT predicted order is well-supported by STM measured values for the same anchors that I gathered from the literature. The  $\beta$  factor and  $A$  values have also predicted and examined against the STM measured and an excellent agreement was found for the 4 linkers.

## Bibliography

1. Chemistry LibreTexts. (2016). *4.12: Uses and Sources of Alkanes*. [online] Available at:  
[https://chem.libretexts.org/Bookshelves/Organic\\_Chemistry/Map%3A\\_Organic\\_Chemistry\\_\(Wade\)/03%3A\\_Structure\\_and\\_Stereochemistry\\_of\\_Alkanes/4.12%3A\\_Uses\\_and\\_Sources\\_of\\_Alkanes](https://chem.libretexts.org/Bookshelves/Organic_Chemistry/Map%3A_Organic_Chemistry_(Wade)/03%3A_Structure_and_Stereochemistry_of_Alkanes/4.12%3A_Uses_and_Sources_of_Alkanes).
2. www.sciencedirect.com. (n.d.). *Cycloalkane - an overview | ScienceDirect Topics*. [online] Available at: <https://www.sciencedirect.com/topics/chemistry/cycloalkane>.
3. M Soler, J., D Gale, J. and García, A. (2002). The SIESTA method for ab initio order-N materials simulation. *Journal of Physics: Condensed Matter*.
4. Parr, R. G., & Weitao, Y. (1994). *Density-Functional Theory of Atoms and Molecules*. Oxford University Press.
5. Kumar, A. (2012). A Brief Introduction to Thomas-Fermi Model in Partial Differential Equations.
6. Lieb, E. H. (1982). Erratum: Thomas-Fermi and related theories of atoms and molecules. *Reviews of Modern Physics*, 54(1), 311.
7. Dreizler, R. M. (1995). Density Functional Theory Vol. 337 of NATO ASI Series B, edited by EKV Gross and RM Dreizler.
8. Hohenberg, P., & Kohn, W. (1964). Inhomogeneous electron gas. *Physical review*, 136(3B), B864.
9. Kohn, W., & Sham, L. J. (1965). Self-consistent equations including exchange and correlation effects. *Physical review*, 140(4A), A1133.
10. Koch, W., Holthausen, M. C., & Kaupp, M. (2001). BUCHER-A Chemist's Guide to Density Functional Theory. *Angewandte Chemie-German Edition*, 113(5), 989-989.
11. Ferrer, J., Lambert, C.J., García-Suárez, V.M., Manrique, D.Z., Visontai, D., Oroszlany, L., Rodríguez-Ferradás, R., Grace, I., Bailey, S.W.D., Gillemot, K.,



- Sadeghi, H. and Algharagholy, L.A. (2014). GOLLUM: a next-generation simulation tool for electron, thermal and spin transport. *New Journal of Physics*, 16(9), p.093029.
12. Ismael, A., Wang, X., Bennett, T.L.R., Wilkinson, L.A., Robinson, B.J., Long, N.J., Cohen, L.F. and Lambert, C.J. (2020). Tuning the thermoelectrical properties of anthracene-based self-assembled monolayers. *Chemical Science*, 11(26), pp.6836–6841.
  13. Wang, X., Bennett, T. and Ismael, A. (2020). Scale-Up of Room-Temperature Constructive Quantum Interference from Single Molecules to Self-Assembled Molecular-Electronic Films. *Journal of the American chemical society*.
  14. Wang, X., Ismael, A., Almutlg, A., Alshammari, M., Al-Jobory, A., Alshehab, A., Bennett, T.L.R., Wilkinson, L.A., Cohen, L.F., Long, N.J., Robinson, B.J. and Lambert, C. (2021). Optimised power harvesting by controlling the pressure applied to molecular junctions. *Chemical Science*, 12(14), pp.5230–5235.
  15. Davidson, R., Ismael, A. and Lambert, C., 2018. Conductance of ‘bare-bones’ tripodal molecular wires. *RSC Advances*, 8(42), pp.23585-23590.
  16. González, M., Ismael, A., Grace, I. and Lambert, C., 2021. Interference Controls Conductance in Phthalocyanine Molecular Junctions. *The Journal of Physical Chemistry C*, 125(27), pp.15035-15043.
  17. Ismael, A. and Lambert, C., 2019. Single-molecule conductance oscillations in alkane rings. *Journal of Materials Chemistry C*, 7(22), pp.6578-6581.
  18. Ismael, A., Alshehab, A., Grace, I. and Lambert, C., 2021. Correction: Molecular-scale thermoelectricity: as simple as ‘ABC’. *Nanoscale Advances*, 3(2), pp.619-619.
  19. Ismael, A., Grace, I. and Lambert, C., 2017. Discriminating single-molecule sensing by crown-ether-based molecular junctions. *The Journal of Chemical Physics*, 146(6), p.064704.

20. Ismael, A., Nichols, R. and Lambert, C., 2019. Single molecule vs. large area design of molecular electronic devices incorporating an efficient 2-aminepyridine double anchoring group. *Nanoscale*, 11(34), pp.15871-15880.
21. Markin, A., Ismael, A., Davidson, R. and Lambert, C., 2020. Conductance Behavior of Tetraphenyl-Aza-BODIPYs. *The Journal of Physical Chemistry C*, 124(12), pp.6479-6485.
22. Naghibi, S., Ismael, A., Grace, I., Lambert, C. and Nichols, R., 2019. Synthetic Control of Quantum Interference by Regulating Charge on a Single Atom in Heteroaromatic Molecular Junctions. *The Journal of Physical Chemistry Letters*, 10(20), pp.6419-6424.
23. Wang, X., Ismael, A., Alshehab, A. and Lambert, C., 2021. Optimised power harvesting by controlling the pressure applied to molecular junctions. *Chemical Science*, 12(14), pp.5230-5235.
24. Wilkinson, L., Grace, I., Ismael, A. and Lambert, C., 2022. Assembly, structure and thermoelectric properties of 1,1'-dialkynylferrocene 'hinges'. *Chemical Science*, 13(28), pp.8380-8387.
25. Gantenbein, M., Ismael, A. and Lambert, C., 2017. Quantum interference and heteroaromaticity of para- and meta-linked bridged biphenyl units in single molecular conductance measurements. *Scientific Reports*, 7(1).
26. Herrero, I., Ismael, A., Grace, I., Lambert, C. and Nichols, R., 2018. Unconventional Single-Molecule Conductance Behavior for a New Heterocyclic Anchoring Group: Pyrazolyl. *The Journal of Physical Chemistry Letters*, 9(18), pp.5364-5372.

27. Ismael, A., Chen, Z., Lambert, C., Hong, W. and Zhang, Q., 2022. Highly Insulating Alkane Rings with Destructive  $\sigma$ -Interference. *Science China Chemistry*, 65.
28. Ismael, A., Grace, I. and Lambert, C., 2017. Connectivity dependence of Fano resonances in single molecules. *Physical Chemistry Chemical Physics*, 19(9), pp.6416-6421.
29. Chen, F., Li, X., Hihath, J., Huang, Z. and Tao, N. (2006). Effect of Anchoring Groups on Single-Molecule Conductance: Comparative Study of Thiol-, Amine-, and Carboxylic-Acid-Terminated Molecules. *Journal of the American Chemical Society*, 128(49), pp.15874–15881.
30. Cheng, Z.-L. ., Skouta, R., Vazquez, H., Widawsky, J.R., Schneebeli, S., Chen, W., Hybertsen, M.S., Breslow, R. and Venkataraman, L. (2011). In situ formation of highly conducting covalent Au–C contacts for single-molecule junctions. *Nature Nanotechnology*, 6(6), pp.353–357.
31. J. R. Widawsky, W. Chen, H. Vazquez, T. Kim, R. Breslow, M. S. Hybertsen and L. Venkataraman, *Nano Lett.*, 2013, 13, 2889–2894.

## Chapter 5

### Non-classical electron transport in the sigma systems of alkane rings

The following investigation was carried out in collaboration with the experimental group led by Professor Zhong-Ning (State Key Laboratory of Structural Chemistry, Fujian Institute of Research on the Structure of Matter, Chinese Academy of Sciences), who synthesised the studied molecules and Professor Wenjing Hong (State Key Laboratory of Physical Chemistry of Solid Surfaces, College of Chemistry and Chemical Engineering, iChEM, Xiamen University), who conducted the experiments. In this chapter, I will present our joint theoretical and experimental work on the electron transport in alkane derivatives, and the results presented here were submitted:

*“Highly insulating alkane rings with destructive  $\sigma$ -interference”*

Wenqiang Cao, Alaa Al-Jobory, Qian-Chong Zhang, Jingyao Ye, Abdullah Alshehab, Kai Qu, Turki Alotaibi, Hang Chen, Junyang Liu, Ali. K. Ismael, Zhong-Ning Chen, Colin J. Lambert and Wenjing Hong.

In chapter 4, I have comprehensively investigated 32 linear alkane chains classified by 4 different terminal anchors including amine, direct carbon, thiol and thiomethyl. In this chapter, I shall investigate a series of alkane chains terminated with thiomethyl and their corresponding symmetric and asymmetric alkane rings, calculate their electrical conductances and Seebeck coefficients using DFT-based simulations. Remarkably, I find that the conductances of the double-branched alkane rings are smaller than those of the corresponding individual chain (which is in agreement with previously published report<sup>38</sup>) and much smaller than the value predicted by Kirchhoff's law. The Seebeck coefficients of the rings are also higher than those of the corresponding chains, which is consistent with the presence of phase coherent tunnelling in the alkane rings. Further characterizations of asymmetric rings reveal that their conductances

and Seebeck coefficients are between those of their corresponding shorter and longer chains. With the elongation of the longer chain, the conductance of the asymmetric ring becomes close to that of the shorter chain. This suppression of conductance in symmetric rings agrees with experimental results using the scanning tunnelling microscope break junction (STM-BJ) method.

## 5.1 Motivation

Characterising the electrical conductance of ring-like molecules is of interest, not only because they possess more than one path for electron transport, which can lead to non-classical behaviour, but also because rings of different sizes have the potential to bind selectively to analyte molecules, with potential sensing applications. Here, I report a combined theoretical and experimental study of electron transport through alkyl rings formed from segments of length  $n$  and  $m$  alkyl units connected via sulphur atoms to form rings. Results are presented for both the electrical conductances and Seebeck coefficients of  $C_mC_n$  rings formed from branches  $n, m = 6, 6; 6, 8; 6, 10; 8, 8; 8, 10$  and  $10, 10$  and also for  $C_m$  chains with  $n = 6, 8$ , and  $10$  alkyl units. The conductances of the  $n, n$  symmetric rings are found to decay exponentially with  $n$ , but at a slower rate than the linear chains. Remarkably, both theory and experiment reveal that the electrical conductances of the symmetric  $C_nC_n$  rings are lower than their asymmetric counterparts, with the  $C_6C_6$  less than both  $C_6C_8$  and  $C_6C_{10}$ , the  $C_8C_8$  less than both  $C_8C_6$  and  $C_8C_{10}$  and the  $C_{10}C_{10}$  less than both  $C_{10}C_8$  and  $C_{10}C_6$ . This highly non-classical behaviour is a signature of phase-coherent tunnelling and quantum interference within the  $\sigma$  systems of these non-conjugated molecules. The symmetric rings are also found to possess the highest Seebeck coefficients, with measured values  $-29, -31$  and  $-26.7 \mu V/k$  for  $C_6C_6, C_8C_8$  and  $C_{10}C_{10}$  respectively, which is consistent with my theoretically predicted trends.

### 5.3 Optimized DFT Structures of Isolated Molecules

I divide the research here in three groups depending on the geometrical details of the studied molecules including alkane chains, symmetric and asymmetric rings. Each group consists of three molecules based on their molecular length. For more information about the transport calculations use in this chapter, see sections 3.2-3.6 in chapter 3.

#### 5.3.1 Geometries of the isolated alkane chains

As I mentioned above, the first group of this chapter is alkane chains. For this group, I choose three molecules by increasing the length of the chain by two  $-CH_2$  units and as follows: **C<sub>6</sub>**, **C<sub>8</sub>** and **C<sub>10</sub>**. The three chains are terminated with two thiomethyl anchors (SMe), as shown in Figure 5.1 (top to bottom respectively).

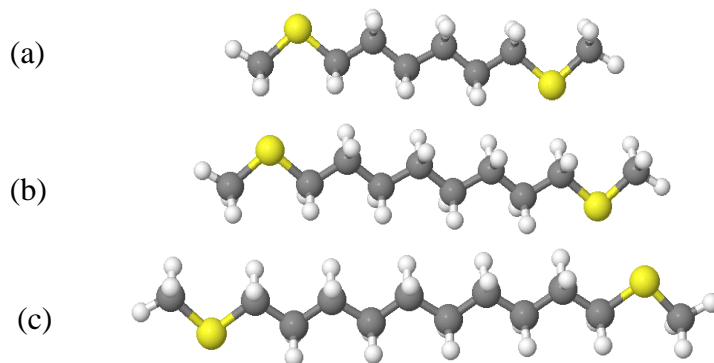


Figure 5. 1. Alkane chains: Fully relaxed isolated molecules, with 6, 8 and 10 carbon atoms (excluding the 2 carbon atoms within the SMe anchors). **(a)**, **(b)** and **(c)**: represent **C<sub>6</sub>**, **C<sub>8</sub>** and **C<sub>10</sub>** chains with (SMe) top to bottom respectively.

#### 5.3.2 Geometries of the isolated symmetric alkane rings

In this section, I combine two alkane chains ( $-CH_2$  units) to form a ring with two sulphur atoms acting as anchor groups. These rings have identical branches (upper and lower). This group

consists of the following three rings **C<sub>6</sub>C<sub>6</sub>**, **C<sub>8</sub>C<sub>8</sub>** and **C<sub>10</sub>C<sub>10</sub>**, as shown in Figure 5.2 (the cavity increases by four  $-CH_2$  units).

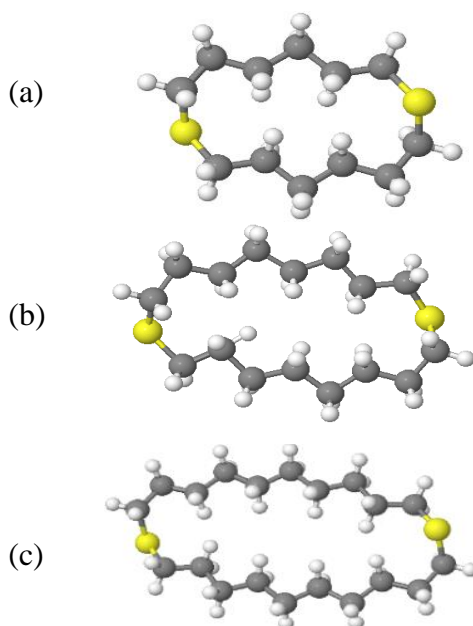


Figure 5. 2. Alkane symmetric rings: Fully relaxed isolated symmetric rings, with 6-6, 8-8 and 10-10 carbon atom branches: **(a)**, **(b)** and **(c)**: represent **C<sub>6</sub>C<sub>6</sub>**, **C<sub>8</sub>C<sub>8</sub>** and **C<sub>10</sub>C<sub>10</sub>** rings with (SMe) top to bottom respectively.

### 5.3.3 Geometries of the isolated asymmetric alkane rings

The procedure of forming symmetric rings will now be repeated, here. However I shall use the first group (chains) to create three asymmetric rings. These rings do not have identical branches ( $n,m$ ) such as, **C<sub>6</sub>C<sub>8</sub>** (**C<sub>6</sub>** combined with **C<sub>8</sub>** through 2 sulphur atoms acting as anchor groups, see Fig. 5.3a), **C<sub>6</sub>C<sub>10</sub>** (**C<sub>6</sub>** combined with **C<sub>10</sub>** through 2 sulphur atoms acting as anchor groups, see Fig. 5.3b) and **C<sub>8</sub>C<sub>10</sub>** (**C<sub>8</sub>** combined with **C<sub>10</sub>** through 2 sulphur atoms acting as anchor groups, see Fig. 5.3c) . As shown in the Figure 5.3 (the cavity increases by two  $-CH_2$  units, 14, 16 and 18 for **C<sub>6</sub>C<sub>8</sub>**, **C<sub>6</sub>C<sub>10</sub>** and **C<sub>8</sub>C<sub>10</sub>** respectively).

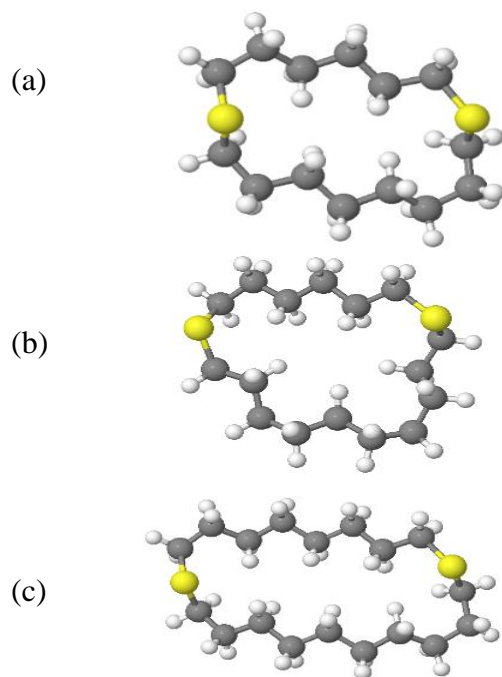


Figure 5. 3. Alkane asymmetric rings: Fully relaxed isolated asymmetric rings, with 6-8, 6-10 and 8-10 carbon atom branches. **(a)**, **(b)** and **(c)**: represents  $C_6C_8$ ,  $C_6C_{10}$  and  $C_8C_{10}$  rings with (SMe) top to bottom respectively.

#### 5.4 Frontier orbitals of the studied molecules

Tables 5.1-5.3 show the frontier orbitals of the isolated molecules. The plots below show iso-surfaces of the HOMO, LUMO, HOMO-1 and LUMO+1 along with their energies of the three groups (chain, symmetric and asymmetric rings).



Table 5. 1. Comparison between the Frontier molecular orbitals of alkane chain, including C<sub>6</sub>, C<sub>8</sub> and C<sub>10</sub> in the gas phase.





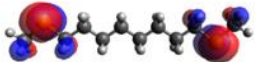
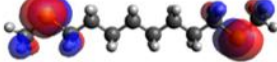
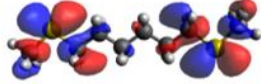
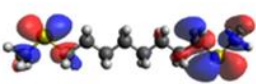
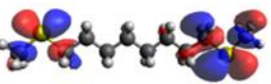
Chains	C <sub>6</sub>	C <sub>8</sub>	C <sub>10</sub>
Mol.			
HOMO eV	 -4.16	 -4.14	 4.13
LUMO eV	 1.02	 1.08	 1.09

Table 5. 2. Frontier molecular orbitals of asymmetric rings, including  $C_6C_8$ ,  $C_6C_{10}$  and  $C_8C_{10}$  in the gas phase.

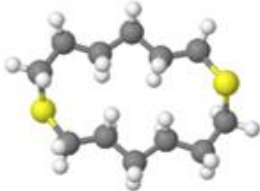
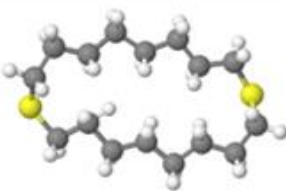
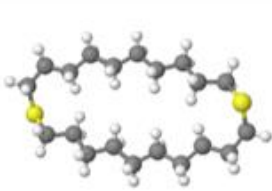
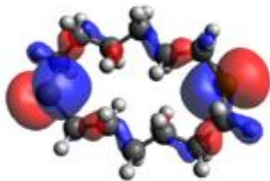
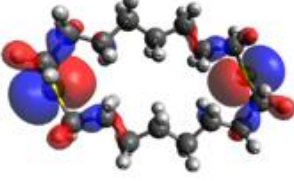
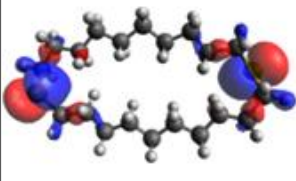
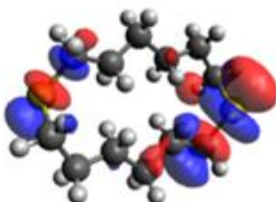
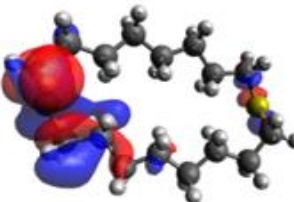
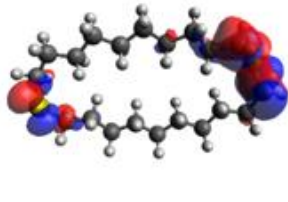

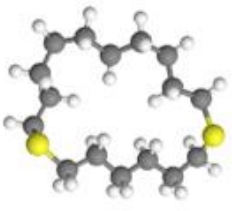

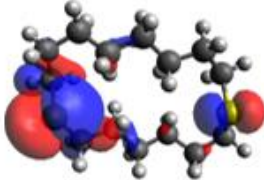
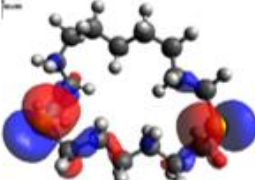
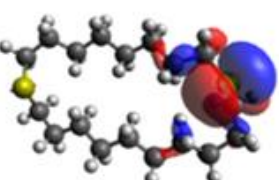
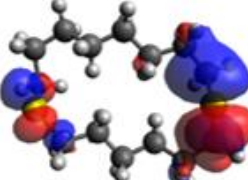
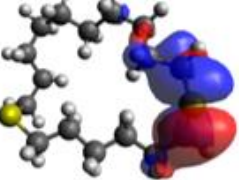
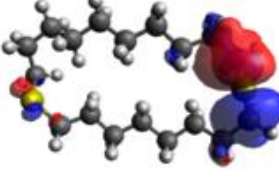
Symmetric rings	$C_6C_6$	$C_8C_8$	$C_{10}C_{10}$
Mol.			
HOMO eV	 -4.24	 -4.25	 -4.24
LUMO eV	 1.06	 1.07	 1.14

Table 5. 3. Frontier molecular orbitals of asymmetric rings, including  $C_6C_8$ ,  $C_6C_{10}$  and  $C_8C_{10}$  in the gas phase.

Asymmetric rings	$C_6C_8$	$C_6C_{10}$	$C_8C_{10}$
Mol.			
HOMO  eV	 -4.15	 -4.24	 -4.18
LUMO  eV	 0.96	 1.11	 0.94

## 5.5 Binding energy of two terminal groups on gold

The binding energy method has been described in chapter 4 (see section 4.5), and the studied molecules have been shown in sections 5.3.1-5.3.3. Now, I am ready to calculate the binding energies of alkane chains terminated with SMe and the corresponding rings terminated with S, as shown in the right panel of Figure 5.4. In the section 4.14 of chapter 4, I already calculated the Au-S covalent binding energy, which was approximately -2 eV and its corresponding equilibrium distance was found to be approximately 2.4 Å. Here, I shall repeat the same procedure that described in the section 4.7 and using the equation (4.1) to calculate (Au-SMe) binding energy. Left panel of Figure 5.4 shows a comparison between the binding energy of an alkane chain with (Au-SMe) and a ring with (Au-S). The Au-SMe covalent binding energy is approximately -0.3 eV. It is clear that the S binding energy is stronger than Au-SMe by approximately 7 times.

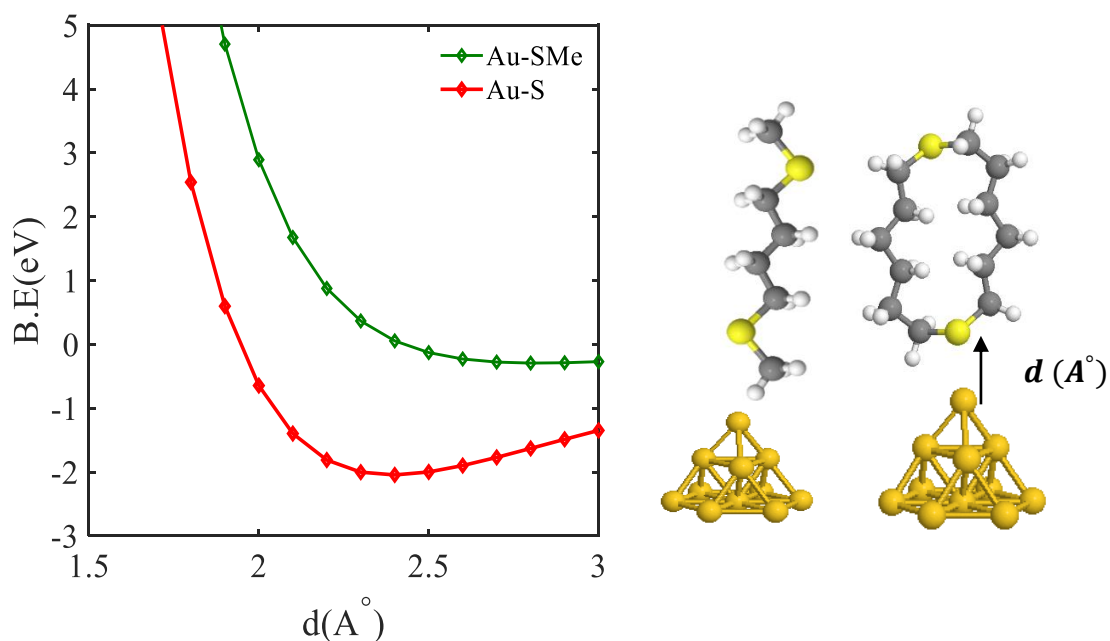


Figure 5. 4. An example of alkane molecule terminated with a thiol anchor and thiomethyl on a gold tip :( Left) Binding energy of C<sub>4</sub> alkane chain and C<sub>6</sub>C<sub>6</sub> symmetric ring to gold as a function of molecule-contact distance. The equilibrium distances (i.e. the minimum of the binding energy curve) are found to be approximately 2.4 and 2.8 Å, for Au-S and Au-SMe (red

and green curves). (Right) its idealised ad-atom configuration at the Au lead interface Au-thiol and Au-SMe. Key: C = grey, H = white, S = light yellow, Au = dark yellow.

## 5.6 DFT Calculations

After relaxing each molecule of the studied group, I calculated the electrical conductance using the GOLLUM quantum transport code [1]. From the ground state Hamiltonian, the transmission coefficient, the room temperature electrical conductance  $G$  and Seebeck coefficient  $S$  were obtained, as described in the sections below.

## 5.7 Optimised DFT Structures of Compounds in their Junctions

Figure 5.5 illustrates 3 alkane chains in Au junctions including C<sub>6</sub>, C<sub>8</sub> and C<sub>10</sub>.

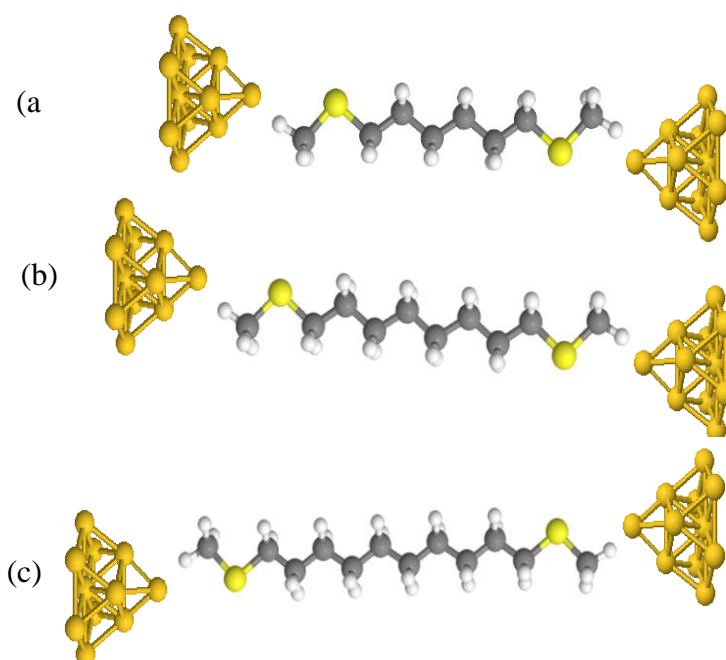


Figure 5. 5. Examples of fully relaxed alkane derivatives in Au|molecule|Au junctions: (a), (b) and (c). 6, 8 and 10 linear chains connect to gold electrodes via thiomethyl anchor groups (Au-SMe).

## 5.8 Transport calculations

The transmission coefficients  $T(E)$ , obtained from using the GOLLUM transport code [1-3], were calculated for alkane chains and rings with different terminal groups such as S and SMe binding to the gold (111) surfaces. I shall investigate in detail the transmission coefficients  $T(E)$ , conductance  $G$  and Seebeck coefficient  $S$  with different anchor groups, then I will compare them against experimental results.

### 5.8.1 Transmission coefficient of alkane chains using (Au-SMe) as terminal group

The Fermi energy is predicted to be approximately mid-gap due to the presence of the SMe anchor group [4-18]. In this study, I choose the DFT-predicted Fermi level (black-dashed line of Figure 5.6), to compare with the experimental results. The transmission coefficients of the alkane chains of different lengths ( $n=6, 8$  and  $10$ ) are shown in Figure 5.6.

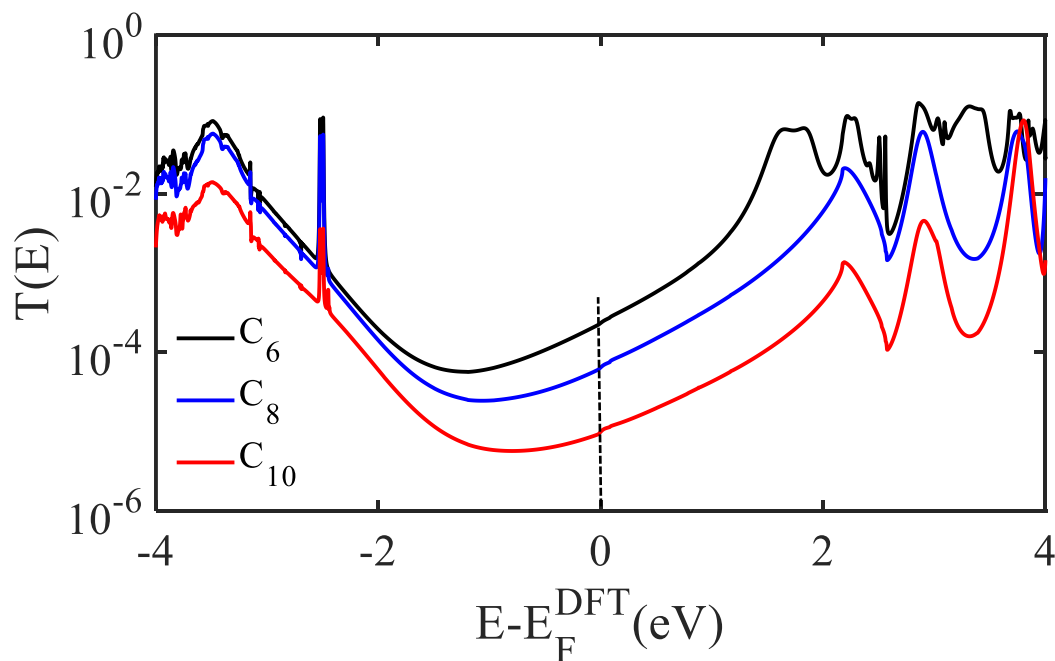


Figure 5. 6. Transmission coefficients of alkanes with 6, 8 and 10 carbon atoms. Transmission coefficients  $T(E)$  of alkane chains against electron energy  $E$ , alkane chain  $C_6$  (black-line), alkane chain  $C_8$  (blue-line), and alkane chain  $C_{10}$  (red-line).

As expected, it is clear from Figure 5.6 that conductance of alkane chains decreases as the length of the molecule increases. The actual logarithmic conductances are -3.7, -4.2 and -5.0 for **C<sub>6</sub>**, **C<sub>8</sub>** and **C<sub>10</sub>** respectively. In the following sections, I will examine conductance behaviour for both symmetric and antisymmetric rings.

### 5.8.2 Transmission coefficient of alkane rings using (Au-S) as terminal group

The transmission coefficients  $T(E)$  were calculated for both the symmetric alkane rings **C<sub>6</sub>C<sub>6</sub>**, **C<sub>8</sub>C<sub>8</sub>** and **C<sub>10</sub>C<sub>10</sub>**, as shown in Figure 5.7, and the asymmetric alkane rings **C<sub>6</sub>C<sub>8</sub>**, **C<sub>6</sub>C<sub>10</sub>** and **C<sub>8</sub>C<sub>10</sub>** shown in the Figure 5.9. Figure 5.8 shows the transmission coefficients of the symmetric rings.

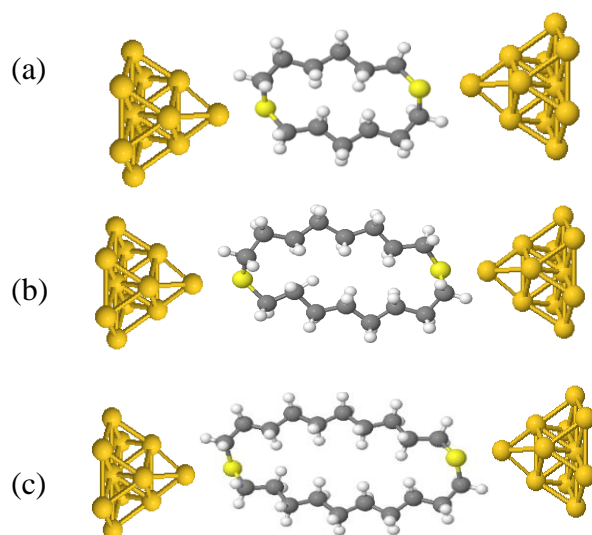


Figure 5. 7. Examples of alkane ring derivatives in Au|molecule|Au junctions: **(a)**, **(b)** and **(c)**: A double-branch  $n = 6, 8$  and  $10$  alkane symmetric rings with (Au-S).

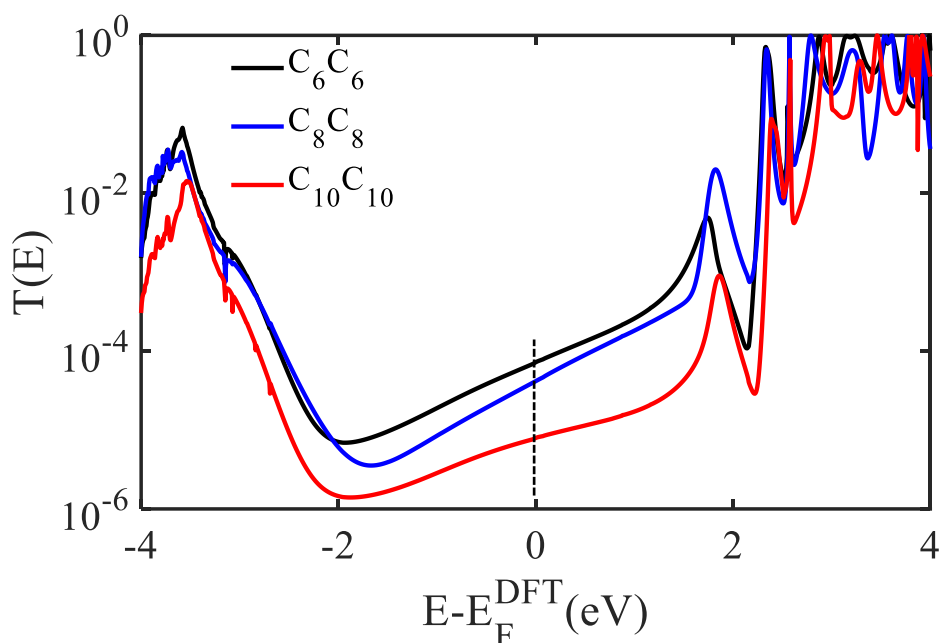


Figure 5. 8. Transmission coefficient curves of alkane symmetric rings. Transmission coefficients  $T(E)$  of alkane symmetric rings against electron energy  $E$ , alkane ring size  $\text{C}_6\text{C}_6$  (black-line), alkane ring size  $\text{C}_8\text{C}_8$  (blue-line), and alkane ring size  $\text{C}_{10}\text{C}_{10}$  (red-line).

The conductance of the symmetric rings decreases as the size of these rings increases as shown in Figure 5.8. The logarithmic conductances are -4.14, -4.38 and -5.10 for  $\text{C}_6\text{C}_6$ ,  $\text{C}_8\text{C}_8$  and  $\text{C}_{10}\text{C}_{10}$  alkane symmetric rings respectively. The transmission coefficients curves are still showing the expected behaviour for both alkane chains and its symmetric rings.

For asymmetric rings, shown in the Figure 5.9, I examined the three different sizes,  $\text{C}_6\text{C}_8$ ,  $\text{C}_8\text{C}_{10}$  and  $\text{C}_6\text{C}_{10}$ . The two branches of these rings are not equal, meaning, one of the branches is longer/shorter by two carbon atoms  $\text{C}_6\text{C}_8$  and  $\text{C}_8\text{C}_{10}$  rings while for  $\text{C}_6\text{C}_{10}$  the difference between the two branches is four carbon atoms.



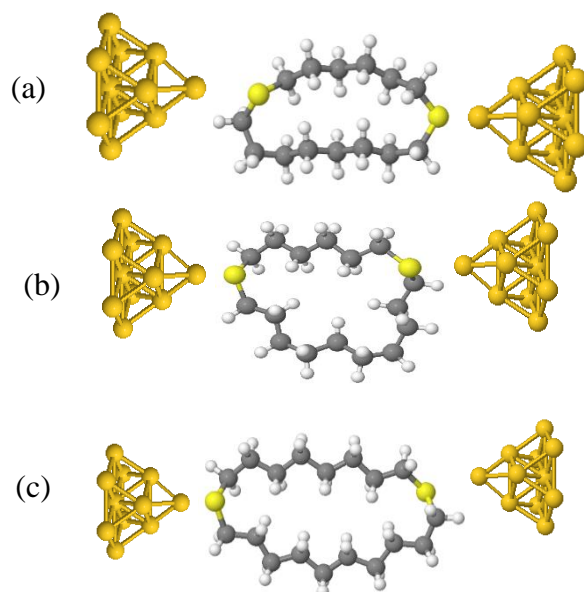


Figure 5. 9. Examples of alkane ring derivatives in Au|molecule|Au junctions: **(a)**, **(b)** and **(c)**: The length of top-branches are  $n = 6$ ,  $6$  and  $8$  while bottom- branches  $n=8$ ,  $10$  and  $10$  asymmetric alkane rings with (Au-S).

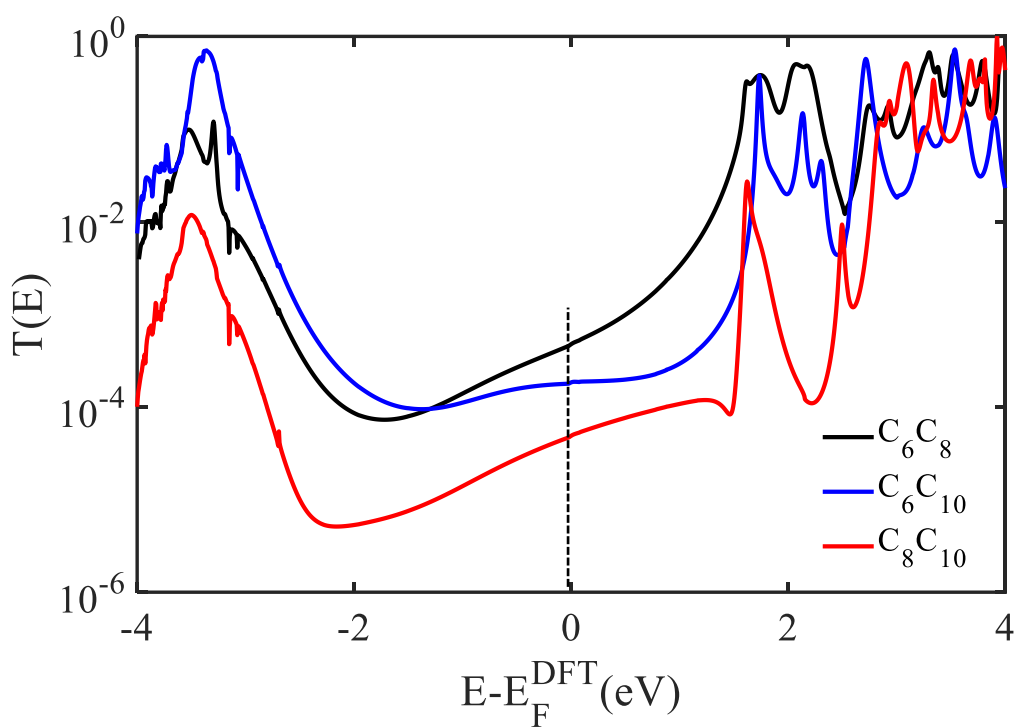


Figure 5. 10. Transmission coefficient curves of alkane asymmetric rings. Transmission coefficients  $T(E)$  of alkane asymmetric rings against electron energy  $E$ , alkane ring size  $\mathbf{C_6C_8}$  (black-line), alkane ring size  $\mathbf{C_6C_{10}}$  (blue-line), and alkane ring size  $\mathbf{C_8C_{10}}$  (red-line).

The conductance of asymmetric rings shows the same trend as the symmetric rings (see Fig. 5.10), with a decreasing conductance as the size of the rings increases as shown in Figure 5.10. The logarithmic conductances are -3.30, -3.73 and -4.31 for  $C_6C_8$ ,  $C_6C_{10}$  and  $C_8C_{10}$  asymmetric rings.

So far, conductances of alkane chains, symmetric and asymmetric rings behave conventionally, meaning that the conductances decrease, as the lengths or cavity sizes of the molecules increase. In the following section, I shall apply the Kirchhoff's law to these nano-scale structures, and I will examine the trend of conductance, to check whether their behaviour is classical or non-classical.

### 5.9 Applying the Kirchhoff's law in the Nano-scale structures

Classically, when electrical circuits are connected in parallel as shown in Figure 5.11, the current has multiple pathways that can travel through them.

Kirchhoff's superposition law states that the total conductance of an electronic circuit in a parallel configuration is the sum of the conductance of the individual branches ( $G_{total} = G_1 + G_2$ ) [19-22].

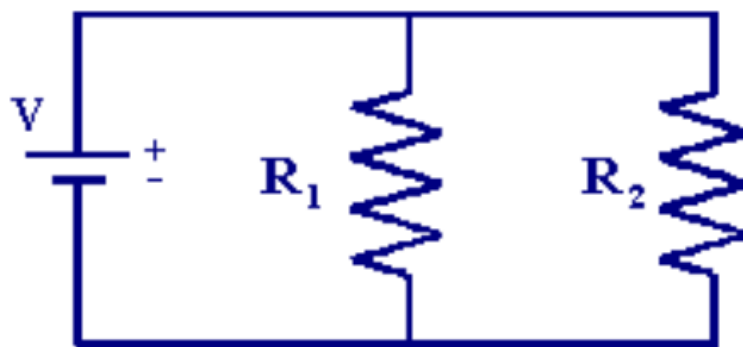


Figure 5. 11. Electrical circuit with resistors ( $R_1$  and  $R_2$ ), where they connected in parallel.

The total resistance is:

$$\frac{1}{R_{total}} = \frac{1}{R_1} + \frac{1}{R_2} \quad (5.2)$$

$$\text{where } G = \frac{1}{R} \text{ (Ampere/Volt = Siemens)} \quad (5.3)$$

From equations (5.2) and (5.3)

$$G_{total} = G_1 + G_2 \quad (5.4)$$

I now examine the question: does Kirchhoff's law work for the nano-scale structures examined in this chapter?

To answer this question, I am going to compare the conductances of three alkane chains, where the electrons have only one passible path to travel as shown in the Figure 5.12(a) against their corresponding symmetric rings. In this case (rings), electrons have more than one passible path as shown in the Figure 5.12(b).

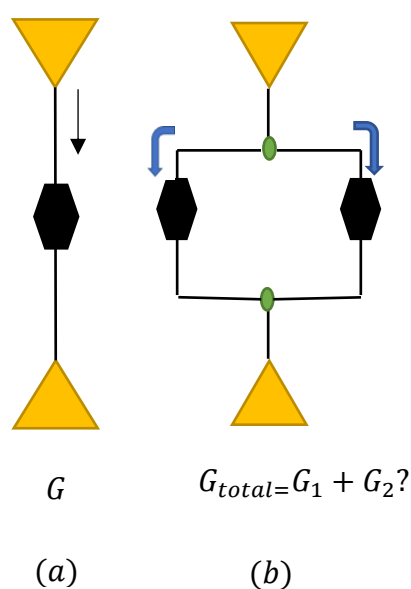


Figure 5. 12. Different scenarios for quantum circuits. **(a)**: The conductance of a molecule is  $G$  (due to there is only one pathway). **(b)**: Classically, the conductance of a ring formed from two conductors connect in parallel, is equal to the sum of the individual conductances ( $G_1 + G_2$ ).

Now, if the Kirchhoff's law works on the studied molecules (chains and rings), then surely the conductances of rings (**C<sub>6</sub>C<sub>6</sub>**, **C<sub>8</sub>C<sub>8</sub>** and **C<sub>10</sub>C<sub>10</sub>**) should be higher than conductances of chains (**C<sub>6</sub>**, **C<sub>8</sub>** and **C<sub>10</sub>**).

### 5.9.1 Conductance of linear chain versus symmetric rings

Here, I am going to investigate the conductance of alkane chains against the conductance of symmetric rings. Also, I am going to check the validity of Kirchhoff's law in these nano-scale structures.

Table 5 .4 summarises the comparison between conductances of chains and symmetric alkane rings at the DFT-predicted Fermi ( $E - E_F = 0$ ). This table proves that the conductances of alkane rings with two parallel conductance paths are lower than those of the corresponding linear chains with only one conductance path. This behaviour is a non-classical trend, meaning, it does not follow the Kirchhoff's law.

Table 5. 4. Conductances of linear chains, **C<sub>6</sub>**, **C<sub>8</sub>** and **C<sub>10</sub>**, and alkane symmetric rings, **C<sub>6</sub>C<sub>6</sub>**, **C<sub>8</sub>C<sub>8</sub>** and **C<sub>10</sub>C<sub>10</sub>**. These results are determined at the DFT-predicted Fermi ( $E - E_F = 0$ ).

Molecule	Conductance $\log(G/G_0)$
<b>C<sub>6</sub></b>	-3.7
<b>C<sub>6</sub>C<sub>6</sub></b>	-4.14
<b>C<sub>8</sub></b>	-4.2
<b>C<sub>8</sub>C<sub>8</sub></b>	-4.38
<b>C<sub>10</sub></b>	-5.0
<b>C<sub>10</sub>C<sub>10</sub></b>	-5.10

### 5.9.2 Conductance of linear chains versus asymmetric rings

In section 5.9.1, I made a comparison between conductances of linear chains and their corresponding symmetric rings ( $C_6C_8$ ,  $C_6C_{10}$  and  $C_8C_{10}$ ). Here, I shall repeat the same comparison, however, this time with asymmetric rings including  $C_6C_8$ ,  $C_6C_{10}$  and  $C_8C_{10}$ .

The conductance of linear chains  $C_6$ ,  $C_8$  and  $C_{10}$  and their asymmetric rings  $C_6C_8$ ,  $C_6C_{10}$  and  $C_8C_{10}$  are investigated in three categories. The first category is denoted  $C_6$ -branch, where there is at least one branch with 6 carbon atoms and it consists of  $C_6$ ,  $C_6C_8$  and  $C_6C_{10}$ . The second category is denoted  $C_8$ -branch, where there is at least one branch with 8 carbon atoms and it consists of  $C_8$ ,  $C_6C_8$  and  $C_8C_{10}$ . The last category, category is denoted  $C_{10}$ -branch, where there is at least one branch with 10 carbon atoms and consists of  $C_{10}$ ,  $C_6C_{10}$  and  $C_8C_{10}$ .

Table 5.5 summarises the comparison between conductances of linear chains and asymmetric rings at the DFT-predicted Fermi ( $E - E_F = 0$ ). The comparison here is more complicated than in Table 5.2, since the two branches are not equal. Therefore, this requires comparing each chain against two different rings and as follows:  $C_6$  versus  $C_6C_8$  and  $C_6C_{10}$ ,  $C_8$  versus  $C_6C_8$  and  $C_8C_{10}$  and  $C_{10}$  versus  $C_8C_{10}$  and  $C_6C_{10}$ . This Table shows three different trends: the conductances of alkane rings with two parallel conductance paths are: equal to or higher or lower than those of the corresponding linear chains with only one conductance path.

The conductance of chain  $C_6$  is lower than  $G$  of  $C_6C_8$  and roughly equal to  $G$  of  $C_6C_{10}$ , similarly, for  $C_8$   $G$  is lower than  $C_6C_8$  and slightly higher than  $C_8C_{10}$ . In contrast, the conductance of the larger chain  $C_{10}$  is lower than both rings  $C_8C_{10}$  and  $C_6C_{10}$ . I can conclude that for small and medium chains  $C_6$  and  $C_8$  the conductance sits between the two conductances of the different cavity ring sizes, while for the large chain  $C_{10}$  the conductance is lower than both rings.

These results are reasonable, if we consider the number of carbon atoms in each branch. To accommodate this point,  $G$  of  $\mathbf{C_6}$  is lower than  $\mathbf{C_6C_8}$ , because this cavity has 14 carbon atoms, whereas  $G$  of  $\mathbf{C_6}$  is roughly equal to  $\mathbf{C_6C_{10}}$  that possesses a bigger cavity (16 carbon atoms). Similarly,  $G$  of  $\mathbf{C_8}$  is lower than  $\mathbf{C_6C_8}$  (small cavity) and slightly higher than  $\mathbf{C_8C_{10}}$  (large cavity).

For the long chain  $\mathbf{C_{10}}$ ,  $G$  is lower than both  $\mathbf{C_8C_{10}}$  and  $\mathbf{C_6C_{10}}$ , however. In other words, it is closer to the large cavity ( $\mathbf{C_8C_{10}}$ ), than the small cavity ( $\mathbf{C_6C_{10}}$ ), which follows the same trend of short and medium chains  $\mathbf{C_6}$  and  $\mathbf{C_8}$ .

The above behaviour partially does not agree with Table 5.2 results, which suggests there is a classical and a non-classical trend. I will discuss this point in more detail in the next section focusing on alkane rings.

Table 5. 5. Conductances of linear chains,  $\mathbf{C_6}$ ,  $\mathbf{C_8}$  and  $\mathbf{C_{10}}$ , and asymmetric alkane rings including  $\mathbf{C_6C_8}$ ,  $\mathbf{C_6C_{10}}$  and  $\mathbf{C_8C_{10}}$ . These results are determined at the DFT-predicted Fermi ( $E - E_F = 0$ ).

Molecule	Conductance $\log(G/G_0)$	Molecule	Conductance $\log(G/G_0)$	Molecule	Conductance $\log(G/G_0)$
$\mathbf{C_6}$	-3.70	$\mathbf{C_8}$	-4.20	$\mathbf{C_{10}}$	-5.0
$\mathbf{C_6C_8}$	-3.30	$\mathbf{C_6C_8}$	-3.30	$\mathbf{C_6C_{10}}$	-3.73
$\mathbf{C_6C_{10}}$	-3.73	$\mathbf{C_8C_{10}}$	-4.31	$\mathbf{C_8C_{10}}$	-4.31

### 5.10 Classical and non-classical trends (families)

In this section, I compare the transmission coefficients of 3 rings that have the same number of carbon atoms in one of the branches (the common branch), while the number of carbon atoms is bigger or smaller in the second branch. Based on that, I have created three families of alkane rings, as shown in Table 5.6. Family-6 includes  $C_6C_6$ ,  $C_6C_8$  and  $C_6C_{10}$  rings, here, the common branch is  $C_6$  and their corresponding transmission coefficients in the Figure 5.13. Family-8, includes  $C_8C_6$ ,  $C_8C_8$  and  $C_8C_{10}$  rings and the common branch is  $C_8$  and their corresponding transmission coefficients in the Figure 5.14. Finally, for family-10, the common branch is  $C_{10}$  and it includes  $C_6C_{10}$ ,  $C_8C_{10}$  and  $C_{10}C_{10}$  rings and their corresponding transmission coefficients in Figure 5.15.

Table 5. 6. Shows three families: family-6, family-8 and family-10. Each family includes three rings, the three rings have a common branch. The common branches of the three rings are  $C_6$ ,  $C_8$  and  $C_{10}$  (family-6, family-8 and family-10 respectively).

Family	Common branch $C_6$	Common branch $C_8$	Common branch $C_{10}$
<b>Family-6</b>	$C_6C_6$	$C_6C_8$	$C_6C_{10}$
<b>Family-8</b>	$C_8C_6$	$C_8C_8$	$C_8C_{10}$
<b>Family-10</b>	$C_{10}C_6$	$C_{10}C_8$	$C_{10}C_{10}$

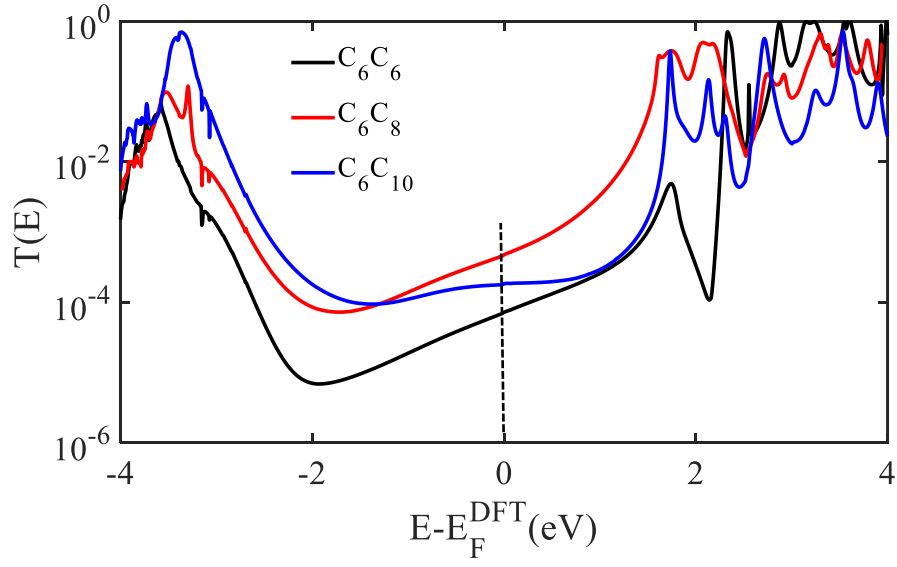


Figure 5. 13. Transmission coefficient curves of the three alkane rings of family-6.

Transmission coefficients  $T(E)$  of family-6 against electron energy  $E$ .

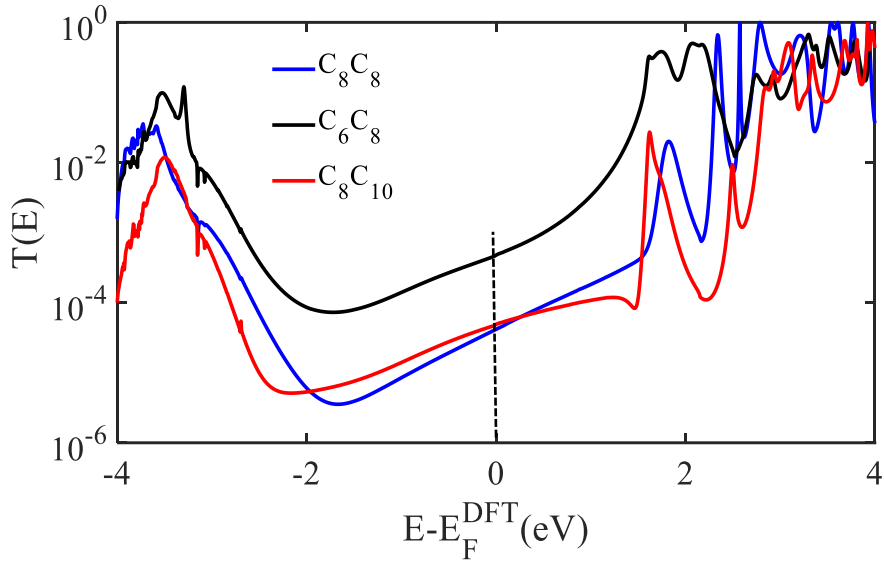


Figure 5. 14. Transmission coefficient curves of the three alkane rings of family-8.

Transmission coefficients  $T(E)$  of family-8 against electron energy  $E$ .



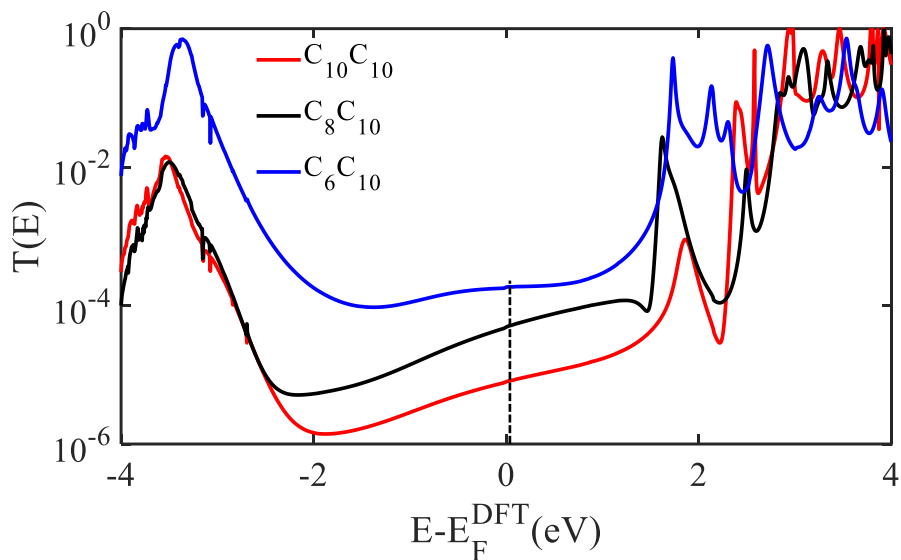


Figure 5. 15. Transmission coefficient curves of the three alkane rings of family-10. Transmission coefficients  $T(E)$  of family-10 against electron energy  $E$

Figure 5.13 clearly demonstrates that family-6 transmission coefficients possess a non-conventional trend, because the  $\text{C}_6\text{C}_6$  ring (the smallest cavity in this family) has the lowest conductance, while the  $\text{C}_6\text{C}_8$  ring (the second biggest cavity in this family) has the largest conductance ( $G = -4.14$  and  $-3.30$  respectively). It is worth mentioning, that the conductance of  $\text{C}_6\text{C}_{10}$  ring lies in between  $\text{C}_6\text{C}_6$  and  $\text{C}_6\text{C}_8$ .

In contrast, family-8 and -10 transmission coefficients show a conventional trend, meaning, the larger the cavity the smaller the conductance. The more classical behaviour is clearly shown in a large family such as family-10, where the conductance of different cavities follows the order  $\text{C}_6\text{C}_{10} > \text{C}_8\text{C}_{10} > \text{C}_{10}\text{C}_{10}$  as shown in Figure 5.15. This trend is less obvious in the medium family (family-8), where the conductance of the three rings follows  $\text{C}_6\text{C}_8 > \text{C}_8\text{C}_{10} \approx \text{C}_{10}\text{C}_{10}$  as shown in Figure 5.14.

Figures 5.13, 5.14 and 5.15 suggest that small cavities (i.e: family-6), tend to follow a non-conventional trend, whereas large cavities (i.e: family-10), tend to follow a conventional trend. Figure 5.16, demonstrates the conventional and non-conventional trend for the three families, these results are summarised in Table 5.5.

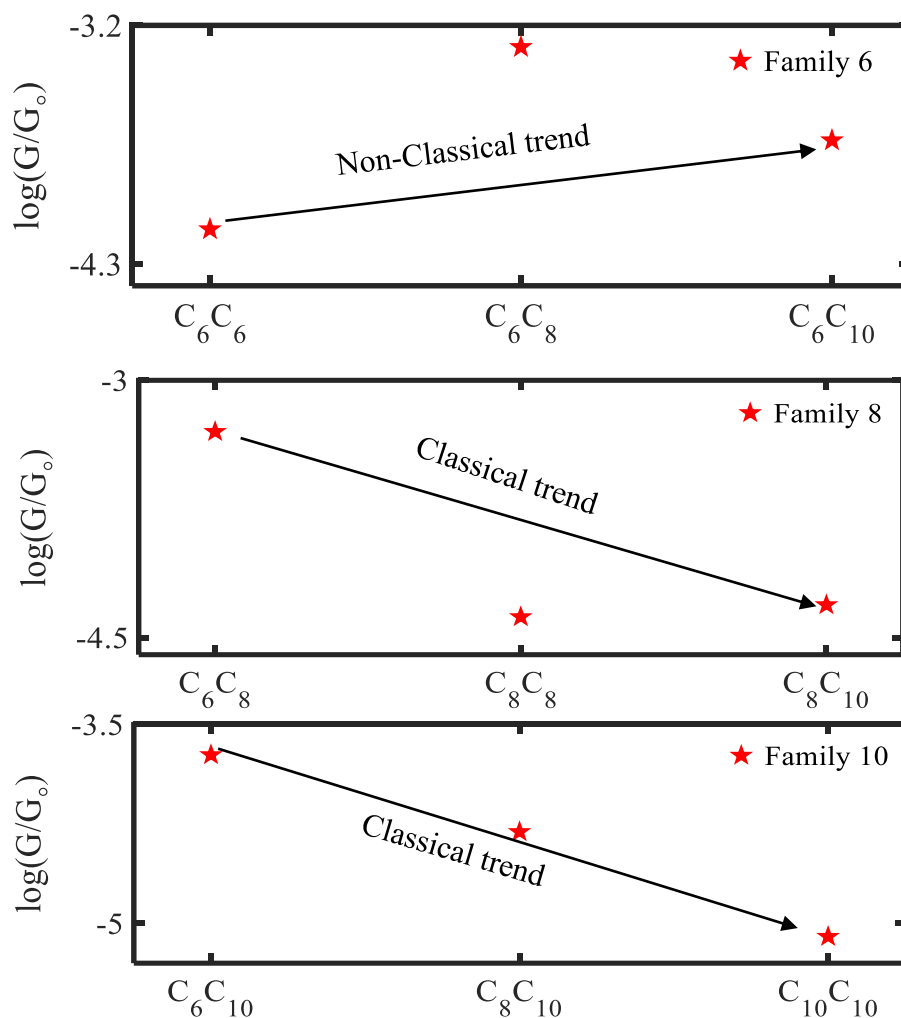


Figure 5. 16. Conventional and non-conventional tunnelling transport of three families. The theoretical conductances of three alkane ring families: small cavity family  $C_6$  including  $C_6C_6$ ,  $C_6C_8$  and  $C_6C_{10}$ , medium cavity family  $C_8$  including  $C_8C_8$ ,  $C_6C_8$  and  $C_8C_{10}$ , and large cavity family  $C_{10}$  including  $C_{10}C_{10}$ ,  $C_6C_{10}$  and  $C_8C_{10}$ .

Table 5. 7. Conductances of three families: small, medium and large (family-6, family-8 and family-10), each family includes three different cavities. These values are determined at the DFT-predicted Fermi energy ( $E - E_F = 0 \text{ eV}$ ).

Family-6		Family-8		Family-10	
Small cavity	Conductance $\log(G/G_0)$	Medium cavity	Conductance $\log(G/G_0)$	Large cavity	Conductance $\log(G/G_0)$
<b>C<sub>6</sub>C<sub>6</sub></b>	-4.14	<b>C<sub>6</sub>C<sub>8</sub></b>	-3.30	<b>C<sub>6</sub>C<sub>10</sub></b>	-3.73
<b>C<sub>6</sub>C<sub>8</sub></b>	-3.30	<b>C<sub>8</sub>C<sub>8</sub></b>	-4.38	<b>C<sub>8</sub>C<sub>10</sub></b>	-4.31
<b>C<sub>6</sub>C<sub>10</sub></b>	-3.73	<b>C<sub>8</sub>C<sub>10</sub></b>	-4.31	<b>C<sub>10</sub>C<sub>10</sub></b>	-5.10

Up to this point, I have theoretically investigated and predicted some relationships employing 9 alkane molecule derivatives. The next step is to test my theoretical DFT simulations against the STM measured values.

### 5.10.1 Comparison between theoretical simulations and experimental measurements

As it mentioned before, this project is a cooperative investigation between theory and experiment. In this section, I will use the STM measurements to test my DFT-simulations and predictions for some electronic properties including conductance and charge transport for the 9 alkane derivatives.

My theoretical simulations predict that the Kirchhoff's law is not applicable in alkane-based nanoscale structures. To prove this point, I made 6 comparisons, where I compared the conductance of 3 single path such as alkane linear chains  $C_6$ ,  $C_8$  and  $C_{10}$  against the conductance of 3 symmetric alkane rings (double even path), such as  $C_6C_6$ ,  $C_8C_8$  and  $C_{10}C_{10}$ . Then, I employed the same 3 single path molecules to check their conductances versus those of asymmetric rings (double uneven path), such as  $C_6C_8$ ,  $C_6C_{10}$  and  $C_8C_{10}$  and find the case with asymmetric rings is more delicate due to the fact that the two paths are not equal.

My DFT simulations about comparing single path versus double even path is shown in Figures 5.6 and 5.8, where the transmission coefficient curves for  $C_6$ ,  $C_8$  and  $C_{10}$  and  $C_6C_6$ ,  $C_8C_8$  and  $C_{10}C_{10}$  plot for different electron energy, although I restrict the comparison at the DFT-predicted Fermi energy (black-dashed line). These results demonstrate that the conductance of single path is higher than double path. The three comparisons contradict Kirchhoff's law (see section 5.9), as clearly shown in Table 5.4.

The validity of my simulations is now going to be tested by the STM measurements. The right panel of Figure 5.17 shows the experimental comparison between linear chains and rings. The measurements prove my simulations to be accurate, meaning that Kirchhoff's law doesn't work in alkane derivatives.

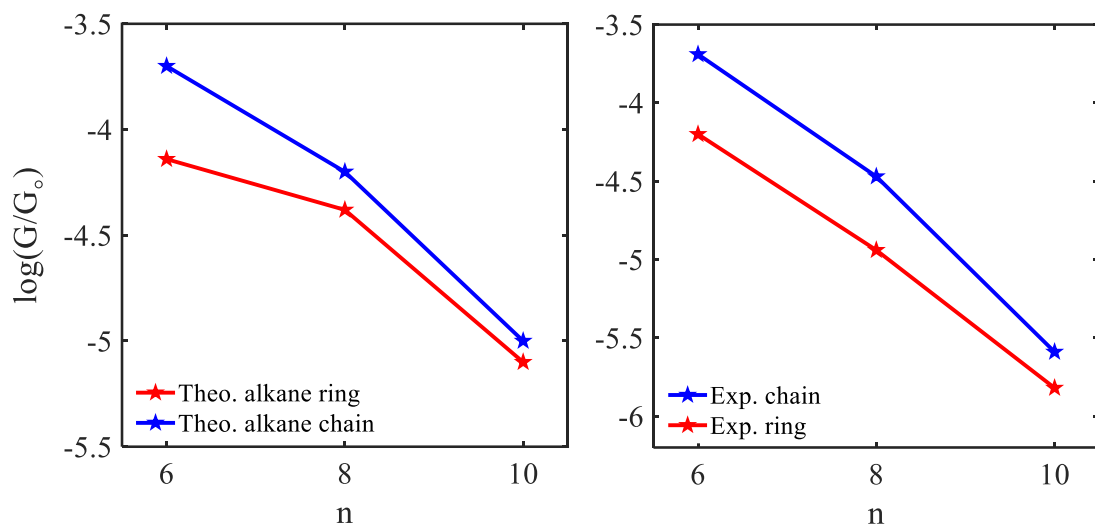


Figure 5. 17. Testing the validity of DFT predictions (the Kirchhoff's law validity). Conductance comparison of linear chains (blue lines) and alkane rings (red lines). (Left panel) represents DFT predictions while (right panel) STM experimental measurements. Note:  $n = C_6, C_8$  and  $C_{10}$  for chains and  $C_6C_6, C_8C_8$  and  $C_{10}C_{10}$  for rings.

Figure 5.18, shows the actual comparison between the theory and experiment for 12 alkane molecules. In general, the DFT calculations are higher than STM measurements. However, the difference decreases with decreasing the length/cavity of the molecules, for instance at  $n=6$ .

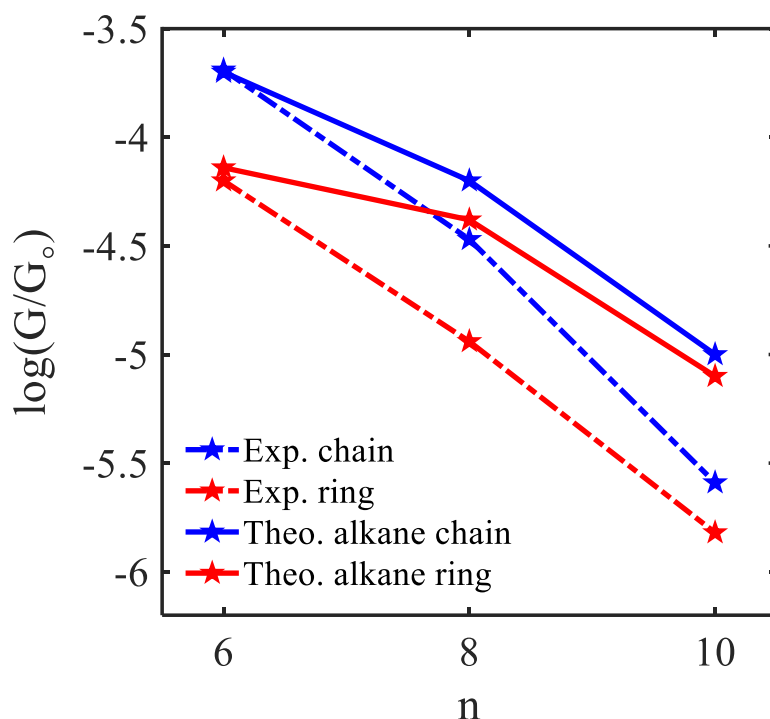


Figure 5. 18. Length dependence conductance of Au|chains/rings|Au junction, with Au–SMe for chains and Au–S for rings covalent bonds connecting the ends of the alkane to the gold electrodes. The blue and dashed blue lines represent the DFT simulations while the red and dashed red lines represent the STM measurements.

After demonstrating that Kirchhoff’s law does not work in the case of chains versus symmetric rings, I am going to test that again but this time against asymmetric rings such as **C<sub>6</sub>C<sub>8</sub>**, **C<sub>6</sub>C<sub>10</sub>** and **C<sub>8</sub>C<sub>10</sub>**.

Since the two branches of the rings are not equal, I am going to compare each linear chain against to 2 rings and as follows: small **C<sub>6</sub>** versus **C<sub>6</sub>C<sub>8</sub>** or **C<sub>6</sub>C<sub>10</sub>**, medium **C<sub>8</sub>** versus **C<sub>6</sub>C<sub>8</sub>** or **C<sub>8</sub>C<sub>10</sub>** and large **C<sub>10</sub>** versus **C<sub>6</sub>C<sub>10</sub>** or **C<sub>8</sub>C<sub>10</sub>**.

As I mentioned above, the case here is more delicate. In general, the DFT simulations suggest that the conductances of rings are higher than the linear chain  $C_6 < C_6C_8$  and  $C_6 \approx C_6C_{10}$ . In contrast, the STM measurements suggest the opposite  $C_6 > C_6C_8$  and  $C_6 > C_6C_{10}$  as shown in Figure 5.19.

Again, in general, the DFT simulations suggest that the conductances of rings are higher than the linear chain  $C_8 < C_6C_8$  and  $C_8 \approx C_8C_{10}$ . For this group the STM measurements agrees with the DFT prediction  $C_8 < C_6C_8$  and  $C_6 < C_8C_{10}$  as shown in Figure 5.20.

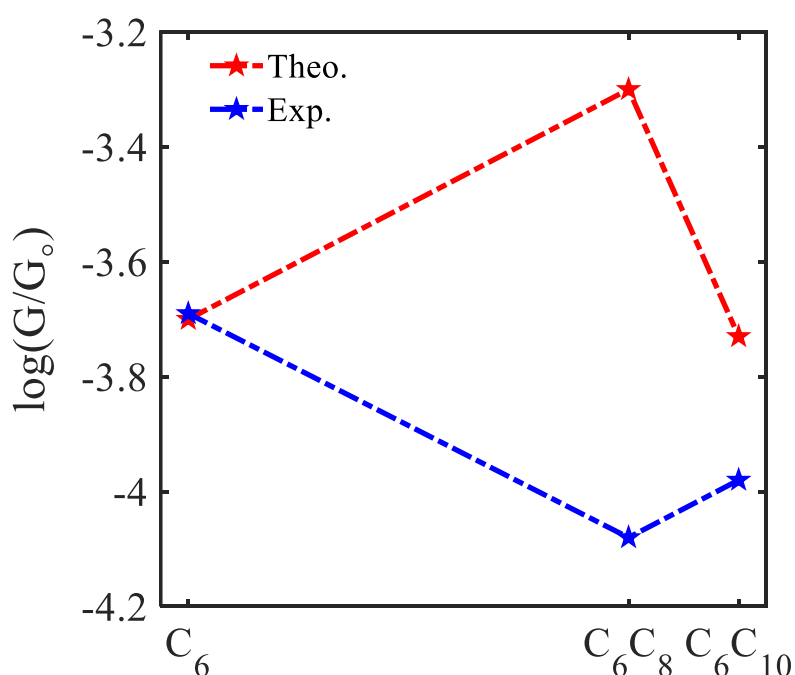


Figure 5. 19. Comparison between DFT simulations against STM measurements of the small group,  $C_6$  versus  $C_6C_8$  or  $C_6C_{10}$ . The red dashed- line represents the theory while the blue dashed- line represents the experiment.

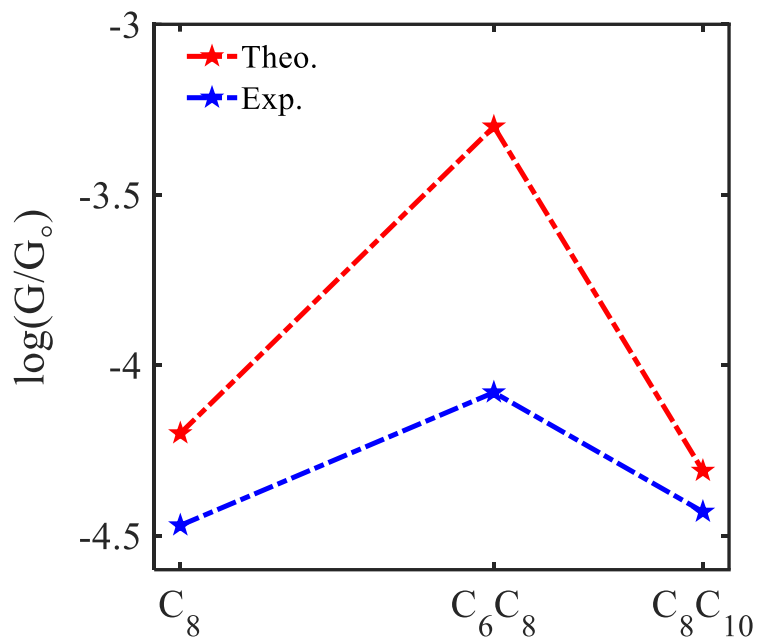


Figure 5. 20. Comparison between DFT simulations against STM measurements of the medium group,  $C_8$  versus  $C_6C_8$  or  $C_8C_{10}$ . The red dashed- line represents the theory while the blue dashed- line represents the experiment.

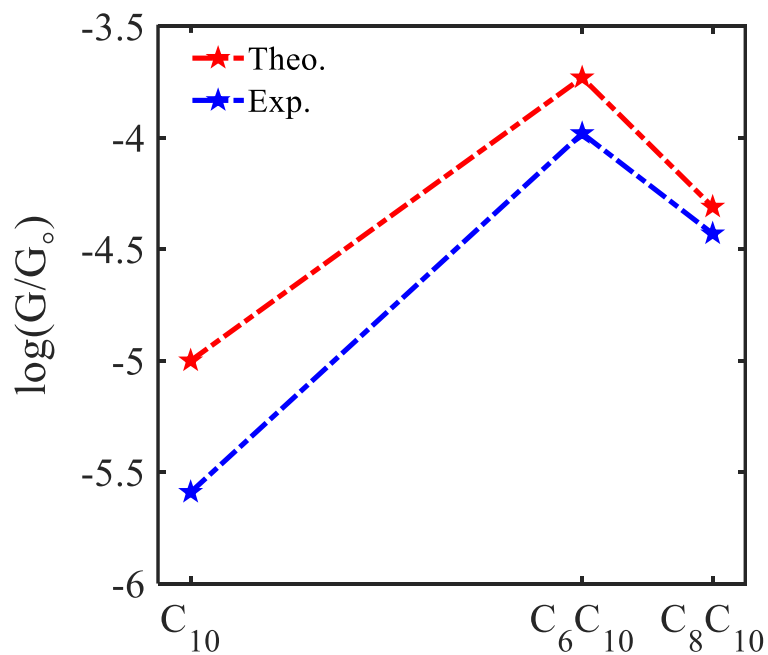




Figure 5. 21. Comparison between DFT simulations against STM measurements of the medium group,  $C_{10}$  versus  $C_6C_{10}$  or  $C_8C_{10}$ . The red dashed- line represents the theory while the blue dashed- line represents the experiment.

Figure 5.21 clearly shows that both simulations and measurements suggest that the conductances of rings are higher than the linear chain  $C_{10} < C_6C_{10}$  and  $C_{10} < C_8C_{10}$ . Overall, I would conclude that in general the DFT simulations predict the conductance of rings is higher than chains. The STM measurements prove that to be correct for two groups medium and large as shown in Figures 5.20 and 5.21.

In section 5.10 above, I created 3 families: family-6, family-8 and family-10, each family consists of 3 rings. Theoretically, I predicted a relationship for each family as shown in Figure 5.16. DFT simulations predict a non-classical trend for family-6 and a classical trend for family-8 and family-10. These predictions will now be checked against the STM measurements. Figure 5.22 shows the STM measurements for the 3 families (black-stars). By comparing them against the predictions (red-stars), one excellent agreement is obtained, especially for the larger cavity (family-10).

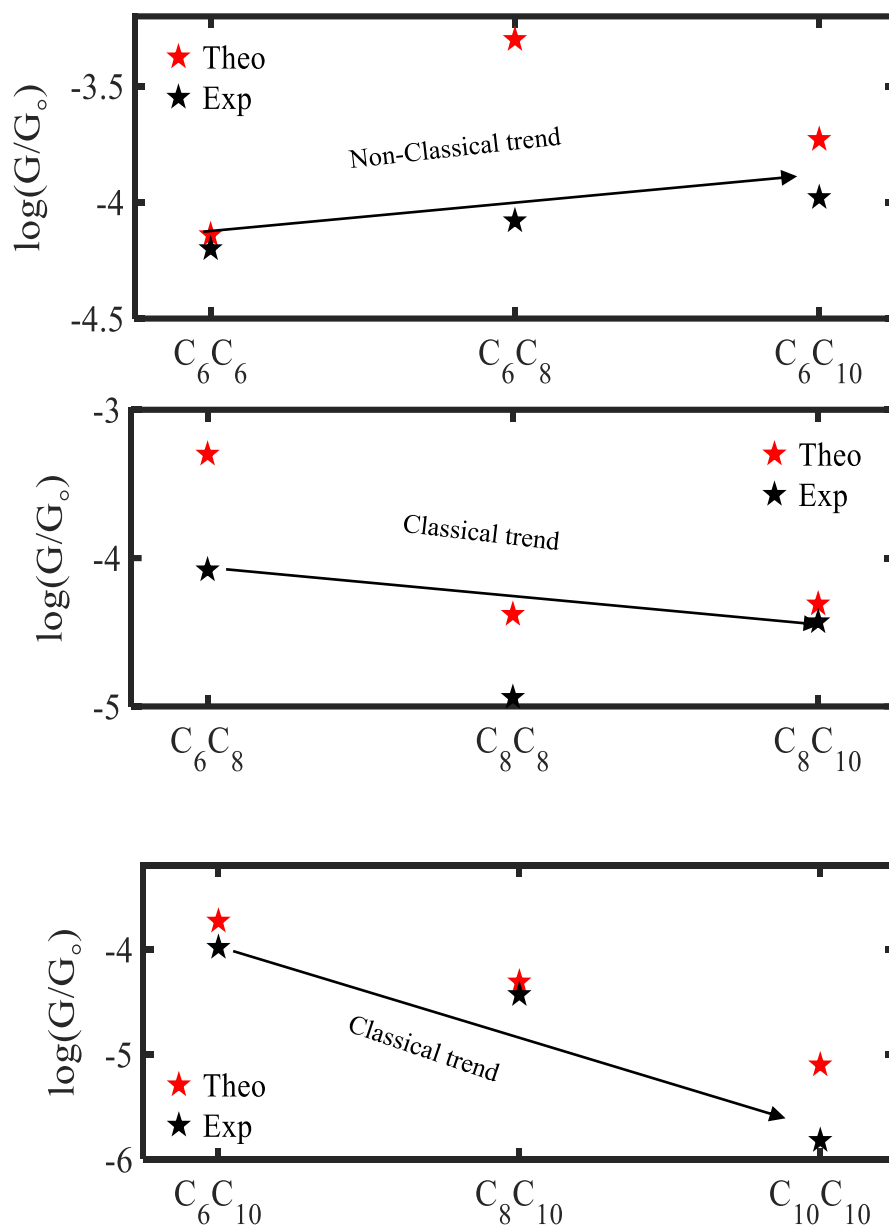


Figure 5. 22. Conventional and non-conventional tunnelling transport. Comparison between the theory and experimental conductances of three alkane ring families: small, medium and large cavities C<sub>6</sub>, C<sub>8</sub> and C<sub>10</sub> respectively.

### 5.10.2 Units of the Y-axis

One can notice that the Y-axes in the sub-plots of Figure 5.22 are not on the same scale. I will now amend the 3 panels of Figure 5.22 to be all from -3 to -6 on Y-axes. The reason behind amending Figure 5.22, is to see a clear picture that helps to understand the trend in each family.

Using the same scales, the top panel of Figure 5.23 (family-6), shows approximately a horizontal line (black arrow), meaning there is no significant change in the conductance of the 3 rings. One explanation for this behaviour, could be that in this family the common branch among the 3 rings is  $C_6$  ( $C_6C_6$ ,  $C_6C_8$  and  $C_6C_{10}$ ), and this path is the shortest in each ring. This suggests that the electrons tend to take the shortest path, and this is why the conductance is independent of increasing the size of the cavity (12, 14 and 16 carbon atoms).

Having that in mind, family-8 includes  $C_6C_8$ ,  $C_8C_8$  and  $C_8C_{10}$  rings and the common branch for this family is  $C_8$ , however, the common branch here is not the shortest branch in  $C_6C_8$  and this is the conductance of  $C_6C_8$  is higher than  $C_8C_8$  and  $C_8C_{10}$  (black arrow-1). Applying the same idea elucidates why the conductances of  $C_8C_8$  and  $C_8C_{10}$  are approximately equal (common equal shortest branch, black arrow-2), as shown in the middle panel of Figure 5.23.

Let us apply the same idea to a large family such as family-10, where the common branch is  $C_{10}$ , and the shortest branch differs from one ring to another  $C_6$ ,  $C_8$  and  $C_{10}$ . According to our assumption, the conductance should decrease by increasing the cavity size of the 3 rings (16, 18 and 20 carbon atoms). This behaviour is clearly shown in the lower panel of Figure 5.23 (black arrow).

These theoretical simulations and the insight they provide are well supported by the STM measurements.

To conclude the conductance comparison in the above sections, the conductances of the  $n,n$  symmetric rings are found to decay exponentially with  $n$ , but at a slower rate than the linear chains. Remarkably, both experiment and theory reveal that the electrical conductances of the symmetric  $C_nC_n$  rings are lower than their asymmetric counterparts, with the  $C_6C_6$  less than both  $C_6C_8$  and  $C_6C_{10}$ , the  $C_8C_8$  less than both  $C_8C_6$  and  $C_8C_{10}$  and the  $C_{10}C_{10}$  less than both  $C_{10}C_8$  and  $C_{10}C_6$ .

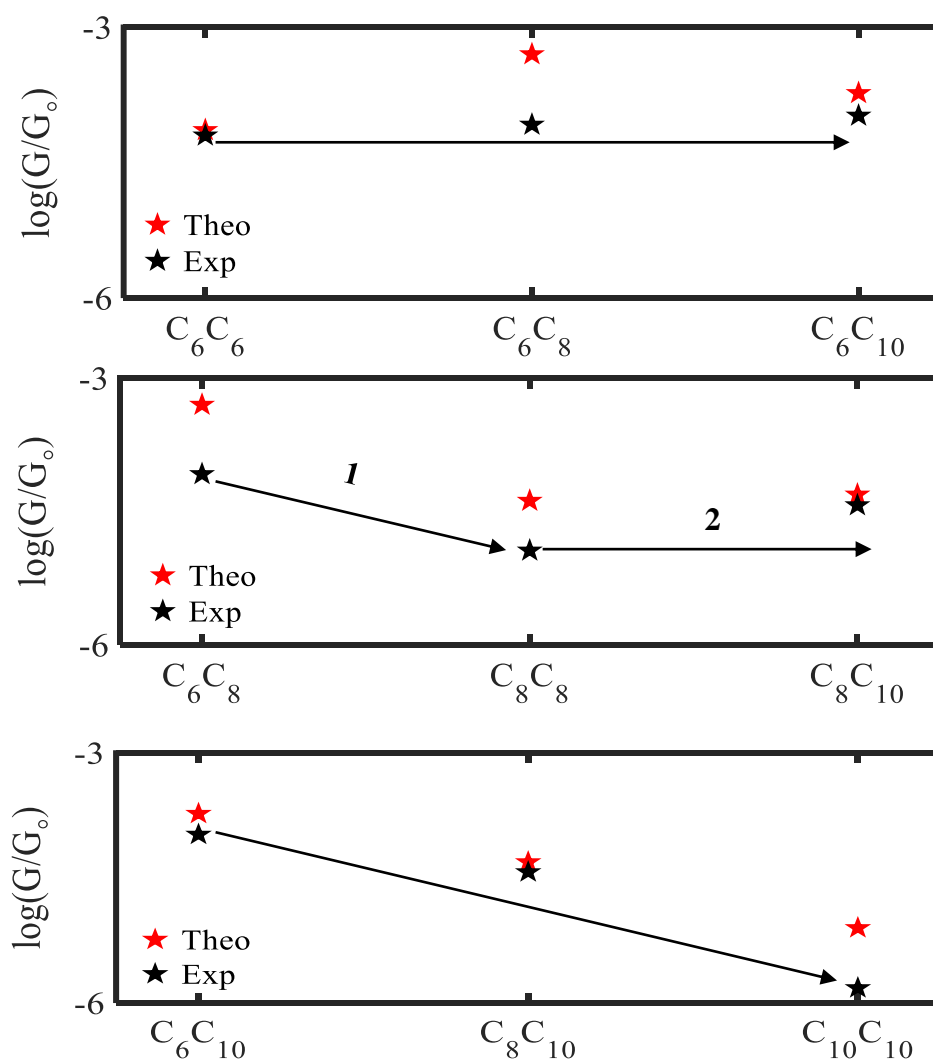


Figure 5. 23. Same plotting scale of Y-axes (amending Figure). Family 6, family 8 and family 10, (top to bottom).

### 5.11 Seebeck coefficient

After computing the electronic structures and properties including transmission coefficients  $T(E)$  for the 9 alkane derivatives (3 linear chains, 3 symmetric rings and 3 asymmetric rings), thermoelectric properties such as Seebeck coefficients  $S$  is going to be computed for the same studied molecules.

For more detail about the thermopower see section 3.2 in chapter 3 [23-29]. Here, I will briefly describe the thermoelectric simulations.

To calculate the Seebeck coefficient of the studied molecular junctions, it is useful to introduce the non-normalised probability distribution  $P(E)$  defined by

$$P(E) = -T(E) \frac{df(E)}{dE} \quad (5.5)$$

Where  $f(E)$  the Fermi-Dirac is function and  $T(E)$  are the transmission coefficients and whose moments  $L_n$  are denoted as follows

$$L_n = \int dE P(E) (E - E_F)^n \quad (5.6)$$

Where  $E_F$  is the Fermi energy. The thermopower,  $S$ , is then given by

$$S(T) = -\frac{1}{|e|T} \frac{L_1}{L_0} \quad (5.7)$$

Where  $e$  is the electronic charge.

It is worth mentioning, that I am going to use the same classifications that I used in the conductance section. Alkane linear chains are denoted **C<sub>6</sub>**, **C<sub>8</sub>** and **C<sub>10</sub>**. Symmetric alkane rings are denoted **C<sub>6</sub>C<sub>6</sub>**, **C<sub>8</sub>C<sub>8</sub>** and **C<sub>10</sub>C<sub>10</sub>** and asymmetric alkane rings are denoted **C<sub>6</sub>C<sub>8</sub>**, **C<sub>6</sub>C<sub>10</sub>** and **C<sub>8</sub>C<sub>10</sub>**.

### 5.11.1 Seebeck coefficients of linear chains

In this section, I shall study Seebeck coefficients of the 3 alkane linear chains, where  $n=6, 8$  and 10, as shown in the Figure 5.5.

Figure. 5.24 shows the thermopower  $S$  evaluated at room temperature for different energy ranges  $E_F - E_F^{DFT}$  of the 3 chains. This Figure shows that the sign of the Seebeck coefficient is negative for the 3 chains. The negative  $S$  is due to the fact that the DFT-predicted Fermi ( $E - E_F = 0$  eV), is slightly closer to LUMO than HOMO as shown in Figure 5.24 (black-dashed line). On the other hand, terminal group such as thiomethyl (SMe), could be HOMO or LUMO dominated according to many theoretical and experimental studies, but I am going test the sing and value against the  $S$  measurements.

Figure 5.24, predict that the Seebeck coefficients of medium and large (**C<sub>8</sub>** and **C<sub>10</sub>**) chains to be similar and higher than the small chain **C<sub>6</sub>**, with -15.0 and -14.6 ( $\mu V/K$ ). One could notice that, the  $S$  increases with increase the length from 6 to 8 carbon atoms.

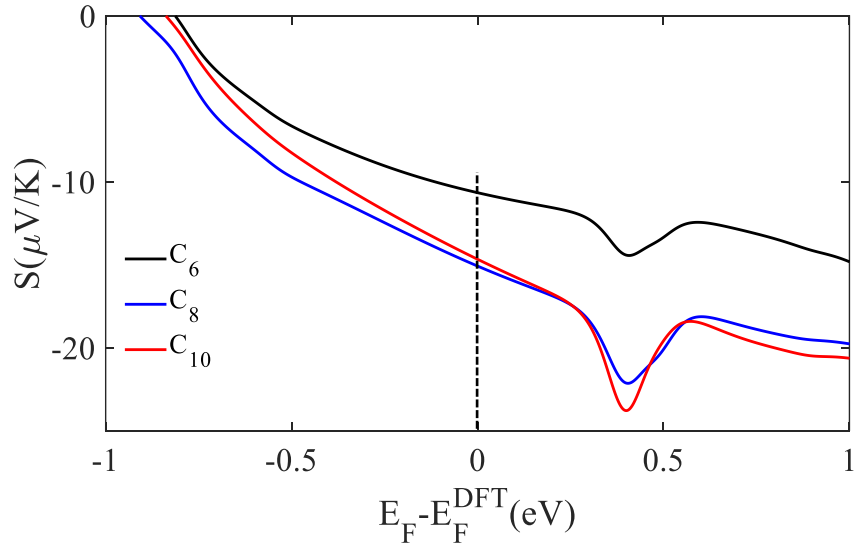


Figure 5. 24. Seebeck coefficient  $S$  as a function of Fermi energy  $E_F$  for 3 alkane chains. Seebeck coefficient  $S$  of alkane chains of size  $C_6$ , alkane chain  $C_8$ , and alkane chain  $C_{10}$ .

### 5.11.2 Seebeck coefficient of symmetric alkane rings

The second group in this study is the symmetric rings, which includes small cavity  $C_6C_6$ , medium cavity  $C_8C_8$ , and large cavity  $C_{10}C_{10}$  shown in the Figure 5.7.

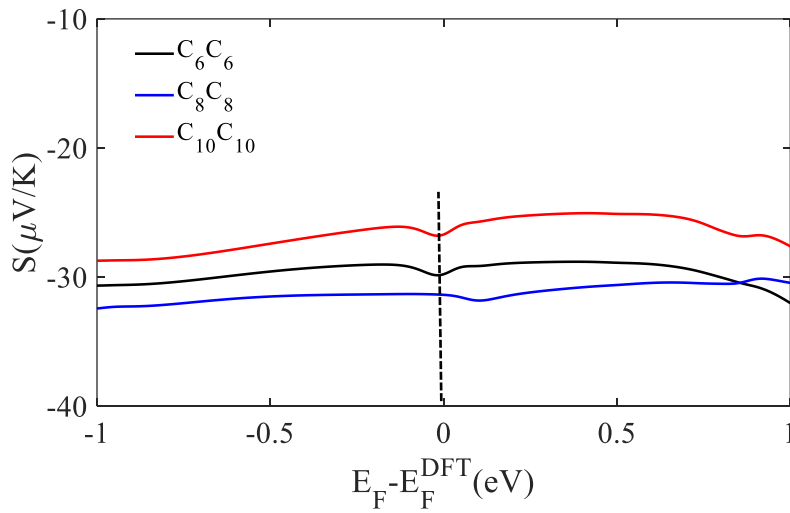


Figure 5. 25. Seebeck coefficients  $S$  as a function of Fermi energy  $E_F$  for 3 alkane symmetric rings. Small symmetric rings of size  $C_6C_6$ , medium size  $C_8C_8$ , and large size  $C_{10}C_{10}$ .

Figure 5.25 above again, shows a negative sign for the 3 symmetric rings, which suggest that the Fermi level is in the vicinity of LUMO than HOMO as shown in Figure 5.25 (black-dashed line).

Figure 5.25, predict that the Seebeck coefficient of the medium ring **C<sub>8</sub>C<sub>8</sub>** possesses the highest Seebeck coefficient with value of -31.4 ( $\mu V/K$ ) followed by the small ring **C<sub>6</sub>C<sub>6</sub>** value of -29.7 ( $\mu V/K$ ) then the lowest value -26.7 ( $\mu V/K$ ) for **C<sub>10</sub>C<sub>10</sub>**.

### 5.11.3 Seebeck coefficient of asymmetric alkane rings

The third group in this study is asymmetric rings, which includes small cavity **C<sub>6</sub>C<sub>8</sub>**, medium cavity **C<sub>6</sub>C<sub>10</sub>**, and large cavity **C<sub>8</sub>C<sub>10</sub>** shown in the Figure 5.9.

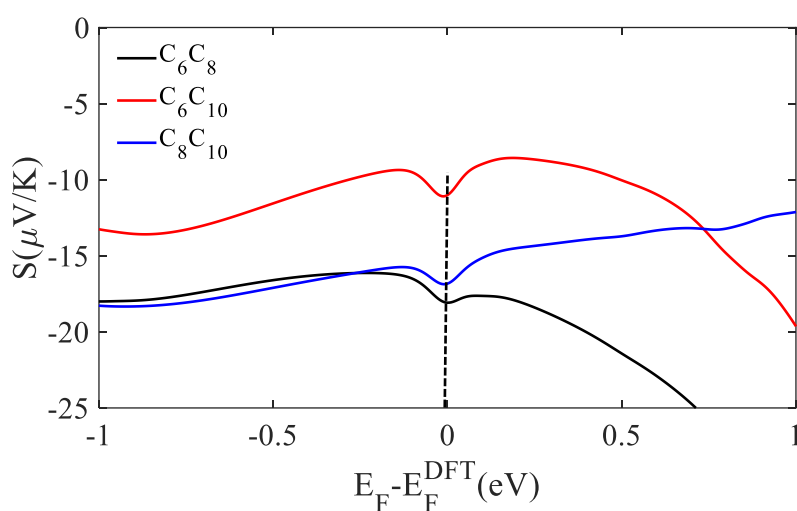


Figure 5. 26. Seebeck coefficients  $S$  as a function of Fermi energy  $E_F$  for 3 alkane rings. Seebeck coefficients  $S$  of asymmetric alkane rings of small cavity **C<sub>6</sub>C<sub>8</sub>**, medium cavity **C<sub>6</sub>C<sub>10</sub>**, and large cavity **C<sub>8</sub>C<sub>10</sub>** respectively.

Figure 5.26 above agrees with Figures 5.25 and 5.24 about the negative sign, which again suggests that the Fermi level is in the vicinity of LUMO than HOMO as shown in Figure 5.26 (black-dashed line).



Figure 5.26, predict that the Seebeck coefficient of the small cavity **C<sub>6</sub>C<sub>8</sub>** possesses the highest Seebeck coefficient with value of -18.0 ( $\mu V/K$ ) followed by the medium cavity **C<sub>8</sub>C<sub>10</sub>** value of -16.8 ( $\mu V/K$ ) then the lowest value -11.0 ( $\mu V/K$ ) for **C<sub>6</sub>C<sub>10</sub>**. The above simulations suggest that the case is more complicated in asymmetric rings.

### 5.11.3 Comparison between theoretical simulations and experimental measurements

In section 5.10.1, I compared my theoretical predictions of conductance against the STM measurements. Here, I am going to do the same for Seebeck coefficients. It is worth mentioning that our collaborator at Xiamen University for technical reason could not measure the Seebeck coefficient for the 9 alkane molecules. For simplicity, I will present the thermopower comparison as a table, where it shows the measured STM values against the DFT predictions.

For alkane linear chains, DFT predicts an increase in  $S$  value by moving from small to medium then a decrease from medium to large chains. The first prediction is well supported by the STM measurements and I cannot check the second prediction as there is no measurements for the large chain as shown in Table 5.8 (top).

For symmetric alkane rings, DFT again predicts similar trend, a slight increase in  $S$  value by moving from small to medium ( $\sim -30$  to  $-31 \mu V/K$ ) then decrease from medium to large cavity. Again, the STM measurements agree well with this prediction, and I cannot check the second prediction for the same reason as shown in Table 5.8 (middle).

For asymmetric rings, DFT predicts an opposite trend, means decrease in  $S$  value by moving from small to medium ( $\sim -18$  to  $-11 \mu V/K$ ) then an increase from medium to large cavity. The STM measurements support the first prediction, and the second prediction cannot be checked as shown in Table 5.8 (bottom).

Finally, the DFT-predicted sign (negative), of the Seebeck coefficient has been proven to be correct for 9 alkane derivatives.

Table 5. 8. DFT predicted versus STM measured Seebeck coefficients of 9 alkane derivatives in  $\mu V/K$  unit.

Molecule type	Molecule	Measured Seebeck coefficient	Calculated Seebeck coefficient
Linear chains	<b>C<sub>6</sub></b>	$-6.76 \pm 0.42$	-10.0
	<b>C<sub>8</sub></b>	$-15.90 \pm 1.16$	-15.0
	<b>C<sub>10</sub></b>	==	-14.6
Symmetric rings	<b>C<sub>6</sub>C<sub>6</sub></b>	$-19.23 \pm 0.31$	-29.7
	<b>C<sub>8</sub>C<sub>8</sub></b>	$-24.94 \pm 0.63$	-31.4
	<b>C<sub>10</sub>C<sub>10</sub></b>	==	-26.7
Asymmetric rings	<b>C<sub>6</sub>C<sub>8</sub></b>	$-14.53 \pm 0.72$	-18.0
	<b>C<sub>6</sub>C<sub>10</sub></b>	$-10.22 \pm 0.16$	-11.0
	<b>C<sub>8</sub>C<sub>10</sub></b>	==	-16.8

== No experimental value is available.

## 5.12 Conclusion

In conclusion, I investigated three alkane chains **C<sub>6</sub>**, **C<sub>8</sub>** and **C<sub>10</sub>** with thiomethyl anchors and found that their conductances decrease when the length of chains increases. Thus, the DFT logarithmic conductance of **C<sub>6</sub>** was -3.7 where the conductance of **C<sub>8</sub>** and **C<sub>10</sub>** were -4.2 and -5 respectively.

Furthermore, I formed symmetric and asymmetric rings from the alkane chains, and I found their conductances also have a conventional behaviour. For symmetric rings, I selected three rings, namely **C<sub>6</sub>C<sub>6</sub>**, **C<sub>8</sub>C<sub>8</sub>** and **C<sub>10</sub>C<sub>10</sub>**, and **C<sub>6</sub>C<sub>6</sub>** has the highest conductance with -4.14 comparing with **C<sub>8</sub>C<sub>8</sub>** and **C<sub>10</sub>C<sub>10</sub>**. In addition, for asymmetric rings, **C<sub>6</sub>C<sub>8</sub>**, **C<sub>6</sub>C<sub>10</sub>** and **C<sub>8</sub>C<sub>10</sub>**, their patterns are not so different from the symmetric rings. **C<sub>6</sub>C<sub>8</sub>** owns the smallest cavity, comparing with **C<sub>6</sub>C<sub>8</sub>** and **C<sub>6</sub>C<sub>10</sub>**, has the largest logarithmic conductance of -3.30.

The most important and unexpected prediction in this chapter is the applicability Kirchhoff's law in the nano-scale structures. Surprisingly, the conductances of alkane chains were higher than that of their corresponding rings, which completely disagrees with classical rules for combining conductances in parallel. Since this study includes, symmetric and asymmetric rings. I formed three families based on the common branch **C<sub>6</sub>**, **C<sub>8</sub>** and **C<sub>10</sub>**. Family-6 consists of **C<sub>6</sub>C<sub>6</sub>**, **C<sub>6</sub>C<sub>8</sub>** and **C<sub>6</sub>C<sub>10</sub>**, which has a non-classical trend. For families-8 and -10, they both have a conventional behaviour.

This chapter also covers the thermoelectric properties such as Seebeck coefficients. For linear chains, for example, a **C<sub>8</sub>** has approximately the largest value of Seebeck coefficient, -15  $\mu\text{V}/k$  comparing with **C<sub>6</sub>** and **C<sub>10</sub>**.

Finally, the DFT predictions and simulations are well supported by the TSM measurements for the 9 alkane derivatives.

Figure 5.27 illustrates and summarizes trend of  $G$  for alkane chains and its corresponding rings.

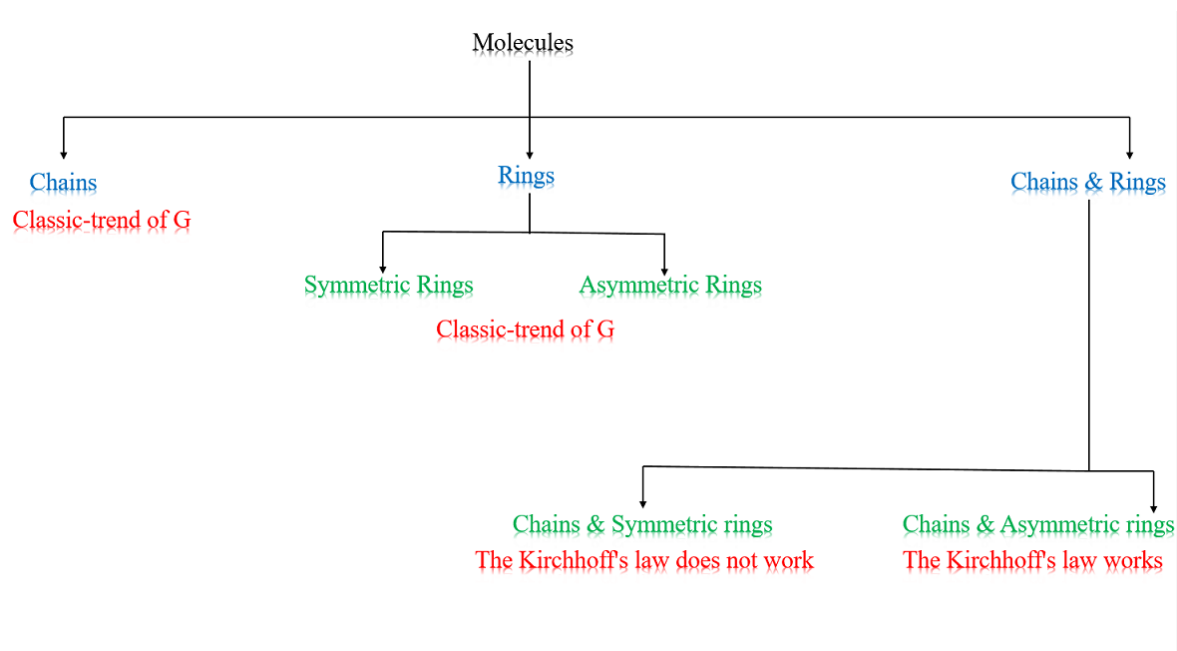


Figure 5. 27. Schematic illustration of chapter 5 summarized the trend of  $G$  for chains and rings.

## Bibliography

1. Ferrer, J., Lambert, C.J., García-Suárez, V.M., Manrique, D.Z., Visontai, D., Oroszlany, L., Rodríguez-Ferradás, R., Grace, I., Bailey, S.W.D., Gillemot, K., Sadeghi, H. and Algharagholy, L.A. (2014). GOLLUM: a next-generation simulation tool for electron, thermal and spin transport. *New Journal of Physics*, 16(9), p.093029.
2. Li, C., Mishchenko, A. and Wandlowski, T. (2011). Charge Transport in Single Molecular Junctions at the Solid/Liquid Interface. *Topics in Current Chemistry*, pp.121–188.
3. Sparks, R.E., García-Suárez, V.M., Manrique, D.Zs. and Lambert, C.J. (2011). Quantum interference in single molecule electronic systems. *Physical Review B*, 83(7).
4. Floyd, T.L. (2007). *Principles of electric circuits: conventional current version*. Upper Saddle River, N.J.: Pearson Prentice Hall.
5. Davidson, R., Ismael, A. and Lambert, C., 2018. Conductance of ‘bare-bones’ tripodal molecular wires. *RSC Advances*, 8(42), pp.23585-23590.
6. González, M., Ismael, A., Grace, I. and Lambert, C., 2021. Interference Controls Conductance in Phthalocyanine Molecular Junctions. *The Journal of Physical Chemistry C*, 125(27), pp.15035-15043.
7. Ismael, A. and Lambert, C., 2019. Single-molecule conductance oscillations in alkane rings. *Journal of Materials Chemistry C*, 7(22), pp.6578-6581.
8. Ismael, A., Alshehab, A., Grace, I. and Lambert, C., 2021. Correction: Molecular-scale thermoelectricity: as simple as ‘ABC’. *Nanoscale Advances*, 3(2), pp.619-619.

9. Ismael, A., Grace, I. and Lambert, C., 2017. Discriminating single-molecule sensing by crown-ether-based molecular junctions. *The Journal of Chemical Physics*, 146(6), p.064704.
10. Ismael, A., Nichols, R. and Lambert, C., 2019. Single molecule vs. large area design of molecular electronic devices incorporating an efficient 2-aminepyridine double anchoring group. *Nanoscale*, 11(34), pp.15871-15880.
11. Markin, A., Ismael, A., Davidson, R. and Lambert, C., 2020. Conductance Behavior of Tetraphenyl-Aza-BODIPYs. *The Journal of Physical Chemistry C*, 124(12), pp.6479-6485.
12. Naghibi, S., Ismael, A., Grace, I., Lambert, C. and Nichols, R., 2019. Synthetic Control of Quantum Interference by Regulating Charge on a Single Atom in Heteroaromatic Molecular Junctions. *The Journal of Physical Chemistry Letters*, 10(20), pp.6419-6424.
13. Wang, X., Ismael, A., Alshehab, A. and Lambert, C., 2021. Optimised power harvesting by controlling the pressure applied to molecular junctions. *Chemical Science*, 12(14), pp.5230-5235.
14. Wilkinson, L., Grace, I., Ismael, A. and Lambert, C., 2022. Assembly, structure and thermoelectric properties of 1,1'-dialkynylferrocene 'hinges'. *Chemical Science*, 13(28), pp.8380-8387.
15. Gantenbein, M., Ismael, A. and Lambert, C., 2017. Quantum interference and heteroaromaticity of para- and meta-linked bridged biphenyl units in single molecular conductance measurements. *Scientific Reports*, 7(1).

16. Herrer, I., Ismael, A., Grace, I., Lambert, C. and Nichols, R., 2018. Unconventional Single-Molecule Conductance Behavior for a New Heterocyclic Anchoring Group: Pyrazolyl. *The Journal of Physical Chemistry Letters*, 9(18), pp.5364-5372.
17. Ismael, A., Chen, Z., Lambert, C., Hong, W. and Zhang, Q., 2022. Highly Insulating Alkane Rings with Destructive  $\sigma$ -Interference. *Science China Chemistry*, 65.
18. Ismael, A., Grace, I. and Lambert, C., 2017. Connectivity dependence of Fano resonances in single molecules. *Physical Chemistry Chemical Physics*, 19(9), pp.6416-6421.
19. Hagen, K.D. (2001). *Introduction to engineering analysis*. Upper Saddle River, Nj: Prentice Hall.
20. Paul, C.R. (2001). *Fundamentals of electric circuit analysis*. New York: John Wiley & Sons.
21. Joachim, C. (2012). Probing intramolecular circuit laws. *Nature Nanotechnology*, 7(10), pp.620–621.
22. Vazquez, H., Skouta, R., Schneebeli, S., Kamenetska, M., Breslow, R., Venkataraman, L. and Hybertsen, M.S. (2012). Probing the conductance superposition law in single-molecule circuits with parallel paths. *Nature Nanotechnology*, 7(10), pp.663–667.
23. Lambert, C.J., Sadeghi, H. and Al-Galiby, Q.H. (2016). Quantum-interference-enhanced thermoelectricity in single molecules and molecular films. *Comptes Rendus Physique*, 17(10), pp.1084–1095.
24. Bennett, T., Ismael, A. and Lambert, C., 2022. Multi-component self-assembled molecular-electronic films: towards new high-performance thermoelectric systems. *Chemical Science*, 13(18), pp.5176-5185.

25. Ismael, A. and Lambert, C., 2020. Molecular-scale thermoelectricity: a worst-case scenario. *Nanoscale Horizons*, 5(7), pp.1073-1080.
26. Ismael, A., Agraït, N. and Lambert, C., 2022. Exploring seebeck-coefficient fluctuations in endohedral-fullerene, single-molecule junctions. *Nanoscale Horizons*, 7(6), pp.616-625.
27. Ismael, A., Bennett, T., Wilkinson, L. and Lambert, C., 2020. Tuning the thermoelectrical properties of anthracene-based self-assembled monolayers. *Chemical Science*, 11(26), pp.6836-6841.
28. Ismael, A., Grace, I. and Lambert, C., 2018. Oscillating Seebeck coefficients in  $\pi$ -stacked molecular junctions. *RSC Advances*, 8(44), pp.24711-24715.
29. Ismael, A., Grace, I. and Lambert, C., 2015. Increasing the thermopower of crown-ether-bridged anthraquinones. *Nanoscale*, 7(41), pp.17338-17342.



## Chapter 6

### Conclusion and Future Work

#### 6.1 Conclusion

In this thesis, I have introduced the principle equations and tools that are used as basis for my work, including the Schrödinger equation, density functional theory (DFT), and the SIESTA code that implements DFT and solves those equations. Moreover, I have presented the theory of single-electron transport, which starts from the Hamiltonian, computes Green's functions and then obtains the transmission coefficient. These methods are described in detail in Chapters 2 and 3, respectively.

Chapter 4 is considered as the first original-results chapter of this thesis, where I started by investigating series of alkane chains using different linker groups including amine ( $\text{NH}_2$ ), thiol (S), direct carbon contact (C), and thiomethyl (SMe). In this chapter, I nominated 8 molecules (4 odd and 4 even), with four different anchor groups. Thus, I have explored in total 32 molecules of alkane chains. I investigated the influence of using different terminated groups on alkane molecules conductance. As expected, the trend of alkane chains conductance was found to be conventional, regardless to the type of linker groups. However, conductance values of these linkers were different depending on the nature of each a terminated group. My theoretical simulations on alkane chains were tested by experimental measurements and an excellent agreement was found.

Chapter 5, is my second results chapter. I investigated three alkane chains  $\text{C}_6$ ,  $\text{C}_8$  and  $\text{C}_{10}$  terminated with thiomethyl anchor, again the same result was found (conductance increases with decreasing the length of chain).

Furthermore, I formed symmetric and asymmetric rings from the alkane chains and found their conductances have a conventional behaviour. For symmetric rings, I selected three rings, namely  $C_6C_6$ ,  $C_8C_8$  and  $C_{10}C_{10}$ .  $C_6C_6$  has the highest conductance with -4.14 compared to  $C_8C_8$  and  $C_{10}C_{10}$ . In addition, for asymmetric rings,  $C_6C_8$ ,  $C_6C_{10}$  and  $C_8C_{10}$ , their patterns are not so different from the symmetric rings.  $C_6C_8$  owns the smallest cavity, comparing with  $C_6C_8$  and  $C_6C_{10}$ , however, it possesses the largest conductance -3.30 .

The most important and controversial prediction in this chapter is the comparison between linear chains against rings (Kirchhoff's law). Surprisingly, conductances of alkane chains were higher than their corresponding ring conductances, which completely disagrees with classical rules for combining electrical conductances. Since this study includes, symmetric and asymmetric rings. I formed three families based on the common branch  $C_6$ ,  $C_8$  and  $C_{10}$ . Family-6 consists of  $C_6C_6$ ,  $C_6C_8$  and  $C_6C_{10}$ , which has a non-classical trend. For families-8 and -10, they both have a classical behaviour.

This chapter also presents a study of the Seebeck coefficients of the above molecules. For linear chains, for example,  $C_8$  has approximately the largest value of Seebeck coefficient,  $-15 \mu V/k$  comparing with  $C_6$  and  $C_{10}$ .

Finally, the DFT predictions and simulations are well supported by the STM measurements for the 9 alkane derivatives.

## 6.2 Future work

In this thesis, I have investigated approximately 32 alkane chains molecules with four anchor groups including amine ( $\text{NH}_2$ ), thiol (S), direct carbon contact (C), and thiomethyl (SMe). The conductance was found to be sensitive to the anchor type and to complete this story, I am planning to employ other linker groups, such as pyridine, cyanide, DBHT and TMS. The current study shows that the direct carbon contact possesses the highest conductance, whereas the amine is the lowest. Similar idea could be applied to the alkane rings.

Another avenue for future exploration is to use different electrodes, for instance graphene [1, 2], platinum or palladium [3] and examine their effect on fluctuation in  $G$  and  $S$ , which might be even higher thermopowers.

I also studied alkane rings in this thesis, which typically have small cavities and contain only two types of atoms: carbon and hydrogen. As part of my future plans, I will also investigate large rings that consist of oxygen atoms as shown in Figure 6.1 [4,5]. During this stage, I am interested in studying the trend of conductance and Seebeck coefficient, perhaps, I will get a new behaviour that I did not discover yet in this thesis.

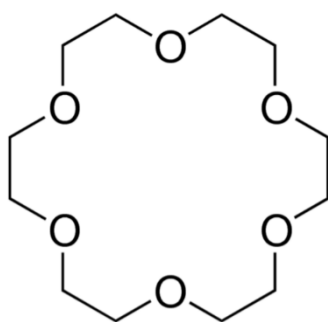


Figure 6. 1. The structure of 1,4,7,10,13,16-Hexaoxacyclooctadecane molecule.

## Bibliography

1. Sadeghi, H., Sangtarash, S. and Lambert, C.J. (2015). Enhancing the thermoelectric figure of merit in engineered graphene nanoribbons. *Beilstein Journal of Nanotechnology*, 6, pp.1176–1182.
2. Zheng, X.H., Zhang, G.R., Zeng, Z., García-Suárez, V.M. and Lambert, C.J. (2009). Effects of antidots on the transport properties of graphene nanoribbons. *Physical Review B*, 80(7).
3. García-Suárez, V.M., Rocha, A.R., Bailey, S.W., Lambert, C.J., Sanvito, S. and Ferrer, J. (2005). Single-channel conductance of H<sub>2</sub> molecules attached to platinum or palladium electrodes. *Physical Review B*, 72(4).
4. Atwood, J. (1987). The oxonium cation in aromatic solvents. Synthesis, structure, and solution behavior of [H<sub>3</sub>O<sup>+</sup>·18-crown-6][Cl<sup>-</sup>H-Cl]. *Journal of the American Chemical Society*, 109(26), pp.8100-8101.
5. Steed, J.W. and Atwood, J.L. (2009). *Supramolecular Chemistry*. Chichester: Wiley-Blackwell.